Department of Physics and Astronomy

University of Heidelberg

Diploma thesis

in Physics

submitted by

Benedikt Gebhard Probst

born in Tübingen

2010

The Pendulum Approximation for Fidelity in Quantum Kicked Rotor Systems

This diploma thesis has been carried out by

Benedikt Gebhard Probst

at the

Institute for Theoretical Physics

under the supervision of

Dr. Sandro Wimberger

The Pendulum Approximation for Fidelity in Quantum Kicked Rotor Systems

The kicked rotor (KR) is one of the prime examples for chaos in nonlinear dynamics. When treating the quantum kicked rotor (QKR) the definition of chaos and instability is more difficult. Peres introduced the fidelity, the overlap of the same initial state evolved in time with two slightly different Hamiltonians, as a measure of stability. For the chaotic case one expects universal properties of the fidelity. The description of integrable systems or systems showing dynamical localization as the QKR is more difficult. We treated the QKR in the chaotic regime near to a quantum resonance in order to apply a pseudo-classical approximation that maps the system to a regular one. This regular system is approximated by the pendulum. In order to describe the rotational trajectories in the pseudo-classical phase space we used the WKB method. This way we could give an analytical expression for the fidelity for single rotors and an approximative expression for ensembles of rotors. The validity of the approximations was tested numerically. We could identify regimes in which the approximations are good. In general, the fidelity of the QKR evolution shows, however, a different behaviour than the one of the pendulum due to crucial differences of the pendulum phase space with respect to the pseudo-classical phase space of the QKR.

Die Pendelnäherung zur Berechnung der Fidelity in gekickten Quantenrotorsystemen

Der gekickte Rotor ist eines der Standardsysteme der nichtlinearen Dynamik, das chaotische Verhalten zeigt. Bei der quantenmechanischen Behandlung des gekickten Rotors ist die Definition chaotischen Verhaltens weniger eindeutig. Peres definierte die Fidelity, den Überlap zweier anfänglich identischer Zustände, deren Zeitevolution leicht unterschiedlich ist, als Stabilitätsmaß eines Quantenzustand. Im Falle chaotischer Dynamik erwartet man universales Verhalten. Im Falle dynamischer Lokalisation wie beim gekickten Quantenrotor oder eines integrabelen Systems ist die Beschreibung schwerer. Um eine pseudoklassische Methode zu verwenden, betrachten wir das System nahe einer Quantenresonanz und näherten das System dort mit dem Pendel an. Um die rotationsartigen Trajektorien zu beschreiben, verwenden wir die WKB Näherung. Auf diese Weise konnten wir einen analytischen Ausdruck für die Fidelity eines Rotors und eine Näherung für Ensembles aus gekickten Quantenrotoren herleiten. Die Gültigkeit dieses Ausdrucks wurde numerisch überprüft. Wir konnten Parameterbereiche finden, in denen die Näherungen gut sind. Im Allgemeinen zeigen der gekickte Quantenrotor und das Pendel jedoch verschiedenes Verhalten aufgrund der wesentlichen Unterschiede zwischen dem pseudoklassischen Phasenraum des Quantenrotors und dem Phasenraum des Pendels.

Contents

Chapter 1

Introduction

Many seemingly simple physical systems exhibit complicated dynamics. There are only a few systems that can be solved easily in closed form as for example the harmonic oscillator or the Kepler problem [Gol06]. Some other ones can still be solved by reducing the solution to well defined integrals as for example the pendulum [Ald80]. There are only a few examples not described in the standard textbooks on theoretical mechanics that can also be solved exactly.

A famous example for a simple system exhibiting complex behaviour is the Henon-Heiles problem, which deals with the motion of a particle in a plane subjected to a non rotationally symmetric potential. Although being Hamiltonian this system shows chaotic behaviour [Tab89]. And even the systems that can be solved may show complex behaviour as soon as one introduces some perturbation. A very famous example introduces a temporal perturbation: the kicked rotor is a free rotor being kicked periodically. If the system is perturbed strongly enough it exhibits chaotic behaviour. This system is of special interest as other systems can locally be approximated by the Kicked Rotor (KR) [Lic92].

Not only is the KR interesting as it is canonical in the context of canonical perturbation theory but it is also a nice example for a lot of phenomena common to nonlinear dynamics. In the KR the occurrence of higher order resonances and the self similar structure in them [Lic85] can be studied. One is also able to study the route to chaos via the Poincaré-Birkhoff theorem and the stochastic layers [Lic92]. The motion in the stochastic layer can be described by a diffusive process [Rec80] within the layer. As long as the stochastic layers are separated no global transport and therefore no global stochasticity is possible. The calculation of the breakdown of the last separating KAM torus as a criterion for global stochasticity is one of the practical examples of the KAM theorem [Gre79].

Problems arise as soon as one tries to treat the system quantum mechanically. One of the most obvious problems is that the language in which we described the chaotic behaviour was formulated using points in phase space. Chaos is mostly characterised by the exponential spreading of initially near phase space points [Lic92]. In quantum mechanics this is not a concept we are able to use. Even if we try to compare the systems by means of classical correspondence we find several fundamental differences. Two examples of purely quantal effects without a classical analogue occurring in the quantum kicked rotor (QKR) are quantum

resonances and dynamical localisation. In the first case the phase of the quantum evolution stabilises the system and leads to ballistic energy growth in contrast to the linear growth that would be expected due to the classical diffusive process [Izr80]. In the second case the resonance condition is broken in order to establish the classical correspondence to observe the diffusive energy growth. Nevertheless, one finds a break down of the diffusive growth after some time [Izr90]. This phenomenon is called dynamical localisation and it can be described in several ways. On the one hand Grempel *et al.* were able to map the problem to the Anderson model from solid state physics [Gre84], on the other hand one can also study this phenomenon by analysing the spectrum of the Floquet operator [Izr90]. In contrast to classical chaos not the classical phase space is used to describe the behaviour but rather the statistics of the Floquet operator or the correlations of on-site energies.

It is difficult to understand how chaotic phase space structures influence the behaviour of a quantum mechanical system. In the beginning of quantum chaos the focus was on describing quantum mechanical phenomena by considering the corresponding classical phase space in the classical limit. The method to do this is the semi-classical approximation. This way one is able to understand how classical structures influence the quantum dynamics. In the case of microwave ionisation of Rydberg atoms the phase space structures can give some insight into the quantum dynamics [Cas88] and in the QKR classical diffusion coefficients give insight into localisation behaviour [Izr90].

In contrast to the classical definition of chaos, where one uses the dynamics of the system as a definition, the quantum mechanical description of chaos relies on static properties as for example level spacing statistics or energy eigenfunctions. One of the most successful theories is random matrix theory which is based on the statistics and symmetries of the matrix ensembles. One of the modern criteria for a chaotic quantum system is the coincidence of the statistical properties of the spectrum with those of a random matrix ensemble [Haa10]. One of the most important formulas, the Gutzwiller trace formula, gives information on the energy level density by evaluating periodic orbits [Gut90] and therefore also describes a static object. Also the considerations in [Izr90] use properties of spacings to describe dynamical localisation. None of these approaches tries to characterise the system by some temporal evolution as is done in the case of classical chaos.

The question of reversibility of temporal evolution is an important concept in classical chaos and thermodynamics. In the case of classical chaos it helps to understand the sensitivity on initial conditions and it plays an important role in thermodynamics to elucidate the relaxation to equilibrium. In thermodynamics an important cornerstone in this context is the $\mathcal{H}$-theorem by Boltzmann. He showed how to obtain an evolution towards an equilibrium state despite reversible microscopic dynamics. As a reply Loschmidt introduced the reversibility paradox, which asks why an equilibrium state may not return to the non-equilibrium state. Boltzmann emphasised the role of initial conditions and the probabilistic interpretation of the second law of thermodynamics in his reply. This behaviour is nowadays known as ergodic behaviour or mixing and course graining [Sch04]. This sensitivity for initial conditions and the phenomenon of “mixing“ is what

connects chaos and thermodynamics. Classical chaos is also characterised by the exponential growth of initially small distances in phase space. This strong dependence on initial conditions makes it very difficult to reverse the time evolution classically whereas the quantum time evolution seems to be more stable [She83].

In 1984 Peres adopted the idea by Loschmidt and introduced it to quantum mechanics [Per84]. The naive picture in which the distance of slightly perturbed initial states spreads exponentially is not applicable in quantum mechanics. The distance in Hilbert space is defined via the overlap of the two states. As the time evolution is unitary this overlap is constant in time and therefore does not give a measure of instability. Peres suggested to focus on a family of perturbed Hamilton operators instead of initial states and to build Loschmidt echo using an unperturbed Hamiltonian for the forward and a perturbed Hamiltonian for the backward evolution and build the overlap of the initial and final state. He suggested that this quantity should differ for chaotic and classical systems. The absolute square of this echo is called the fidelity of an initial state.

Since the time when Peres introduced this concept of stability a more detailed view of the field has been developed. It showed that he chose a rather untypical case for classifying regular motion and therefore his classification of regular and stochastic motion breaks down in general[1]. It turned out that the choice of initial states is very crucial, especially in integrable systems. Unlike the chaotic case the integrable case shows some structure in the phase space that influences the behaviour of fidelity. This makes it very difficult to define characteristic or universal properties that allow us to distinguish between chaotic and regular behaviour in contrast to the initial idea of Peres [Gor06].

For chaotic systems several regimes for the fidelity decay can be defined. in the case of weak perturbations quantum mechanical perturbation theory can be applied. One of the important conditions is that the eigenenergies and vectors are Gaussian distributed and uncorrelated. The perturbation leads to a Gaussian decay. The regime of Gaussian decay is therefore called the perturbative regime. If the perturbation is increased the perturbative treatment breaks down and one needs to focus at semi-classical considerations. In this regime Fermi's golden rule leads to a Lorentzian level density and, as the fidelity can also be regarded as the Fourier transform of the level density, we obtain an exponential decay. This regime is called Fermi's Golden Rule regime. The finite dimension of the Hilbert space leads to fidelity saturation. The visibility of these regimes depends on their onset. The perturbative regime, for example, is visible as soon as the finiteness of the Hilbert space dominates the time averaged correlation function. Jalabert and Pastawski even showed a semi-classical mechanism for an exponential decay in which the time scale is defined by the classical Lyapunov exponent and therefore is independent of the perturbation [Jal01]. However, it is complicated to observe a crossover between golden rule and Lyapunov decay [Jac01]. These different regimes just discussed are described in the context of correlation functions in [Gor06].

In integrable systems universal properties cannot be expected as they do not

[1] There are even cases in which regular motion leads to a faster fidelity decay in regular systems [Gor06].

show a universal phase space. To show the universal properties one needs to know that the system shows some strong mixing behaviour in order to be independent of the initial state. The loss of this property can also show up in systems that are expected to be chaotic. Dynamical localisation for example can be a problem in order to define this universal properties [Gor06]. As already mentioned the kicked rotor model is an example where such a behaviour appears.

One of the examples of physical systems that can be mapped onto the QKR is the motion of atoms in a periodic potential. The periodicity can be reduced to the motion on a circle via the Bloch theorem [Nol05]. This system is called the atom optic kicked rotor (AOKR). Due to the description via Bloch waves this model has an additional parameter. This parameter is the quasimomentum which is a conserved quantity. Measurements on this system by Oberthaler *et al.* demonstrated the existence of quantum accelerator modes [Obe99]. They observed that a part of the atoms was accelerated. The effect turned out to be pure quantum and is related to gravity. Fishman *et al.* were able to give a theoretical explanation for this surprising phenomenon [Fis03, Fis02]. They rescaled the system near to resonance and defined a pseudo-classical limit. The phase space defined in this pseudo-classical limit showed some islands that were large enough to carry quantum states, and therefore to explain this accelerated behaviour. In general this pseudo-classical limit maps the dynamics onto a phase space having regular structure although the system was far from the classical limit and completely chaotic. The standard semi-classical limit was not able to explain this accelerator modes but the pseudo-classical limit could explain the behaviour. This example shows how in systems that seem chaotic some regular structures may arise.

In the last years quite some work has been done on the fidelity of the QKR. Sankaranarayanan and Lakshminarayan calculated the fidelity of a rotor near a classical nonlinear resonance island [San03]. They assumed a completely regular classical phase space. They predicted revivals for motion on the island. For motion along rotational orbits they also tested their theory. Weinstein and Hellberg used the kicked top and the QKR for numerical studies [Wei05]. In both publications they used localised wave packets and the system was in the regular regime. They observed the different decay regimes we discussed earlier. However their results are not supported by any analytical expectation.

Our focus is somehow different as we are interested in the chaotic regime. To describe the system in the chaotic regime we assume near resonant kicking, which allows us to use the pseudo-classical technique developed in [Fis03]. This technique maps the AOKR system to a kicked rotor system with reduced kicking strength. Therefore we can describe the system near to a resonance by regular structures although it is completely chaotic. An example of the phase space we can use is given in fig. 3.3. The phase space is characterised by a resonance island and rotator like KAM tori.

It is very hard to translate between the pseudo-classical picture and the particle description in the original Schrödinger equation. A coherent state in the pseudo-classical picture will have a very complicated structure when represented in the original variables. The bridge to experiment therefore will be to express the

wave function in Bloch states which correspond to angular momentum eigenstates and to describe the dynamics by describing the dynamics of the Bloch states. In order to describe the dynamics of a cloud of atoms we need to average over the phase space cell. In this thesis we focused at the calculation of the dynamics of such a Bloch state. Unfortunately in the mentioned literature mostly coherent states were used and we cannot compare our results directly with their treatment.

Abb *et al.* were able to describe analytically the rapid decay and the revivals for states corresponding to the principal nonlinear resonance island in the pseudo-classical phase space [Abb09]. They used a van Vleck propagator and the harmonic oscillator approximation for the island. Building the average over the complete phase space cell they numerically observed a slow decay. This slow decay is attributed to the rotator like rotors and therefore is not described by a theory for island states. This thesis is the continuation of their work. We try to develop a theory for the rotational orbits in order to describe the slow decay. To describe the QKR we use the pendulum approximation of the pseudo-classical model and quantise it using the WKB method.

Outline of the thesis

We will start the thesis with the introduction of the theoretical preliminaries in chapter 2. We will introduce the KR model and show its properties. The QKR will be introduced and we will discuss its differences with respect to the classical model. In order to introduce the pseudo-classical approximation we review the semi-classical approximation. The discussion of the pendulum approximation will start in chapter 3, where will introduce the approximation and give some properties of the model. We will present some pseudo-classical comparison of the pendulum approximation with the QKR. After we have introduced the pendulum approximation we will continue with the description of the pendulum in WKB approximation in chapter 4. The major result of this chapter will be formulas for the fidelity of a single rotor and also for ensembles of rotors in pendulum approximation. The validity of the several approximations will be tested numerically in chapter 5. We will conclude in chapter 6.

Chapter 2

Theoretical Preliminaries

In this chapter we will give the theoretical preliminaries for this thesis. We will start by introducing the classical model of the kicked rotor (KR) which can be described by the standard map. This map is one of the most important example systems in the theory of nonlinear dynamics because a lot of interesting behaviour can be explained based on this model [Lic92]. We will explain the properties of this mapping and show that increasing the kicking strength leads to chaotic regions in the phase space. After we introduce the classical model, we will introduce the quantum version in the context of the atom optic kicked rotor (AOKR) which introduces an additional parameter into the model. This quantum analogon shows unexpected phenomena. We will show how ballistic energy growth arises in quantum resonances and how dynamical localisation can be understood by considering spectral properties.

If we treat the quantum kicked rotor (QKR) near to a quantum resonance we can introduce a rescaling that allows us to define the problem in a pseudo-classical limit. For a better understanding of this technique we introduce a more formal version of semi-classics starting from path integrals. Using the semi-classical approximation as a formal approximation we can define the pseudo-classical limit near to a resonance which is called ϵ-classical limit. This pseudo-classical limit allows us to to map the chaotic KR onto a nearly integrable KR.

After the introduction of the QKR dynamics we will introduce the concept of fidelity. Fidelity was defined by Peres in 1984 as a measure of stability of the time evolution of a quantum state [Per84]. The state of a cloud of cold atoms can be described by an incoherent sum of plane waves. In order to describe them we will introduce the fidelity for an incoherent ensemble of plane waves. We will review two examples of theories describing the fidelity of the QKR in different regimes. We will first review the results by Wimberger *et al.* [Wim06] for the resonant kicked rotor and then the result by Abb *et al.* [Abb09] for near resonant kicked rotors. The later authors used the ϵ-classical technique which will also be used in this thesis in a different regime and a different representation.

2.1 Classical Kicked Rotor

We will first give a formal introduction of the KR model, discuss its important properties and give some physical implementations later.

2.1.1 The Kicked Rotor Model (KR)

The model of the kicked rotor describes a classical particle moving on a circle being kicked by δ-like kicks in a fixed direction as illustrated in fig. 2.1. Using the angular momentum I and the angle θ we can give the Hamiltonian

$$H(I,\theta,t) = \frac{I^2}{2} + k\cos\theta \sum_{n=-\infty}^{\infty} \delta(t - n\tau), \tag{2.1}$$

where τ is the kicking period and k is the kicking strength. Inserting this into Hamilton's equations we obtain

$$\dot{\theta} = I \tag{2.2a}$$

$$\dot{I} = k\sin\theta \sum_{n=-\infty}^{\infty} \delta(t - n\tau). \tag{2.2b}$$

By integrating these equations over one period we find the standard map

$$I_{t+1} = I_t + k\sin\theta_t \tag{2.3a}$$

$$\theta_{t+1} = \theta_t + \tau I_t. \tag{2.3b}$$

By rescaling $J \equiv I\tau$ we obtain a more common version

$$J_{t+1} = J_t + K\sin\theta_t \tag{2.4a}$$

$$\theta_{t+1} = \theta_t + J_t, \tag{2.4b}$$

where we defined the stochasticity parameter to be $K \equiv \tau k$. For the discussion of the classical dynamics we will use this iterative mapping. By means of an extended phase space we can interpret this map as the Poincaré map when defining the Poincaré section by the periodic time coordinate.

This map is one of the cornerstones of chaos in nonlinear systems. A rich variety of phenomena can be studied in this system including higher order resonances and self similarity [Lic85]. The above mapping also shows a transition to global chaos [Gre79] and diffusion in the chaotic phase space [Lic92]. A comprehensive description can be found in [Lic92]. We will now state some of its important properties.

The phase space of the particle moving on a circle is a cylinder. A closer look on the eqs. (2.4) shows that the equations are invariant under the transformation $J \to J + 2\pi m$. The periodic structure of the phase space can be respected by defining J modulo 2π. Doing this we can reduce the phase space of the kicked rotor from the cylinder to a torus. The standard map as a formal map is therefore defined on a torus in the literature. Nevertheless, the phase space of the particle

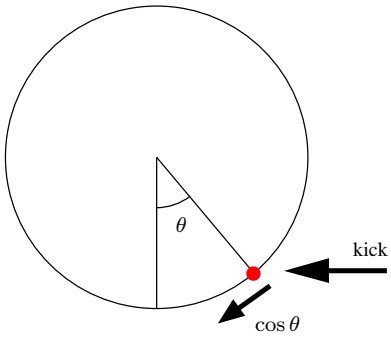

Figure 2.1: In the model of the kicked rotor we assume a particle moving on the circle being kicked from the side.

moving on a circle remains the cylinder. This difference between the formal description on the torus and the physical description on a cylinder is important as leaving the phase space cell on the upper border means entering the next phase space cell from the bottom. From the view of the torus we enter the structure from the bottom but we are in the next cell and have a larger momentum. Moving through the cells therefore can result in energy growth.

This behaviour can be understood by the stroboscopic property of the Poincaré map. The stroboscopic map maps $(J_t, \vartheta_t) \to (J_{t+1}, \vartheta_{t+1})$ but does not say anything about the behaviour between t and $t+1$. In the free evolution part of the dynamics the trajectory might rotate several times. The momentum which corresponds to this rotations is the amount of momentum that is cancelled by the modulo operation in the definition of J. Later we will mention that the motion in the chaotic part can be described by a diffusive process. The transition to global stochasticity can be understood as the breakdown of the last barrier in J direction.

To give an idea why K is called the stochasticity parameter we give some Poincaré plots for different K. In fig. 2.2 we show phase spaces for different K. With growing K the island grows and higher order resonances appear. In the separatrix a stochastic layer develops which builds up a stochastic net. In fig. 2.2(c) we show a phase space slightly below the limit to global stochasticity calculated in [Gre79]. The portion of the phase space which is separated from the stochastic net by the last KAM tori is marked with red arrows. If the stochasticity parameter is large enough the phase space is completely chaotic. Nevertheless there is no strict prove to that and small local structures cannot be excluded [Lic92].

In [Lic92] it is shown that the trajectories in the stochastic layer can be described by a diffusion process. This shows up in linear energy growth on average. In the case of the QKR this diffusive growth will break down.

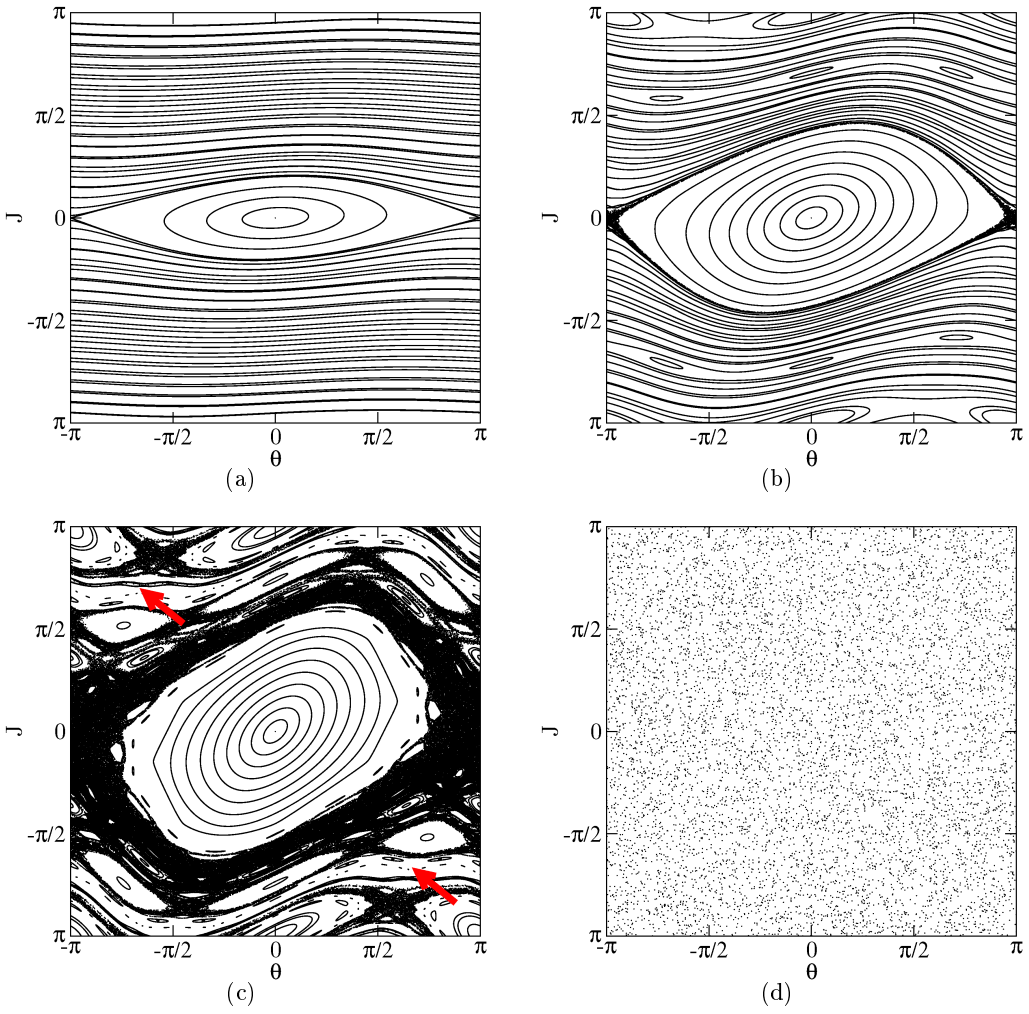

Figure 2.2: In this figure we show the phase space of the standard map. In (a) we show $K = 0.1$, in (b) we show $K = 0.5$, in (c) we show $K = 0.97$ and , in (d) we show $K = 10$. For all plots we used the same 80 starting values. in (a) to (c) we iterated them 10000 times and in (d) 100 times. We can see that with growing K the main resonance grows and the stochastic layer develops. Higher order nonlinear resonances develop and build a net of stochastic layers. The last remaining KAM tori are indicated in (c) by red arrows. They can be recognised as they separate the neighbouring stochastic layers.

2.1.2 Physical Example – Particle in a Periodic Kicking Potential

Let us now discuss different physical realisations of the KR model. It was originally introduced to describe the dynamics of plasmas and the particles in accelerator beams. These days the kicked rotor model can be implemented using cold atoms.

We discuss the motion of a particle in a periodic potential in detail. In accordance to the atom optics kicked rotor we assume a cosine potential that is switched on periodically to implement a kick. The corresponding Hamiltonian is

$$H(p,q,t) = \frac{p^2}{2m} + V_0 \cos\left(2\pi\frac{q}{a}\right) \sum_{n=-\infty}^{\infty} \delta(t - n\tilde{\tau}), \tag{2.5}$$

where a is the grid size, V_0 is the potential depth and $\tilde{\tau}$ is the kicking period and m is the mass of the particle. In order to obtain the kicked rotor Hamiltonian eq. (2.1) we need to rescale the spatial variable by $k_r = \pi/a$. To be in accordance with eq. (2.1) we need to introduce a shift in x. Momentum and time can be scaled to characteristic values. We will present a rescaling that already reflects the quantum nature of the moment. We will use the recoil energy $E_r = k_r^2\hbar^2/2m$ and the Talbot time T. Using this scales we introduce

$$k = \frac{V_0 T}{\hbar}, \qquad \theta = 2k_r x \mod 2\pi, \qquad P = \frac{p}{2k_r\hbar}, \qquad \tau = \frac{8E_r T}{\hbar}\tilde{\tau} \tag{2.6}$$

and obtain the kicked rotor Hamiltonian as $H_{KR}(t) \equiv H(t)/8E_r$. A similar rescaling has been used by Fishman *et al.* in [Fis03].

In physical systems there is not such a thing as a real δ-kick. Therefore we need to consider the characteristics of a δ-kick. This consideration is important when focusing on experimental realisations. In experiments with cold atoms the interaction potential in eq. (2.5) is an effective potential which by definition is just valid for a finite pulse duration. In order to qualify for a δ-pulse the pulse needs to be short compared to the changes of the spatial coordinate. This can be seen when considering eq. (2.2). There the kick takes place in the equation for the momentum but not in the spatial variable. This means that the spatial coordinate is constant during the kick.

2.2 Quantum Kicked Rotor (QKR)

When talking about QKR we will mean mostly the atom optics kicked rotor (AOKR). In contrast to the QKR model the AOKR describes atoms moving in a linear potential rather than a circular motion. Therefore the AOKR contains an additional parameter in contrast to the QKR model discussed for example in [She83, Izr90]. We will first introduce the model starting from the Hamiltonian presented in the last section. Introducing the Bloch states we can replace the linear operator $\hat{x}$ by the periodic angular operator $\hat{\theta}$. This way we obtain an additional parameter β.

Nevertheless, we begin with the rescaled model Hamiltonian

$$\hat{H} = \frac{\hat{p}^2}{2} + k\cos\hat{x}\sum_{n=-\infty}^{\infty}\delta(t-n). \tag{2.7}$$

We will now treat the problem by introducing $\theta \equiv x \mod (2\pi)$. When describing the particle in the circle the momentum operator directly becomes the angular momentum operator. It is important to remind that we treat the QKR and not directly the AOKR. The transition to the AOKR will be done by introducing β-rotors and the associated redefinition of the momentum operator. Integrating the corresponding Schrödinger equation we obtain the operator that maps the state after one kick to the one after the next kick. This operator is called the Floquet operator. For the kicked rotor we obtain the following Floquet operator

$$\hat{\mathcal{U}} = \mathrm{e}^{-\frac{\imath}{\hbar}\left(k\cos\hat{\theta}+\tau\frac{\hat{p}^2}{2}\right)}. \tag{2.8}$$

This operator has two independent parameters. The dynamics are not any more defined by the stochasticity parameter alone. We redefine our variables in order to get rid of the Planck constant

$$p' = \frac{p}{\hbar} \qquad k' = \frac{k}{\hbar} \qquad \tau' = \hbar\tau. \tag{2.9}$$

Writing the Floquet operator in this variables we obtain

$$\hat{\mathcal{U}} = \mathrm{e}^{-k'\imath\cos\hat{\theta}}\mathrm{e}^{-\imath\tau\frac{\hat{p}'^2}{2}}. \tag{2.10}$$

In this rescaling we see that the limit $\hbar \to 0$ corresponds to $k' \to \infty$, $\tau \to 0$ and $K = \text{const.}$. For now we will stay with the quantum case and therefore will drop the primes.

As the Hamiltonian is invariant under translations by the spatial period of the potential (in our scaling equal to one) we can apply the Bloch theorem. This theorem states that the eigenfunctions of the stationary Schrödinger equation with a periodic potential can be expressed by a plane wave and some periodic function. This means we can write eigenfunctions as

$$\psi(x) = \mathrm{e}^{\imath\beta x}\psi_\beta(x) \tag{2.11}$$

where $\psi_\beta(x) = \psi_\beta(x+2\pi)$ and β can be chosen to be in $[0,1]$. In this scaling β represents the fractional momentum and is conserved and is therefore called quasimomentum. Such a state $\psi_\beta(x)$ that is extended to the line by multiplication of $\mathrm{e}^{\imath\beta x}$ is called a β-rotor. We will see later how a β-rotor is connected to a state on a line.

The angular momentum operator is defined by $\hat{\mathcal{N}} \equiv -\imath\partial_\theta$ and is therefore the direct analogon of the momentum operator $\hat{p}$. The angular momentum eigenfunctions are given as

$$\langle\theta|n\rangle = \frac{1}{\sqrt{2\pi}}\mathrm{e}^{\imath n\theta}, \tag{2.12}$$

where n is the angular momentum quantum number.

To determine the Bloch functions that correspond to a state $|\psi\rangle$ we can build

$$\langle\theta|\Psi_\beta\rangle \equiv \frac{1}{\sqrt{2\pi}}\sum_n \langle n+\beta|\psi\rangle \mathrm{e}^{\imath n\theta}. \tag{2.13}$$

This angular representation corresponds to the $\psi_\beta(x)$ introduced above. The difference is that the β-rotor $|\Psi_\beta\rangle$ is a more abstract object. The it is a state on the circle that is connected to a state in the periodic potential $|\psi\rangle$. The state in the periodic potential is not periodic by definition and might be a wave packet. This state is constructed by β-rotors via

$$\langle x|\psi\rangle = \frac{1}{\sqrt{2\pi}}\int_0^1 \mathrm{d}\beta \mathrm{e}^{\imath\beta x}\langle x \mod 2\pi|\Psi_\beta\rangle. \tag{2.14}$$

We can decompose the momentum into a fractional and an integer part by $p = n+\beta$ where $n \in \mathbb{N}$ and $\beta \in [0,1)$. Using this we can give the momentum representation as

$$\langle p|\psi\rangle = \frac{1}{\sqrt{2\pi}}\int_0^{2\pi} \mathrm{d}\theta\langle\theta|\Psi_\beta\rangle \mathrm{e}^{-\imath n\beta}. \tag{2.15}$$

In this picture a β-rotor corresponds to an β component of the wave function. This concept is known in solid state physics as the band model. The integer momentum n corresponds to the band number and β corresponds to the wave number k. The correspondence gets clearer when we take a plain wave state $|p_0\rangle$ and give the corresponding representation in β-rotors. This β-rotor is given by

$$\Psi_\beta(\theta) = \frac{1}{\sqrt{2\pi}}\delta(\beta-\beta_0)\mathrm{e}^{\imath n_0\theta}, \tag{2.16}$$

where $n_0 \in \mathbb{N}$ is the integer part of the momentum and $\beta \in [0,1)$ is the quasi-momentum such that $p_0 = n_0 + \beta_0$. The β-rotors are always connected to a state in physical space. This is the same problem as expressing a wave packet using the Bloch states. Nevertheless we just need to formulate our model for β-rotors. Later we will give an example how to describe the physical behaviour by representing it in β-rotors.

To deal with movement in a periodical structure we now rewrite the Floquet operator in the language of β-rotors. This means that we replace the momentum operator $\hat{p}$ by the decomposition into integer and fractional momentum. This means we replace $\hat{p} \to \hat{\mathcal{N}} + \beta$. The Floquet operator reads

$$\hat{\mathcal{U}}_\beta = \mathrm{e}^{-\imath k\cos\hat{\theta}}\mathrm{e}^{-\imath\frac{\tau}{2}(\hat{\mathcal{N}}+\beta)^2} \tag{2.17}$$

and can be written by means of the β-rotors using the Anger-expansion eq. (A.6). The resulting matrix elements are

$$\langle n|\hat{\mathcal{U}}_\beta|l\rangle = (-\imath)^{n-l}J_{n-l}(k)\mathrm{e}^{-\imath\frac{\tau}{2}(\beta+l)^2}. \tag{2.18}$$

In order to determine the dynamics of the system we could calculate the eigenvalues of this equation and use it to represent the initial state by eigenfunctions.

Their evolution is simple. The eigenvalues are connected to quasienergies ϕ_n which are defined by [Haa10]

$$\hat{\mathcal{U}}|u_n\rangle = \mathrm{e}^{\imath\phi_n}|u_n\rangle, \tag{2.19}$$

where $|u_n\rangle$ is an eigenstate of the Floquet operator. These quasienergies are defined modulo 2π. If we have a time independent Hamiltonian the quasienergies coincide with the energies of the system modulo 2π. This consideration is important as we will later compare our time dependent problem to a time independent approximation. Due to the folding we cannot unfold the quasienergy spectrum. As we have an infinite number of levels the quasienergies are dense in the interval $[0, 2\pi)$. A eigenstate of the Floquet operator however can be localised and therefore pick out some quasienergies that seem to be discrete. Considerations of that kind are important to understand dynamical localisation.

We will use the Floquet operator to implement our numerics later in subsection 2.2.3. A nice introduction of the QKR Hamiltonian and into the system of the QKR[1] is given in [Izr90]. A derivation of this operator for a particle in a periodic potential is given in [Fis02], where they analyse the kicked rotor in a gravitational field but also discuss the case without gravity as it is their starting point for the modelling of quantum accelerator modes. The quasienergy statistics are analysed in [Izr86]. This is also the foundation of the understanding of the phenomenon of dynamical localisation discussed in subsection 2.2.2.

2.2.1 Quantum Resonance

We will now have a closer look at the free evolution part of the Floquet operator. This part has still two parameters we can fix by the experiment: the kicking period τ and the quasimomentum β. Carrying out the square in the exponent we can drop the β^2 term as it only contributes a common phase independent of k and n which means that it will cancel in building the fidelity that will be defined later. Using this we can write the free evolution as

$$\mathrm{e}^{\imath\left(\hat{\mathcal{N}}^2\frac{\tau}{2}+\tau\hat{\mathcal{N}}\beta\right)}. \tag{2.20}$$

A quantum resonance means that this term is $\mathbb{1}$. A higher quantum resonance means that some power of this operator fulfils this condition. In order to include the case of higher resonances we will chose $\tau = 4\pi p/q$ where $p, q \in \mathbb{N}$ and q is called the order of the resonance. For a resonance of order q the qth power of the free evolution is unity. This leads to the resonance condition

$$\mathrm{e}^{-\imath 2\pi\frac{p}{q}n^2}\mathrm{e}^{-\imath 4\pi n\beta\frac{p}{q}} = \mathrm{e}^{\imath 2\pi\frac{m}{q}}. \tag{2.21}$$

by taking the qth power and using the identity[2] $\exp(\imath 2\pi q n^2) = \exp(\imath 2\pi q n)$ we can reduce this condition to

$$pn + 2pn\beta = m. \tag{2.22}$$

[1] It is important to mention that this is not the AOKR. In the QKR there is no β which comes just by introducing the Bloch theorem to the periodic potential.

[2] The only interesting question is whether the integer factor in the exponent is even or odd. If n is even so is also n^2 and the same for odd.

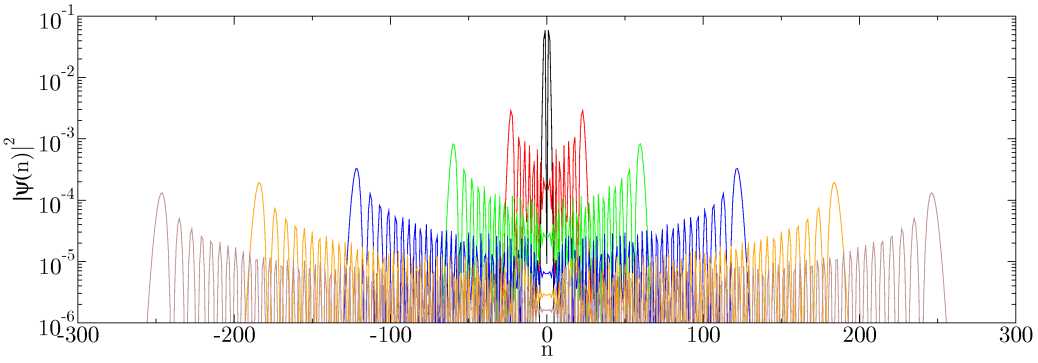

Figure 2.3: In this figure we show the spreading in momentum space for a resonant rotor with $\tau = 2\pi$, $\beta = 0.5$ and $k = 0.8\pi$. The data shows the momentum distribution for $t = 1, 10, 25, 50, 75, 100$ from black to brown. We can see that the edge of the momentum distribution spreads linearly and therefore the energy grows ballistic.

So we need to chose β in order to fulfil this relation. The complete resonance condition reads

$$\tau = 4\pi\frac{p}{q} \qquad p, q \in \mathbb{N} \qquad \beta = \frac{l}{2p} \qquad 0 \leq l < 2p \qquad l \in \mathbb{N}. \tag{2.23}$$

We will focus on the primary resonance with $q = 2$, $p = 1$ and $\beta = 1/2$ in this thesis. In the course of this section we will now discuss some of the special features of this resonance. For the higher orders one needs to focus on higher powers. In [Izr80] also these cases are discussed.

For the resonant case the energy grows ballistically. This can be seen by calculating the energy expectation value for an initial state whose angular momentum is n_0

$$\begin{aligned} E(t) &= \langle\psi(t)|\frac{\hat{\mathcal{N}}^2}{2}|\psi(t)\rangle && \text{(2.24a)}\\ &= \langle\psi(0)|\hat{\mathcal{U}}^{t\dagger}\frac{\hat{p}^2}{2}\hat{\mathcal{U}}^t|\psi(0)\rangle && \text{(2.24b)}\\ &= -\frac{1}{8\pi^2}\int_0^{2\pi} \mathrm{d}\theta \mathrm{e}^{in_0\theta}\mathrm{e}^{\imath tk\cos\theta}\frac{\partial^2}{\partial\theta^2}\mathrm{e}^{-in_0\theta}\mathrm{e}^{-\imath tk\cos\theta} && \text{(2.24c)}\\ &= \frac{k^2t^2}{4} + \frac{n_0^2}{2}, && \text{(2.24d)} \end{aligned}$$

which is the mentioned ballistic energy growth. This is in strong contrast to the classical rotor where we had linear growth of energy. This resonance is of pure quantum nature. It shows how the phase as a property of the wave function is able to stabilise the quantum evolution. Later we will detune the kicking period τ slightly in order to destroy this stabilisation. Therefore we will be able to define a pseudo-classical limit which allows us to apply semi-classical methods in a totally chaotic regime and to understand why there are regular structures in the pseudo-classical phase space despite the chaotic regime.

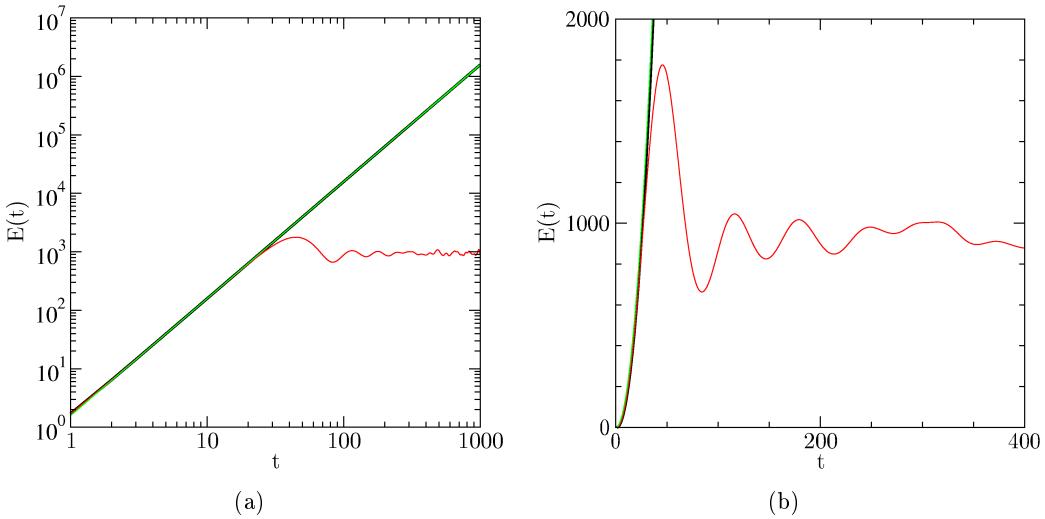

Figure 2.4: In this figure we show the energy expectation value of a plane wave state with $n = 0$ evolved in time. In black we show the case of the resonant kicked rotor with $k = 0.8\pi$, $\beta = 0.5$ and $\tau = 2\pi$. In red we show a rotor slightly detuned by $\tau - 2\pi = 0.001$. In green we show the expectation eq. (2.24). In (a) we show the data in logarithmic scaling to show the ballistic growth and the saturation of the non resonant rotor. In the linear scaling (b) the process of saturation is presented in detail.

The energy growth comes from a spreading of the wave function in momentum space. The spread in the momentum distribution is demonstrated in fig. 2.3. The momentum spreads linearly in time in momentum space.

2.2.2 Dynamical Localisation

For non-resonant rotors one observes localisation of the wave function [Gia91]. This can be seen by looking at the energy evolution in fig. 2.4. We can see that the energy of the non resonant rotor saturates after some time. This can be understood in several ways.

One way is to consider the quasienergy levels contributing to the evolution. The discrepancy between the quantum resonant and the slightly detuned motion is an indication that the quasienergies which are involved in the evolution have a finite spacing and therefore cannot describe an evolution which grows infinitely. After some time which is related to the quasienergy density the growth therefore has to stop. One way to understand this behaviour is to express the initial state by eigenfunctions of the Floquet operator. It turns out that this representation only contains a limited amount of quasienergies. Therefore the time evolution of this state has to show periodic or pseudo periodic behaviour after some time as a limited number of pseudo energies show a finite level spacing. The localisation length can be related to the diffusion constant and the kicking strength [Izr90, Gia91].

Another approach is to use the transfer matrix formulation from solid state physics. In [Gre84] the non resonant kicked rotor is mapped onto a tight binding model with hopping. It can be shown that this coefficients are not random but

pseudo-random [Bre92]. Nevertheless they seem to be random enough to lead to Anderson localisation.

In the regime we are interested in we eventualy have dynamical localisation. This localisation is important in our numerics because it limits the size of the vector needed to describe long time evolutions in contrast to the resonant case.

2.2.3 Numerical Implementation

To deal with the problem numerically we have two possibilities. On the one hand we can use the matrix representation of the Floquet operator to calculate the wave functions successively. On the other hand we can evaluate the kick in the angular representation and the free evolution in the momentum representation. The later procedure has the advantage that the single iteration steps are phase shifts in the corresponding representation.

By expanding the Floquet operator in angular momentum eigenstates we can obtain a matrix. This matrix has to be unitary in order to conserve probability. This unitarity is violated when truncating the matrix. On the other hand the nonunitarity can be used to estimate the truncation error. For the time evolution we need to carry out one matrix multiplication for each time step which scales with N^2 where N is the size of the state vector.

Using different bases for the kick and the free evolution leads to simple calculation of the single steps but instead we have the problem of changing the basis. This basis change is by definition a Fourier transform. We can evaluate this transformation very efficiently with the fast Fourier transformation (FFT). Using the FFT this method scales with $N \ln N$. A disadvantage is that this method is by definition unitary as the discrete Fourier transform has this property and therefore truncation errors cannot be estimated by testing the trace. For this method one needs to check the convergence by changing the vector size.

In our implementations we used the method in which we change the basis. It is more efficient and due to the dynamic localisation in our regime we do not need very large vectors. Due to the localisation our wave function also does not tend to reach the boundaries where the truncation or the boundary conditions would gain importance.

2.3 Semi-classical Approximation from the Path Integral

Semi-classics can be introduced in several ways into quantum mechanics. Most textbooks separate the phase and the amplitude of the wave function and do some approximations[3] which is not straight forward. To understand better to which extend the semi-classical approximation is an approximation to quantum mechanics, we would like to review the semi-classical approximation in the context of path integrals shortly. In this way the semi-classical approximation is defined

[3]Mostly the argument is that the wave function does not change on the scale of the de Broglie length and that the curvature is small. To see why this corresponds to the terms that are dropped is not trivial. In [Sak09] an illustration of these approximations is given. Nevertheless, the approximations are justified afterwards there.

as the stationary phase approximation (SPA) to the path integral formulation of quantum mechanics. The advantage of this approach is that we can see where the approximation takes place. In our special case it is important to mention that this approximation is a formal approximation to a Hamiltonian in a special shape. Interpreting semi-classics as an approximation to special operators allows us to understand the ϵ-classics we will introduce later.

The path integral representation of the propagator is given as [Sch96]

$$G(x,t;y) = \int_{(y,0)}^{(x,t)} \mathrm{d}x(\tau) \exp\left(\frac{\imath S[x(\tau)]}{\hbar}\right), \tag{2.25}$$

where the integration is over all paths going from $(y,0) \to (x,t)$, τ is the internal time of the path and $S[x(\tau)]$ is the classical action corresponding to the path. The problem is now to calculate this integral. The integral is defined as the continuity limit of the sum over discrete time differences.

One technique to approximate an integral over a fast oscillating function is the stationary phase integration. It deals with integrals of the type

$$F(\lambda) = \int_{-\infty}^{\infty} \mathrm{d}t\, \mathrm{e}^{\imath\lambda f(t)} \tag{2.26}$$

by expanding $f(t)$ around an extremal point with $f'(t_0) = 0$. This leads us to

$$F(\lambda) = \int \mathrm{d}t\, \exp\left[\imath\lambda f(t_0) + \frac{1}{2}\imath\lambda t_0^2 f''(t_0) + \cdots\right]. \tag{2.27}$$

Truncating this expansion after the second order term we can evaluate the integral by means of Fresnel integrals and obtain

$$F(\lambda) = \sqrt{\frac{2\pi\imath}{\lambda f''(t_0)}}\, \mathrm{e}^{\imath\lambda f(t_0)}. \tag{2.28}$$

For a better understanding of this approximation we will have a short look at integrals of the type

$$K(\lambda) = \int_{-\infty}^{\infty} \mathrm{d}t\, \mathrm{e}^{\imath\lambda t^2} \mathrm{e}^{\imath a\lambda t^3} \mathrm{e}^{\imath b\lambda t^4}. \tag{2.29}$$

Here we can expand the last two exponentials and obtain this way

$$K(\lambda) = \int_{-\infty}^{\infty} \mathrm{d}t \mathrm{e}^{\imath\lambda t^2} \left[1 + \imath\lambda a t^3 + \imath\lambda b t^4 - \frac{1}{2}\lambda^2 a^2 t^6 + \cdots\right] = \sqrt{\frac{\imath\pi}{\lambda}}\left[1 - \frac{\imath 3b}{4\lambda} + \frac{\imath 15a^2}{16\lambda} + \cdots\right]. \tag{2.30}$$

By writing K this way we see that the SPA result is the leading term of an expansion in $1/\lambda$. In this sense the SPA is the dominating term of the expansion as it scales with $1/\sqrt{\lambda}$ in contrast to the other terms that scale with $1/\lambda^n$. We introduced the SPA in the context of complex exponential functions whose exponent is defined by a function f. In order to apply this technique to the path integral we have to extend this to functionals.

Finding the trajectory leading to stationary action and therefore stationary phase leads to the Hamilton-Jacobi equations. The WKB propagator is then obtained by expanding the action S around this extremal solution in a functional way and using the SPA. The expansion of the action in functional variations is not as simple as the procedure presented above. One needs to go to the discretised form of the integral and write the action in discretised form. The second variation can be expressed using a tridiagonal matrix. The eigenvalues and eigenvector can be given and this way one is able to evaluate the Gaussian integral. In the continuity limit the pre factor is defined by a differential equation which can be identified by the continuity equation for trajectories of the classical mechanics. This is a very short sketch of the procedure given in [Sch96]. In the end it leads to the WKB propagator

$$G_{WKB}(x,t;y,0) = \sum_{\alpha} \sqrt{\det\left(\frac{\imath}{2\pi\hbar}\frac{\partial^2 S_\alpha}{\partial x \partial y}\right)}\, \mathrm{e}^{\frac{\imath}{\hbar}S_\alpha}, \tag{2.31}$$

where the sum is over classical trajectories, which are indexed by α, and S_α is the action for a trajectory connecting x and y in time t. This form of the WKB propagator is also called van Vleck propagator. In section 4.1 we will continue this review by transforming this propagator from time to energy. This is also the way the WKB propagator is given in most textbooks.

In the end we have to remember that the semi-classical approximation is a SPA approximation of the full propagator. For the quality of the approximation in eq. (2.28) it is important to have a large λ. In the semi-classical expansion presented above this quantity is $1/\hbar$. This prefactor defines how strong the non-extremal paths contribute. In the next chapter we will rescale the Floquet operator in a way that this prefactor is the reciprocal of the detuning from quantum resonance. This allows us to use this approximation in a regime where the $\hbar \to 0$ limit is not valid.

2.4 Dynamics near Quantum Resonance

We will now go back and consider our system near to the resonance[4] with $\tau = 2\pi l$, where l is an integer, and define the detuning of the kicking period ϵ by

$$\tau = 2\pi l + \epsilon. \tag{2.32}$$

Now we introduce a new angular momentum operator $\hat{I} = |\epsilon|\hat{\mathcal{N}}$. We will return to the Floquet operator now. Introducing eq. (2.32) into eq. (2.17) we obtain

$$\hat{\mathcal{U}} = \mathrm{e}^{\imath k\cos\hat{\theta}}\mathrm{e}^{\imath\pi l\hat{\mathcal{N}}^2+\frac{\epsilon}{2}\hat{\mathcal{N}}^2+\tau\hat{\mathcal{N}}\beta} = \mathrm{e}^{\imath k\cos\hat{\theta}}\mathrm{e}^{\imath\pi l\hat{\mathcal{N}}+\frac{\epsilon}{2}\hat{\mathcal{N}}^2+\tau\hat{\mathcal{N}}\beta}, \tag{2.33}$$

where we already dropped the β^2 term as it will just be a common phase and we used $\exp(\imath 2\pi q n^2) = \exp(\imath 2\pi q n)$. Introducing the rescaled momentum operator we obtain

$$\hat{\mathcal{U}} = \mathrm{e}^{-\frac{\imath}{\epsilon}\left(\tilde{k}\cos\hat{\theta}+\mathrm{sign}(\epsilon)\frac{\hat{I}^2}{2}+\hat{I}(\tau\beta+\pi l)\right)}, \tag{2.34}$$

[4] We change here the convention for the resonance slightly. We fixed $q = 2$ and give therefore τ as a multiple of 2π. To emphasise this we switch from p to l.

where we defined $\tilde{k} = \epsilon k$. This operator is similar to the original Floquet operator with the difference that, instead[5] of $\hbar$, now a factor ϵ appears.

In section 2.3 we introduced the semi-classical approximation as an approximation to the propagator in path integral formulation in the case of small $\hbar$. We have now the same type of operator but a factor of $1/|\epsilon|$ instead of $1/\hbar$ controlling the deviation from the trajectory of extremal action. Motivated by the last section we will now use the same approximations we used there for $\hbar$ here for $|\epsilon|$. The limit $\epsilon \to 0$ will be called ϵ-classical limit.

This considerations allow us to give the QKR Hamiltonian near to the resonance as the formal quantisation of another system in the ϵ-classical limit. The rescaled operator is again a combination of free evolution and a kick. This corresponds to an ϵ-classical mapping of a KR with different kicking strength $\tilde{k} = \epsilon k$

$$I_{t+1} = I_t + \tilde{k} \cos \theta_t \tag{2.35a}$$
$$\theta_{t+1} = \theta_t \pm I_t + (\tau\beta + l\pi), \tag{2.35b}$$

where the sign is fixed by the sign of ϵ. By a simple transformation we can reduce this mapping to the standard mapping. We introduce $J_t = I_t \pm (\tau\beta + l\pi)$ and $\vartheta_t = \theta_t + \pi/2 \pm J_t$,which leads to the well-known standard map

$$J_{t+1} = J_t + \tilde{k} \sin \vartheta_t \tag{2.36a}$$
$$\vartheta_{t+1} = \vartheta_t + J_t. \tag{2.36b}$$

The properties of this mapping have already been discussed in subsection 2.1.1.

Going near to a quantum resonance allows us to describe the dynamics of the system by the same system with a reduced kicking strength. The ϵ-classical system and the corresponding classical system are both kicked rotors but with a different kicking strength. If k is chosen to be in the deep chaotic regime we can reduce its effect by going near to a quantum resonance as ϵk gets smaller and may even be in the near integrable regime.

This technique was developed in [Fis03] to describe the dynamics of quantum accelerator modes. In the system of the kicked rotor in the gravitational field the gravity breaks the periodicity of the potential. By going into an accelerated frame one is able to restore this periodicity. The additional terms nevertheless makes the phase space structure much richer. The observed quantum accelerator modes can be understood as states trapped on islands in this phase space [Fis03].

2.5 Fidelity

It is difficult to recognise chaotic behaviour in quantum mechanics. One reason is that the idea to characterise chaos by the behaviour of nearby points in phase space is not valid any more. Stability against variation of the initial state is meaningless because of the unitarity of the time evolution. In 1984 Peres introduced

[5] We set $\hbar$ to 1 so this limit cannot be seen in our case. We had to revert the rescaling in eq. (2.9) in order to introduce $\hbar$ at the right positions.

the idea not to perturb the initial state but to perturb the time evolution [Per84]. This means one uses two slightly different time evolutions of an initial state $|\psi_0\rangle$ and compares the overlap. We assume that δ is the parameter characterising the perturbation of the Hamiltonian. The fidelity amplitude is defined as

$$f_\delta(t) \equiv \langle\psi_0|\hat{\mathcal{U}}_0^\dagger(t)\hat{\mathcal{U}}_\delta(t)|\psi_0\rangle, \tag{2.37}$$

where $\hat{\mathcal{U}}_\delta(t)$ is the time evolution operator as a function of the perturbation parameter δ. The fidelity is defined as its modulus

$$F(t) \equiv |f_\delta(t)|^2. \tag{2.38}$$

We introduced the fidelity as the comparison between a state evolved with two slightly different time evolutions. Another picture can be given by defining the echo operator

$$\hat{M}_\delta(t) \equiv \hat{\mathcal{U}}_0(-t)\hat{\mathcal{U}}_\delta(t) = \hat{\mathcal{U}}_0^\dagger(t)\hat{\mathcal{U}}_\delta(t). \tag{2.39}$$

This operator resembles the idea by Loschmidt to characterise the reversibility by evolving a state for t and then reverse the evolution with a different Hamiltonian. This is known in classical statistical physics as the Loschmidt echo [Gor06]. The fidelity can be interpreted as the quantum analogue of this classical concept. This was also Peres initial idea to characterise the chaotic behaviour in quantum systems by comparing this theoretical concept with the classical limit.

To compare to the classical limit we need to introduce the fidelity for an ensemble. Fidelity is an expectation value of the echo operator for an initial state. We define the fidelity for an initial ensemble with statistical operator $\hat{\rho}_0$ as

$$F(t) = |\mathrm{tr}(\hat{\rho}_0\hat{M}_\delta)|^2. \tag{2.40}$$

This definition is consistent with the definition above when inserting the statistical operator of a pure state $\hat{\rho}_0 = |\psi_0\rangle\langle\psi_0|$ as the initial state.

In this thesis we aim to calculate the fidelity for a special system and a special ensemble. Our focus is less on comparison to universal properties of fidelity. Nevertheless, we will give the connection of fidelity to correlation functions. We introduce the perturbation potential V by

$$H(t) = H_0(t) + \delta V(t). \tag{2.41}$$

By switching to the interaction picture we can express the echo operator by means of the perturbation potential

$$M_\delta(t) = \hat{T}\exp\left(-\frac{\imath}{\hbar}\delta\int_0^t \mathrm{d}t'\; V_I(t')\right), \tag{2.42}$$

where $\hat{T}$ is the time ordering operator and $V_I \equiv \hat{\mathcal{U}}_0^\dagger(t)\hat{V}(t)\hat{\mathcal{U}}_0(t)$ is the perturbation potential in the interaction picture. Expanding the exponential function in a power series, truncating after the second order and taking the expectation value we obtained

$$f_\delta(t) = 1 - \frac{\imath\delta}{\hbar}\int_0^t \mathrm{d}t'\;\langle V_I(t')\rangle - \frac{\delta^2}{\hbar^2}\int_0^t \mathrm{d}t'\int_{t'}^t \mathrm{d}t''\;\langle V_I(t')V_I(t'')\rangle, \tag{2.43}$$

where the brackets mean building the expectation value for the initial state $\langle \hat{A} \rangle \equiv \mathrm{tr}(\hat{\rho}_0 \hat{M}_\delta)$. Taking the modulus square

$$F(t) = 1 - \frac{\delta^2}{\hbar^2} \int_0^t \mathrm{d}t' \int_0^t \mathrm{d}t'' \, C(t', t''), \tag{2.44}$$

where $C(t', t'') \equiv \langle V_I(t') V_I(t'') \rangle - \langle V_I(t') \rangle \langle V_I(t'') \rangle$ is the two point correlation function of the perturbation. This allows the reduction on considerations of correlation functions. In this linear response formulation fast decay of correlations in the perturbation implies slow decay of fidelity.

Using some universal properties for the correlation one is able to define several universal regimes of fidelity decay. In order to obtain this universal behaviour it is important to be independent of the choice of the initial state. The other important question is whether the system distributes the wave function fast over the Hilbert space in order to obtain universal behaviour. When building a theory for universal properties one has to assume either quantum mixing, which means fast spreading, or random initial states, or averaging over the Hilbert space. Chaotic systems that provide quantum mixing are systems in which universal behaviour is possible. Systems that supply dynamical localisation or are governed by regular states complications arise as they suppress quantum mixing. A possibility is to obtain universal properties in these systems by averaging over the Hilbert space or choosing a random initial state, which somehow replaces the spreading over the phase space. As we did not focus on comparisons to such approaches we would like to refer to the review of the topic by Gorin *et al.* [Gor06] and the references therein.

2.5.1 Fidelity in QKR

The definition of fidelity we gave is consistent to the literature on fidelity in general. For the system of the QKR it is more handy to write the fidelity slightly differently. In the context of the QKR we will define the fidelity as

$$F(t) = |\langle \hat{\mathcal{U}}_{k_1}^{-t} \hat{\mathcal{U}}_{k_2}^{t} \rangle|^2, \tag{2.45}$$

where due to the discrete time the evolution can be given as a power of the Floquet operator and the unperturbed time evolution is regarded to be the one with kicking strength k_1 and the perturbed one the one with kicking strength k_2. The perturbation parameter therefore is $\delta k = k_2 - k_1$.

In experiments the atoms are placed as a cloud in the kicking potential. It was shown that it is possible to describe this cloud by an incoherent ensemble of plane waves [Wim04, Bha99]. The density operator of an incoherent ensemble of plane waves is defined by

$$\hat{\rho}_0 = \int \mathrm{d}p f(p) |p\rangle\langle p|, \tag{2.46}$$

where $f(p)$ is the probability density for the momentum p. This density operator needs to be expressed by means of β-rotors. As each plain wave has a defined

quasimomentum using an ensemble of β-rotors is equivalent to using plane waves. The statistical operator of a β-rotor corresponding to $f(p)$ is given as

$$\hat{\rho}_\beta = (P(\beta))^{-1} \sum_n f(n+\beta)|n\rangle\langle n|, \tag{2.47}$$

where the probability of finding a β-rotor is $P(\beta) \equiv \sum_n f(n+\beta)$. The statistical operator can therefore be written as

$$\hat{\rho}_0 = \int_0^1 \mathrm{d}\beta \; P(\beta)|\Psi_\beta\rangle\langle\Psi_\beta|. \tag{2.48}$$

Inserting this into eq. (2.40) we obtain by carrying out the trace

$$F(t) = \left| \int_0^1 \mathrm{d}\beta \; P(\beta)\langle\Psi_\beta|\hat{\mathcal{U}}_{k_2}^t \hat{\mathcal{U}}_{k_1}^{t\dagger}|\Psi_\beta\rangle \right|^2. \tag{2.49}$$

The ensemble average therefore takes into account the phase of the overlaps. It is important to mention that this average is nevertheless an average over an incoherent ensemble although we account for the phase of the overlap. We defined the fidelity as the expectation value of the echo operator which itself is defined as an overlap between wave functions and therefore carries a phase. If we would average over a coherent ensemble of rotors we would have off-diagonal terms in the density operator and therefore also overlaps between two rotors with different β.

For a Gaussian ensemble $P(\beta)$ is a sum over shifted Gaussian distributions which is the definition of the Theta-function [Abr64]. Using Poisson's summation formula we can give an approximation [Wim04, Wim03]

$$P(\beta) = 1 + 2\mathrm{e}^{-2\pi^2\sigma^2} \cos(2\pi\beta) + O(\mathrm{e}^{-8\pi^2\sigma^2}). \tag{2.50}$$

If the distribution $f(p)$ is sufficiently broad ($\sigma > 1$) we can assume a constant density of quasimomenta.

For the quantum kicked rotor there are already two cases where a theory exists. On the one hand Wimberger *et al.* developed a theory for a full ensemble using resonant kicking [Wim06]. On the other hand Abb *et al.* developed a theory for ensembles corresponding to the oscillatory trajectories in pseudo-classical phase space near to quantum resonance [Abb09]. We will give a short review on their findings.

2.5.2 Fidelity in QKR – Resonant Rotors

In the case of the resonant rotor the kick just contributes a constant phase. This is only that simple in the case of resonant β. If just τ is resonant and β is non resonant we get a similar Floquet operator

$$\hat{\mathcal{U}}_\beta = \mathrm{e}^{-\imath k \cos\hat{\theta}} \mathrm{e}^{-\imath\xi\hat{\mathcal{N}}}, \tag{2.51}$$

where $\xi \equiv \pi l(2\beta \pm 1) \mathrm{mod}(2\pi)$ is the additional phase due to the non resonant β. Iterating this mapping we obtain

$$\hat{\mathcal{U}}_\beta^t \psi_\beta(\theta) = \mathrm{e}^{-\imath k \sum_{s=0}^{t-1} \cos(\theta - s\xi)} \psi_\beta(\theta - t\xi) = \mathrm{e}^{-\imath k |W_t| \cos(\theta + \arg(W_t))} \psi_\beta(\theta - t\xi), \quad (2.52)$$

where we summed up the cosines. We used the geometric sum and obtain

$$\sum_{s=0}^{t-1} \cos(\theta - s\xi) = \cos\left(\theta - \frac{t-1}{2}\xi\right) \frac{\sin\frac{\xi}{2}t}{\sin\frac{\xi}{2}}, \quad (2.53)$$

and defined

$$\arg(W_t) = -\frac{t+1}{2}\xi + \phi_t \quad (2.54)$$

$$|W_t| = \left| \frac{\sin\frac{\xi}{2}t}{\sin\frac{\xi}{2}} \right|, \quad (2.55)$$

where ϕ_t restores the sign which was lost due to taking the absolute value in the definition in $|W_t|$. Transforming the wave function to momentum representation we obtain

$$\langle n|\hat{\mathcal{U}}_\beta^t \psi_\beta\rangle = \mathrm{e}^{-\imath n \arg(W_t)} \int_0^{2\pi} \frac{\mathrm{d}\theta}{\sqrt{2\pi}} \mathrm{e}^{-\imath n\theta - \imath k |W_t| \cos\theta} \psi_\beta(\theta - t\xi - \arg(W_t)). \quad (2.56)$$

For plane waves the ψ_β are also plane waves filtering the right β. This means the β-rotor for a plane wave with $p_0 = n_0 + \beta_0$, where $n_0 \in \mathbb{N}$ and $\beta_0 \in [0, 1)$, reads as

$$\psi_\beta(\theta) = \frac{1}{\sqrt{2\pi}} \delta(\beta - \beta_0) \mathrm{e}^{\imath n_0 \theta}. \quad (2.57)$$

Using this representation we can give our momentum coefficients as

$$\langle n|\hat{\mathcal{U}}_\beta^t \psi_\beta\rangle = \mathrm{e}^{-\imath n \arg(W_t)} J_{n-n_0}(k|W_t|), \quad (2.58)$$

where $J_n(x)$ is the Bessel function of first kind. Using the angular representation we can calculate the fidelity of such a rotor as

$$F(t) = \left| \langle \hat{\mathcal{U}}_{k_1,\beta}^t \psi_\beta | \hat{\mathcal{U}}_{k_2,\beta}^t \psi_\beta \rangle \right|^2 = \left| \int_0^{2\pi} \mathrm{d}\theta \langle \hat{\mathcal{U}}_{k_1,\beta}^t \psi_\beta | \theta \rangle \langle \theta | \hat{\mathcal{U}}_{k_2,\beta}^t \psi_\beta \rangle \right|^2 \quad (2.59)$$

$$= \left| \int_0^{2\pi} \mathrm{d}\theta \mathrm{e}^{\imath \delta k |W_t| \cos(\theta)} \right|^2 = J_0^2(|W_t|\delta k), \quad (2.60)$$

where $\delta k = k_2 - k_1$ is the difference in kicking strength. An interesting case is the case of $\xi = 0$ which corresponds to resonant β. From the definition we find $|W_t|(\xi = 0) = t$. Therefore the resonant fidelity decays like the Bessel function.

In order to describe the evolution of a wave packet we now use this result to calculate the fidelity for the density operator. As we showed in the last section for sufficiently wide $f(p)$ this corresponds to a uniform distribution. Therefore

we have to evaluate the average over $\beta \in [0,1)$ which corresponds to the average over $\xi \in [-\pi,\pi]$. So we find, using the periodicity of the trigonometric functions

$$\int_0^1 \mathrm{d}\beta J_0(|W_t|\delta k) = \int_{-\pi}^{\pi} \frac{\mathrm{d}x}{2\pi} J_0(\delta k \sin(tx)\csc(x)) \tag{2.61}$$

$$= \int_{-\pi}^{\pi} \frac{\mathrm{d}x}{4\pi^2} \sum_{r=0}^{t-1} \frac{2\pi}{t} J_0(\delta k \sin(x)\csc(xt^{-1} + 2\pi r t^{-1}), \tag{2.62}$$

where we introduced $x \equiv \xi/2$. It is important to mention that we need that we integrated over a complete period of the sine, because we had problems doing the transformation $x \to x/t$ in such a simple way. Using the periodicity of the sine makes it also impossible to repeat this derivation for partial ensembles. For large times the sum over r approximates an integral over the continuous variable $\alpha \equiv 2\pi r/t$. This allows us to write the sum as an integration:

$$\int_0^1 \mathrm{d}\beta J_0(|W_t|\delta k) = \frac{1}{(2\pi)^2} \int_{-\pi}^{\pi} \mathrm{d}x \int_0^{2\pi} \mathrm{d}\alpha J_0\big(\delta k \sin(x)\csc(\alpha)\big). \tag{2.63}$$

Using (11.4.7) from [Abr64] we can give the fidelity in the long time limit as

$$F_{t\to\infty}(\delta k) = \frac{1}{(2\pi)^2} \left(\int_0^{2\pi} \mathrm{d}\alpha J_0^2(\delta k \csc(\alpha)/2) \right)^2. \tag{2.64}$$

The integral can be evaluated numerically and is presented in fig. 2.5. The result is quite surprising as this states that there is a fidelity saturation although the kicked system can be completely chaotic. Such a saturation is untypical even for integrable systems.

This prediction was tested by Wu *et al.* [Wu09]. They used an atom interferometer to implement the fidelity. As perturbation they used different kicking strengths in the two arms of the interferometer. The interference signal at the output corresponds to the square root of the fidelity. The experimental result and the theoretical prediction is shown in fig. 2.5.

2.5.3 Fidelity in QKR – Near Resonant Rotors

We will give a short sketch of the method used in [Abb09] and the results therein. In the end we will show a plot of the initial angles θ' ending in θ after a certain time t that illustrates why we did not follow this approach further.

For near resonant rotors we can apply the ϵ-classical technique. This means we use the ϵ-classical system and apply semi-classical methods to describe the quantum mechanical time evolution operator. The van Vleck propagator is used in ϵ-classical representation

$$\hat{\mathcal{U}}^t_{\beta,k} \propto \frac{1}{\sqrt{2\pi}} \sum_s \left| \frac{\partial\theta}{\partial\theta'} \right|^{-1/2} \mathrm{e}^{\imath/\epsilon\Phi_s(\theta,t) - \imath(\pi/2)\nu_s}, \tag{2.65}$$

where s are the classical trajectories connecting θ' and θ in the time t, and Φ is the corresponding action and ν_s are Maslov indices. As they are near to resonance

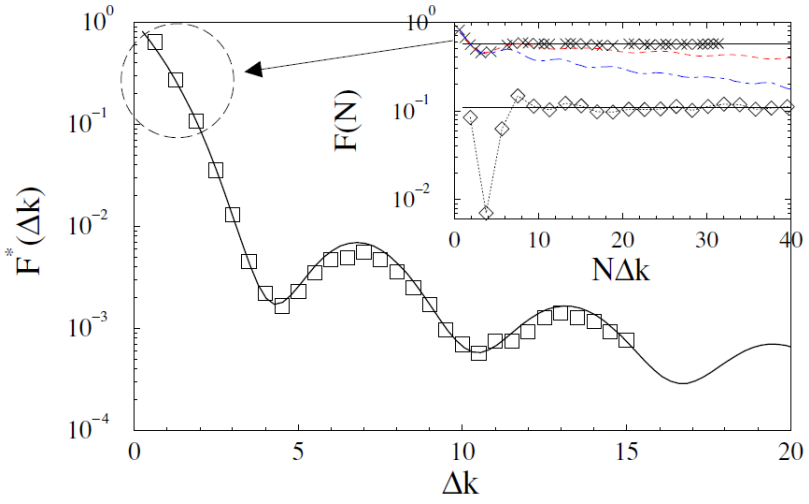

(a)

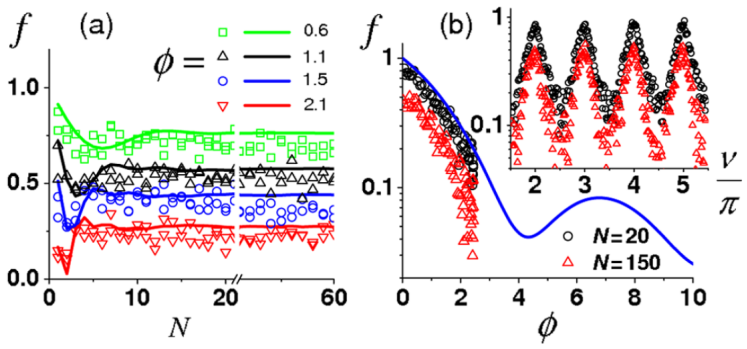

(b)

Figure 2.5: In this figure we show the results for ensembles of resonant kicked rotors with $\beta \in [0, 1]$. In (a) we present a figure from [Wim06] showing the theoretical expectation for the saturation value of the fidelity. In the inset the temporal evolution for $\delta k = 0.6283$ (crosses) and $\delta k = 1.885$ (diamonds) are shown. For the case of $\delta k = 0.6283$ also the result for a detuning of $\epsilon = 0.025$ (dashed) and $\epsilon = 0.1$ (dot-dashed) are shown. In (b) we show a figure from [Wu09] presenting their experimental results with $f = \sqrt{F}$. In the left plot the interferometer output against kick number is plotted and in the right plot the saturation value against the kicking strength (for exact definitions we refer to the paper).Reprinted figure (b) with permission from Wu *et al.* , Phys. Rev. Lett., **103**, 034101 (2009). Compyright by the American Physical Society. Reprinted figure (a) with permission IOP Publishing and the author from Wimberger *et al.*, Journal of Physics B, **39**, (2006) L145.

they can use the pendulum approximation which we will define in chapter 3. As they just take states on the island into account they use the harmonic oscillator approximation for the pendulum. This way they can give the trajectories and the action analytically

$$\theta'(\theta,t) = \sec[\theta - \bar{\beta}\sin(\omega t)] \tag{2.66}$$

$$\Phi(\theta,t) = \bar{\beta}\theta[\sec(\omega t) - 1] - (\omega^{-1}\bar{\beta}^2 + \omega\theta^2)\tan(\omega t)/2, \tag{2.67}$$

where $\omega = \sqrt{\tilde{k}}$. The intrinsic momentum $\bar{\beta} \equiv -\pi + \tau\beta$ will be discussed in chapter 3. Abb *et al.* assume a delocalised initial state. This variables are inserted into the van Vleck propagator and it is used to calculate the fidelity. The average over a small interval near to the resonant β is taken. In the limit of $\epsilon \to 0$ and $t\sqrt{\epsilon}$ =constant the average over a small stripe can be approximated by an integral from $-\infty$ to ∞, which can be evaluated by means of Fresnel integrals. This way they obtain the following expression for the fidelity of an ensemble near to resonance

$$F(k_1,k_2,t) = \frac{\epsilon^2\omega_1\omega_2}{8\pi^2 b^2 4\omega_1\omega_2 - \omega_+^2\cos(\omega_- t) - \omega_-^2\cos(\omega_+ t)|}, \tag{2.68}$$

where $\omega_{1/2} = \sqrt{\tilde{k}_{1/2}}$, $\omega_\pm = \omega_1 \pm \omega_2$ and b is defined as the two times the width of the ensemble which means $\beta \in [0.5 - b, 0.5 + b]$. Evaluating the fidelity without averaging over β one finds

$$F_{\text{res}}(k_1,l_2,t) = \frac{\epsilon}{2\pi}\frac{1}{|\omega_2\cos(\omega_1 t)\cos(\omega_2 t) - \omega_1\cos(\omega_2 t)\sin(\omega_1 t)|}. \tag{2.69}$$

We can see that the periodicity of the first fidelity is at $T_{12} \equiv 2\pi/|\omega_-|$ and in the second fidelity for $T_{12}/2$. This is illustrated in fig. 2.6. There we can see that every second revival vanishes as more of the nonlinear island (corresponding to new resonant values of β) is populated.

The initial idea was to use this type of theory for pendulum orbits that are rotator like. We also derived a perturbation method in order to obtain $\theta'(\theta,t)$. The result described the pendulum good in the beginning. But already at around 900 kicks we had problems with multiple trajectories[6]. Using this trajectories to calculate the fidelity lead to a Bessel like decay. This means that the approximation breaks down too fast. Using a method not relying on trajectories leads to much better results as we will see in chapter 4.

2.6 Context of the Thesis

This thesis is meant to be the continuation of the works by Wimberger *et al.* [Wim03, Wim06] and Abb *et al.* [Abb09] using the technique developed by Fishman *et al.* [Fis02, Fis03]. Our aim is a better understanding of how the quantum

[6]When using the van Vleck propagator one needs to sum over all classical trajectories. As the number of trajectories contributing changes aking them in account is difficult especially as our theory did not cover the bending leading to multiple trajectories.

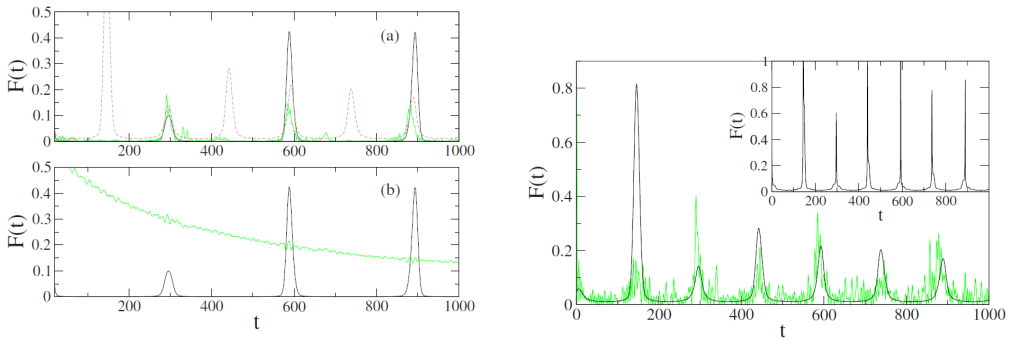

Figure 2.6: In this figure we show figure 1 and 2 from [Abb09]. In (a) an ensemble of 5000 rotors with $\Delta\beta = 0.05$, $\epsilon = 0.01$, $k_1 = 0.6\pi$, $k_2 = 0.8\pi$ and $\tau - \epsilon = 2\pi$ is shown. The solid lines are the theoretical result for a narrow ensemble and the dashed line for a single resonant β-rotor. The numerical data is shown in green. For comparison we show the corresponding resonant rotor in the right figure. The analytical fidelities are smoothed in order to control the singularities. The non smoothed data is shown in the inset. In (b) the ensemble with $\Delta\beta = 1$ is presented. Reprinted figure with permission from Abb *et al.* , Phys. Rev. E, **80**, 035206(R) (2009). Compyright by the American Physical Society.

resonance influences the behaviour of the QKR in the chaotic regime. In this thesis we always use kicking strengths of about $k \approx 0.7\pi$ and kicking period $\tau \approx 2\pi$ which means that we are in the classical limit in the completely chaotic regime of the standard classical analogue.

Nevertheless the phenomenon of quantum resonance is completely independent of the classical regime. In [Wim03] the QKR is treated quantum mechanically without respecting the structure in the classical limit. The fidelity can be evaluated in this framework and shows saturating behaviour [Wim06]. This is a behaviour that is unexpected as the system is chaotic in the classical limit. So one would expect a decay of fidelity. The expected decay, however, is motivated by semi-classical methods that are not relevant in our case as the system is also in the deep quantum regime. In this regime general expectations are not easy to define as most of the tools used are not valid.

Quantum resonance is a very special condition and the question is what happens if the resonance condition is slightly violated. This question leads to the definition of the ϵ-classical limit in [Fis03]. In [Wim06] also the fidelity of near resonant ensembles was evaluated and a decay of the former saturated fidelity was observed. Intuitively this can be understood as the perfect match of the phases is destroyed which stabilised the fidelity. A first approach to describe this decay by the phase space obtained in the ϵ-classical limit was done by Abb *et al.* [Abb09]. The ϵ-classical phase space showed regular structures and therefore semi-classical methods could be applied. The phase space contains two different regimes. Abb *et al.* focused onto the island like states and could developed an analytical theory describing the revivals of the fidelity and the behaviour of this revivals when averaging over several island states.

These island states are, however, cover only a small amount of the pseudo-

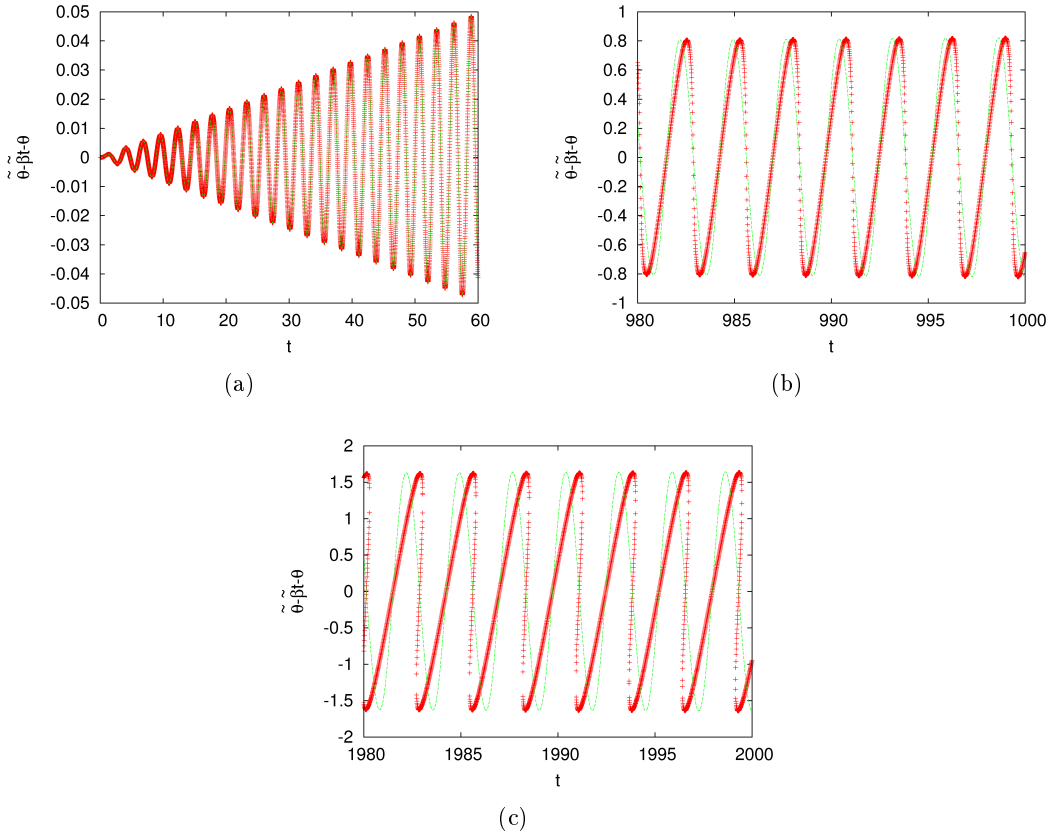

Figure 2.7: In this figure we show the difference of pendulum trajectories to the trajectory of the free rotor. We show the initial angle $\theta'(\theta, t)$ which ends in θ after the time t. The angle calculated by the pendulum is $\tilde{\theta}$ the initial angle is θ and the angle a free rotor would have is $\tilde{\beta}t$. In contrast to the definition in chapter 3 $\bar{\beta}$ is called $\tilde{\beta}$ here. Therefore we plot the deviation from the free rotor by plotting $\tilde{\theta} - \tilde{\beta} - \theta$. We show the system with $\epsilon = 0.001$, $k = 0.6\pi$ and $\beta = 0.135$. In red we show the numerical data and in green an approximative result we obtained. In (a) we show the initial behaviour. In (b) we show an intermediate regime and a later regime in (c). We can see that the problem of multiple orbits arises quite early. This bending is not modelled by the analytical result.

classical phase space cell. In the resonant limit the island even vanishes so that the revivals can not be observed in the resonant case. On the other hand a vanishing island also means that the approach of Abb *et al.* cannot describe the decay of the saturation that is illustrated by the green solid line in fig. 2.6(b). The saturation and the decay of the saturation therefore is a property of the rotator like states which are excluded in the theory by Abb *et al.*. In order to describe the decay one needs to focus at the rotator like orbits. We will also use the pendulum approximation but treat the rotating orbits. We will focus on the question whether the pendulum approximation can describe the rotator like rotors.

Chapter 3

Pendulum Approximation

On the classical level, the kicked rotor (KR) can be described by a stroboscopic map called the standard map. This map maps the state after a kick to the state after the next kick. It looks very simple but can have very complex behaviour. The KR is a time-dependent problem which cannot be solved in closed form. It is easier to deal with time-independent Hamiltonian description for which we have more methods to treat. Especially the semiclassical quantisation procedures are mostly for the time-independent case. One possibility to obtain a time-independent approximation for the kicked rotor is to truncate the Fourier expansion of the kick in order to take only the slow and constant terms into account. The result of this crude approximation is the pendulum approximation.

In this chapter we will derive this approximation. We will give a procedure to implement it numerically. After that we will discuss the spectral properties. To compare the pendulum approximation to the QKR we will give the Husimi function and compare the two quantum mechanical evolutions.

3.1 Pendulum Approximation for the KR

We will shortly review the derivation of the pendulum approximation as presented in [Lic92]. This review is for the classical system and therefore is formulated using canonical variables. To apply it to our problem we need to introduce the ϵ-classical variables in the next step which is done in the section 3.1.1.

The KR is a time-dependent problem that is formulated in discrete time. For many applications it is useful to have some formulation in continuous time as the formalism of Hamiltonian mechanics is formulated in this way and we can use its methods only if we have the right formulation. The Hamilton-Jacobi theory for example is formulated for trajectories in continuous time and so is the action we obtain. In order to apply the tool kit of Hamiltonian mechanics we need a formulation in continuous time. We expand the periodic δ function in a Fourier series in eq. (2.1) and obtain

$$H = \frac{I^2}{2} + K\cos\theta \sum_{m=-\infty}^{\infty} \mathrm{e}^{\imath 2\pi m t}. \tag{3.1}$$

If we now assume that θ is a slow variable it is reasonable to consider only the lowest frequencies $m = 0, \pm 1$. This leads us to

$$H = \frac{I^2}{2} + K\cos\theta + 2K\cos\theta\cos 2\pi t. \tag{3.2}$$

If we now assume that the third term averages to zero we arrive at the pendulum approximation for the standard map.

$$H_0 = \frac{I^2}{2} + K\cos\theta. \tag{3.3}$$

To avoid confusion we note that the approximation as we presented it here is not in the variables we used in chapter 2, but are supposed to be general canonical variables. If we want to apply this well known approximation to the problem of the QKR near resonance we have to introduce the ϵ-classical variables and $\tilde{k}$ now. This is done in the next subsection.

3.1.1 Application of the Pendulum Approximation to the ϵ-classical QKR

In section 2.4 we introduced a detuning which allowed us to map the full problem to a system which is much more regular. This system was again a KR system. By introducing new variables J and ϑ we could reduce it to the standard map. These variables are the variables which also need to be inserted into the pendulum approximation. We obtain

$$H(J,\vartheta) = \frac{J^2}{2} + \tilde{k}\cos\vartheta. \tag{3.4}$$

Although we used J in the pendulum Hamiltonian the physical momentum is I and it has to be reintroduced to the Hamiltonian.

As the phase space of pendulum and KR have different topologies we have to take a closer look at the transformation and the role of β in this context. The momentum J is defined modulo 2π which introduces a certain arbitrariness into the choice of the phase space cell. The transformation (see eq. (2.35-2.36)) therefore reads

$$J + 2\pi m = I + \tau\beta + l\pi, \tag{3.5}$$

assuming $\epsilon > 0$. The periodicity reflects the fact that the KR phase space is periodic in J. Unfortunately the pendulum phase space in not. This is illustrated in fig: 3.1. We can see that the pendulum describes the KR only in one phase space cell. Therefore we have to choose m to correspond to the right phase space cell.

In the pendulum approximation the resonance is at $J = 0$ which fixes the relation between β and I up to $2\pi m$. We will assume that the particle is placed in the phase space cell at rest which means in an state with angular momentum zero whose wave function constant in spatial representation. In this interpretation the

$\tau\beta$ term covers the interval $[0, \tau+\epsilon]$ which is equal to $[0,\tau]$ in first order approximation[1]. For the pendulum approximation to be valid we need to choose m such that the β value of interest maps near to $J \approx 0$ or at least $J \in [-\pi, \pi]$. As soon as $l \neq 0$ we have multiple resonant β and therefore also multiple combinations of m and β mapping to a case in which the pendulum approximation is valid.

As we do not discuss higher resonances in this thesis we will focus on the $l = 1$ case with only one resonant β. In this case the $\tau\beta$ term scans an interval $[0, 2\pi]$ in first approximation. To map this into a range in which the pendulum approximation is valid we need to choose $m = 1$ so that our special transformation reads[2]

$$J = I + \tau\beta - \pi = I + \bar{\beta} \tag{3.6}$$

where we defined $\bar{\beta} \equiv -\pi + \tau\beta$.

We will use β and $\bar{\beta}$ equivalently. As we will always assume the $I = 0$, β and $\bar{\beta}$ can be interpreted as a momentum offset or an intrinsic momentum of the particle. Each β value has an unique corresponding $\bar{\beta}$. We will use the notation of an over bar for this correspondence and switch between the different quantities without further notice. Which quantity is used should be clear from the context. As $\bar{\beta}$ is defined in the transformation, in every ϵ-classical expression will be $\bar{\beta}$ and never β. We will however never give $\bar{\beta}$ values but just use β values in order to easy comparison to be the original QKR. This means we will also give β values even if the data is calculated in some semiclassical expression.

After having done the transformation we can give the ϵ-classical Hamiltonian for the pendulum approximation

$$H(I, \vartheta) = \frac{1}{2}(I + \bar{\beta})^2 + \tilde{k}\cos\vartheta. \tag{3.7}$$

We can see that the transformation leads to a intrinsic shift in the momentum in contrast to the simple pendulum. Before we discuss the implications for the spectrum of this shift we give the numerical method we use to calculate the pendulum data.

3.1.2 Numerical Implementation

In order to implement the pendulum numerically we use some matrix representation. We use the representation in angular momentum eigenstates. In this representation the matrix reads

$$\langle n|H|m\rangle = \langle n|\frac{1}{2}(\hat{I}^2 + \bar{\beta})^2 + \tilde{k}\cos\hat{\theta}|m\rangle \tag{3.8}$$

$$= \frac{1}{2}(n\epsilon + \bar{\beta})^2\delta_{n,m} + \frac{\tilde{k}}{2}\langle n|\left(\mathrm{e}^{\imath\hat{\theta}} + \mathrm{e}^{-\imath\hat{\theta}}\right)|m\rangle \tag{3.9}$$

$$= \frac{1}{2}(n\epsilon + \bar{\beta})^2\delta_{n,m} + \frac{\tilde{k}}{2}(\delta_{n,m+1} + \delta_{n,m-1}), \tag{3.10}$$

[1] This also results in a shift of the island which can be seen when comparing states that correspond to the symmetry $J \leftrightarrow -J$ which is not exactly equal to $\bar{\beta} \leftrightarrow -\bar{\beta}$. In our case we do not not make use of this symmetry and therefore we can neglect this effect.

[2] It is important to keep in mind that we decided to take $\epsilon > 0$.

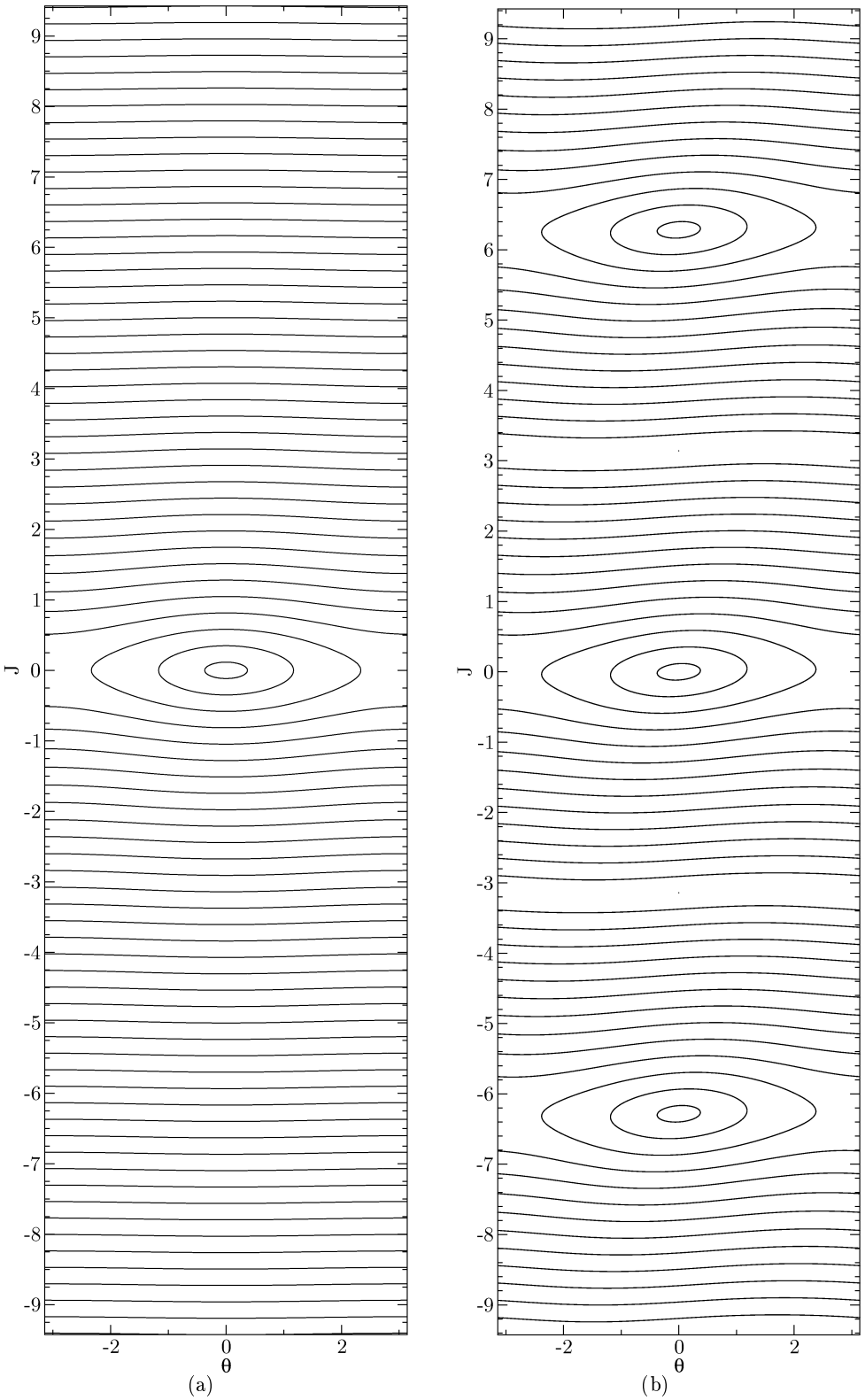

Figure 3.1: In this plot we show the phase space of the pendulum and the kicked rotor. We show data for $K = 0.1$. The pendulum phase space is shown in (a) and the kicked rotor phase space is shown in (b). We can see that the pendulum approximation describes the phase space only near the island and lacks the periodic structure completely.

where we used

$$\langle n|\mathrm{e}^{\imath k\hat{\theta}}|m\rangle = \int_0^{2\pi} \mathrm{d}\theta \int_0^{2\pi} \mathrm{d}\theta' \langle n|\theta\rangle\langle\theta|\mathrm{e}^{\imath k\hat{\theta}}|\theta'\rangle\langle\theta'|m\rangle \tag{3.11}$$

$$= \frac{1}{2\pi}\int_0^{2\pi} \mathrm{d}\theta \int_0^{2\pi} \mathrm{d}\theta' \mathrm{e}^{-\imath n\theta}\mathrm{e}^{\imath k\theta}\delta(\theta-\theta')\mathrm{e}^{\imath m\theta'} \tag{3.12}$$

$$= \frac{1}{2\pi}\int_0^{2\pi} \mathrm{d}\theta \mathrm{e}^{\imath(m-n+k)\theta} = \delta_{n,m+k}. \tag{3.13}$$

To get the spectrum and the temporal evolution we need to diagonalise this matrix. Doing this we obtain the eigenvalues E_i^k and the transformation matrix to the eigenbasis Q_k. Using them we can write

$$D_k \equiv \mathrm{Diag}(E_i^k; i \in \mathbb{N}) = Q_k H^k Q_k^\dagger. \tag{3.14}$$

In order to obtain the temporal evolution of a initial state $|\Psi_0\rangle$ we have to expand it in momentum energy eigenstates as the temporal evolution is trivial in this representation. Defining $c_m = {}_k\langle m|\Psi_0\rangle$, where $|m\rangle_k$ is an energy eigenstate and $|l\rangle$ is an angular momentum eigenstate we can give the temporal evolution as

$$|\Psi(t)\rangle = \sum_n \mathrm{e}^{-\imath\frac{t}{\epsilon}E_n^k} c_n |n\rangle_k = \sum_{n,l} \mathrm{e}^{-\imath\frac{t}{\epsilon}E_n^k} c_n |l\rangle\langle l|n\rangle_k. \tag{3.15}$$

The $\langle l|m\rangle_k$ are the entries of Q_k. We compute the c_m initially, apply the phase rotation which corresponds to the exponential and transform it back to the angular momentum representation using Q_k.

For the evaluation of fidelity we need to compare different k so we need ${}_{k_1}\langle m|n\rangle_{k_2}$ which can be obtained by multiplying Q_{k_1} and $Q_{k_2}^\dagger$. The procedure of obtaining the fidelity from energy eigenstates is described in section 4.2.

To implement this procedure we need to calculate the eigenvector and eigenvalues of the matrix eq. (3.10). This matrix is tridiagonal which allows us to use specialised routines. We used the LAPACK implementation of the Intel math kernel library (MKL). For the diagonalisation we used the subroutine DSTEV which uses the QR or LR method for the diagonalisation [And99]. This routine also gives the transformation matrix which we called Q_k and the eigenvalues sorted by their value.

For the estimation of the truncation error it is important to notice the structure of the matrix. Its diagonal dominates except for the entries where $\bar{\beta} \approx n\epsilon$. In the parts where the matrix is diagonally dominant the diagonal elements are very near to the actual eigenvalue [Sch05a]. If the diagonal is not dominant its values are no good estimates. Then the eigenvalues may be dominated by the hopping entries. This means truncating in the offdiagonally dominant regime leads to wrong behaviour. The effect of truncation is less severe as long as the truncation is in the regime of dominating diagonal.

3.1.3 Implications of β for the Spectrum

The spectrum of the pendulum is well known [Ald80]. Unfortunately the spectrum is just discussed without the intrinsic momentum offset β, which changes the

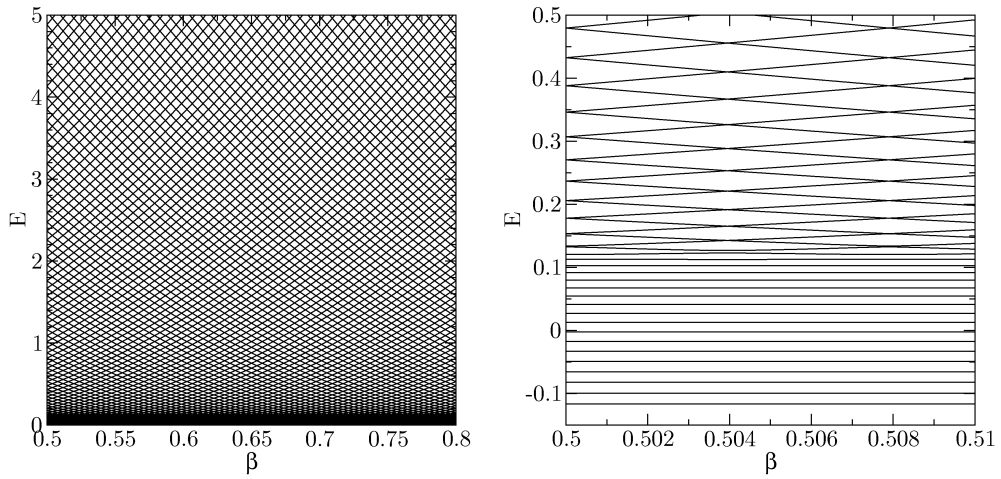

Figure 3.2: In this figure we show the spectrum of a pendulum with $\epsilon = 0.05$ and $k = 0.8\pi$. In (a) we show an overview. In (b) we show the low levels from (a) in detail and demonstrate the transition of island like states to rotor like states.

spectrum. This influence will now be discussed.

The spectrum can be understood qualitatively in a semiclassical view. Therefore we need to have a look at fig. 3.2. There we show the spectrum of a pendulum as a function of β. We can see that there is a fixed amount of levels which are nearly independent of β. On the other hand there are levels who have a quadratic dependency with β; some falling, some rising, resulting in a mesh like structure. The independent levels can be understood as some harmonic oscillator like states which have an equal spacing. They correspond to the harmonic oscillator approximation. In the picture of quantised action in the phase space [Gut90] we see that the area in phase space surrounded by harmonic oscillator orbits is the same even if the centre of the island is shifted in phase space. In the case of rotating orbits the surrounded area in phase space is the area between the trajectory and the $J = 0$ axis. This area is very sensitive to a shift in phase space. The existing of falling and rising levels to left and right rotating states. This behaviour can also nicely be seen in fig. 4.2. The step in the momentum corresponds to the island and the values showing linear behaviour are the rotor like states.

This behaviour can be understood in the context of solid state theory. There one introduces the Bloch states for the free electron and calculates the band gap by taking the leading order Fourier coefficient of the potential into account [Ash06]. This corresponds to a cosine potential which is also the case for the pendulum. The structure of the spectrum therefore can be understood as a band structure of a deep lattice. The island states correspond to a regime with a very large band gap. The band gap decreases quickly after some threshold. This argument motivates the existence of avoided crossings which unfortunately be understood in a semiclassical way.

3.2 Phase Space Observations

We already discussed the similarity of the phase spaces of kicked rotor and pendulum. In this discussion we focused only at the classical phase space. Now we will discuss how much of this similarity also occurs in the quantum picture. We will introduce a phase space function which allows us to understand in which part of the phase space the wave function lives in order to understand which aspects of the dynamics of the QKR is described by the pendulum approximation.

3.2.1 The Husimi Function

In semiclassics one works with some spatial or momentum representation to define a wave function. For a better understanding of the influence of phase space structures to the wave function it would be desirable to have a phase space density function to describe the quantum mechanical state. There are infinitely many functions to achieve this and the problem is to find a physical one [Bal06]. Therefore we have to state additional requirements.

The Wigner function at least satisfies the mixture property. This means that the phase space function is just dependent on the state operator and not on the pure states it is represented in. However the Wigner function is not positive and can therefore not be interpreted as a phase space density. The negative values in the Wigner functions are often interpreted as the occurrence of purely quantum phenomena [Sch01, Ken04].

Another function satisfying the positivity but not the mixture property is the Husimi function. It is strictly positive but one is unable to calculate the right momentum or local probability distribution. The basic idea is to project the state of the system onto the state that is nearest to the point in phase space which is the coherent state. The coherent states $|p,q\rangle$ form an over complete system which means [Sch96, Bal06]

$$\int \mathrm{d}p\mathrm{d}q \ |p,q\rangle\langle p,q| = 2\pi\hbar\mathbb{1}. \tag{3.16}$$

The Husimi function is defined by means of these coherent states as

$$\rho_H(p,q) = (2\pi\hbar)^{-1}\langle p,q|\rho|p,q\rangle. \tag{3.17}$$

For a pure state $\rho = |\Psi\rangle\langle\Psi|$ this means

$$\rho_H(p,q) = (2\pi\hbar)^{-1}|\langle p,q|\Psi\rangle|^2. \tag{3.18}$$

One way of motivating the Husimi function is the projection onto coherent states. But it is also possible to show that the Husimi function is the Wigner function convoluted with the coherent state [Bal06].

Coherent State on the Circle

In most textbooks coherent states are defined as the ground state of the harmonic oscillator [Fri06]. However this construction only works for the particle moving

on the line. For the particle moving on the circle some considerations need to be done.

In [Gaz09] the procedure of defining coherent states is discussed in a general context. Although the focus is more on coherent state quantisation a general concept for constructing coherent states is given. For the motion on the circle the coherent state is

$$|J,\alpha\rangle = \frac{1}{\sqrt{N(J)}}\left(\frac{\sigma}{\pi}\right)^{1/4}\sum_{n\in\mathbb{Z}} \mathrm{e}^{-\frac{\sigma}{2}(J-n)^2}\mathrm{e}^{-\imath n\alpha}|e_n\rangle, \tag{3.19}$$

where σ is a regularisation parameter, J and α parametrise the classical phase space, $|e_n\rangle$ is a basis of the Hilbert space and $N(J)$ is a normalisation factor which is connected to the elliptic theta function. The Gaussian distribution of momenta comes from the particular choice of weight motivated by experimental accessibility.

For the construction of the coherent state we choose the angular momentum basis. The regularisation is chosen such that the coherent state is equal to the harmonic oscillator approximation on the island. In order to evaluate the Husimi function we need to calculate the overlap of a coherent state at (I_0,θ_0) with the state whose Husimi function we want to calculate at several points in the phase space.

To fix the regularisation parameter σ we use the harmonic oscillator approximation for the pendulum. As σ is related to the width of the Gaussian we can relate it to the harmonic oscillator by taking the ground state in momentum representation and compare the exponents. The result is

$$\sigma = \sqrt{\frac{\epsilon}{k}} = \frac{\epsilon}{\sqrt{\tilde{k}}}. \tag{3.20}$$

Taking this together a coherent state in our picture is

$$\langle n|I_0,\theta_0\rangle = \frac{1}{\tilde{N}(I_0)}\ \mathrm{e}^{-\frac{(I_0-\epsilon n)^2}{\epsilon\sqrt{\tilde{k}}}}\mathrm{e}^{\imath n\theta_0}, \tag{3.21}$$

where $\tilde{N}$ is a normalisation and we switched to $\hat{I} = \epsilon\hat{\mathcal{N}}$ as momentum.

3.2.2 Numerical Realisation of the Husimi Function

To implement the evaluation of the Husimi function in an efficient way we reduce it to a Fourier transform. How this is done can be seen most easily by writing the Husimi function with the coherent state inserted

$$\rho_H(I_0,\theta_0) = (2\pi\epsilon)^{-1}\sum_n \frac{1}{\tilde{N}(I_0)}\ \mathrm{e}^{-\frac{(I_0-\epsilon n)^2}{\epsilon\sqrt{\tilde{k}}}}\mathrm{e}^{\imath n\theta_0}\Psi_n = (2\pi\epsilon\tilde{N}(I_0))^{-1}\sum_n F_n(I_0)\mathrm{e}^{\imath n\theta_0}, \tag{3.22}$$

where we separated a factor only dependent on n and I_0 from the exponential carrying the θ_0 dependence. The $F_n(I_0)$ are defined as

$$F_n(I_0) \equiv \mathrm{e}^{-\frac{(I_0-\epsilon n)^2}{\epsilon\sqrt{\tilde{k}}}}\Psi_n. \tag{3.23}$$

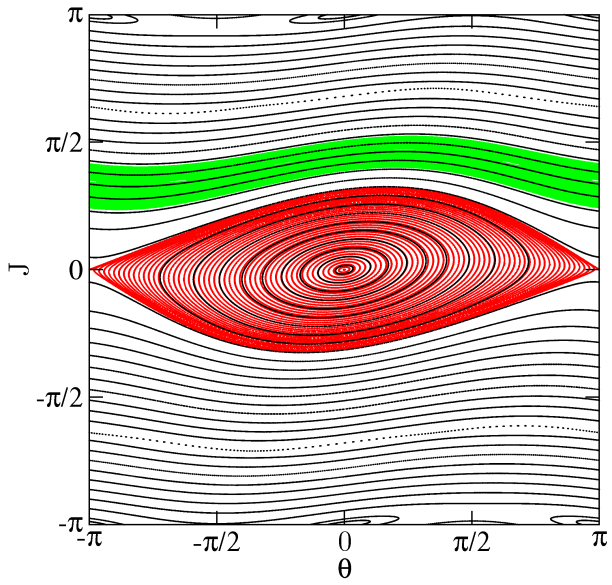

Figure 3.3: In this figure we show the ϵ-classical phase space of the QKR for $k = 25$, $\epsilon = 0.01$ and $\tau = 2\pi + \epsilon$. In green we show the part of the phase space corresponding to the state with $\beta = 0.7$ and n red the state corresponding to $\beta = 0.5$.

Rewriting the Husimi function this way, we can interpret eq. (3.22) as a Fourier transformation of $F_n(I_0)$. If we choose the vector size as a power of 2 we can use the Fast Fourier Transformation (FFT) for the numerical implementation. This way we obtain the values for all θ_0 corresponding to I_0 in one step.

3.3 Comparison of the Phase Spaces

Until now we gave the pendulum approximation to the kicked rotor and introduced the numerical procedure of the Husimi function on cylindrical phase space. We will now use the Husimi function to compare the quantum dynamics of pendulum and kicked rotor as it allows us to look at a phase space function. This way we can see whether the time evolution follows the expectations of the ϵ-classical phase space. This is important as the pendulum approximation uses this phase space.

value of our approximation we choose one rotor corresponding to the rotating regime and one for a state near to the resonance, which corresponds to the island. This is shown in fig. 3.3. There we show the region of phase space which corresponds to a β-rotor. We placed 100 phase space points on a horizontal line with $J = -\pi + \tau\beta$ and evolved them for 100 kicks and recorded all positions.

We can now compare this to the quantum evolution by having a look at the Husimi function. They are obtained by evolving a β-rotor in time and calculating the Husimi function. Some snapshots for QKR and pendulum are shown in fig. 3.4 and fig. 3.5. In fig. 3.4 we show Husimi plots for a $\beta = 0.5$ rotor corresponding to the red regime in fig. 3.3. We can see that the initial state corresponds to a delo-

calised state which starts to rotate on the island. It sticks near to the separatrix and rotates in the middle. This corresponds to the ϵ-classical expectations. In fig. 3.5 we show a rotor with $\beta = 0.7$ which corresponds to the green regime in fig. 3.3. We can see that the state rotates and gets folded after some time. This is also the reason why an approach using an van Fleck propagator gets problematic as we observe multiple orbits quite early as was demonstrated in fig. 2.7. Nevertheless, the pendulum reproduced the qualitative behaviour quite well in both cases.

3.4 Summary

We have now compared the phase space of the pendulum and the QKR in a ϵ-classical and quantum picture. Therefore we had to choose the right phase space cell in the transformation $I \to J$. We introduced the Husimi function for a state on a circle and used it to visualise the evolution of a initial β-rotor in the ϵ-classical picture. We used the pendulum and the QKR time evolution and compared it. We found that they coincide very well in the Husimi function. We could also convince us that the ϵ-classical interpretation of rotational and oscillatory type orbit holds.

In the next chapter we will use the WKB approximation to calculate the spectrum and the energy eigenfunctions of the pendulum. This will allow us to obtain a better understanding of the spectrum of the pendulum. The WKB will formalise the heuristic argument we gave earlier for the behaviour of the levels in fig. 3.2 at least for the rotating type levels.

The most important result of this chapter is the correspondence of pendulum and QKR in the Husimi picture. The pendulum as a time-independent system is much easier to treat as the time-dependent QKR. Instead of dealing with the more abstract concept of Floquet operators we can deal with the Hamilton operator and its eigenvalues which can be translated to quasienergies of the QKR easily. The picture of the pendulum as a perturbed free rotor that was shortly mentioned in the discussion of the band model is also of importance. This concept will arise several times in the next chapters. In this chapter the QKR was reduced to the pendulum. Thus solving the pendulum in WKB approximation gives deeper insight to the QKR. Nevertheless we still have to check the quality of the pendulum approximation. We will do this numerically in chapter 5.

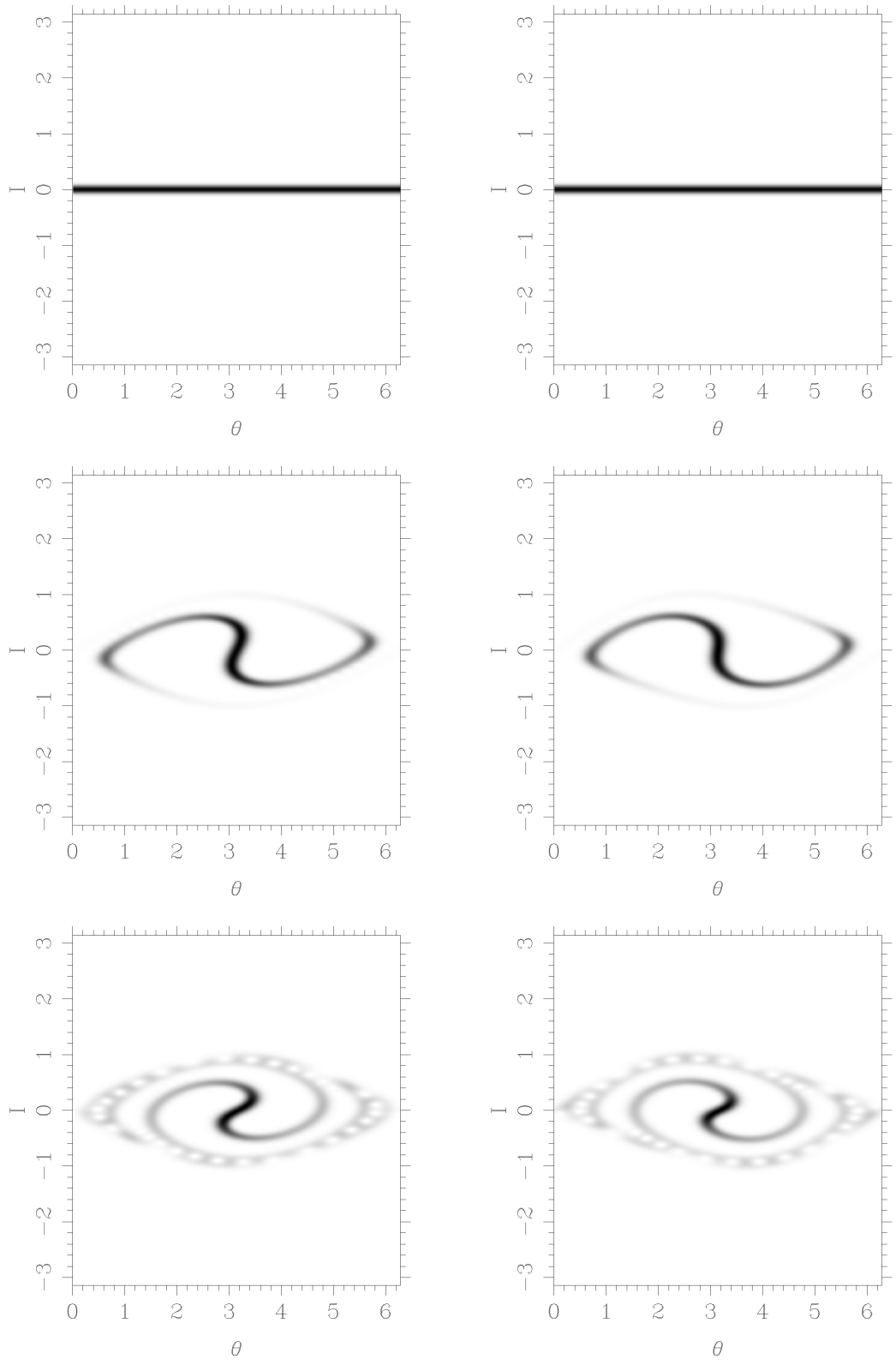

Figure 3.4: In this figure we show Husimi plots for the pendulum and QKR with $\epsilon = 0.01$, $k = 25$ and $\beta = 0.5$. In the left column we show pendulum states and on the right side we show Pendulum data. From top to bottom we show $t = 0, 10, 30$. We can see that the correspondence is quite good.

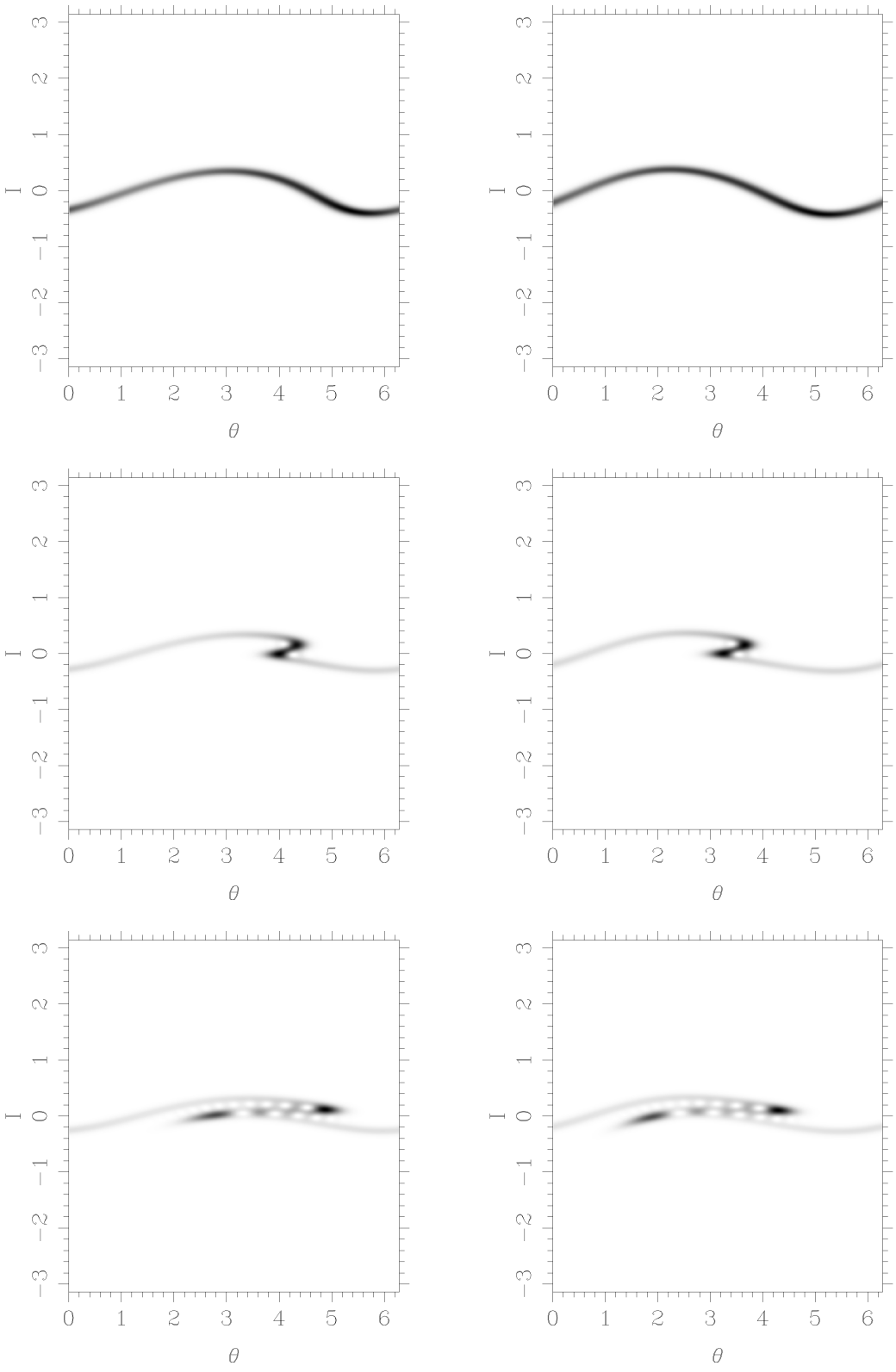

Figure 3.5: In this figure we show Husimi plots for the pendulum and QKR with $\epsilon = 0.01$, $k = 25$ and $\beta = 0.7$. In the left column we show pendulum states and on the right side we show QKR data. From top to bottom we show $t = 2, 7, 12$. The initial state is the same as in fig. 3.4 in the first row. In between the snapshots the state rotates once through the phase space from left to right. We can see that the correspondence is quite good.

Chapter 4

WKB Theory for the Pendulum

As shown in chapter 2 an approach using trajectories and the van Vleck propagator is problematic as the orbits are very complicated and the problem of multiple orbits arises quite early. This means taking an approach which is based on finding trajectories connecting two angles in a specific time is problematic. One solution is to switch to a method that is dealing with trajectories with a certain energy and not fixing the time. The WKB method is one of these methods. It enables us to get the classical Greens function and with it the eigenenergies. Using the Greens function we can construct the eigenstates needed to compute the fidelity.

In this chapter we will first show how the WKB method is related to the van Vleck propagator. The phase space of the pendulum is a cylinder where the angle is the periodic coordinate. Therefore we have to have a closer look at the derivation of the WKB method in order to understand how and why we can apply the WKB approximation. We will specialise the equations to our problem. After that we will show how we can obtain the fidelity by expanding in energy eigenstates and eigenenergies. In section 4.3 we will calculate the energies and the angle representation of the energy eigenstates and calculate the fidelity of a pendulum in WKB approximation. In order to get a first impression of the value of the approximation we will compare the fidelity using WKB to numerical data for the pendulum. In the end we give an analytical formula for ensembles.

4.1 Review of the WKB Approximation

In most quantum mechanics textbooks (e.g. [Sch05b, Sak09]) the WKB approximation is introduced by separating phase and amplitude of the wave function. After introducing this ansatz into the Schrödinger equation one assumes that the potential is constant on scales of the de Broglie wavelength and drops all terms containing $\hbar$. This way one obtains the Hamilton-Jacobi equation for the phase and an expression for the WKB wave function. We would like to present a different approach as it is not clear what happens on connected phase spaces in the usual WKB approach following the procedure presented in the textbooks mentioned.

We will present the procedure introduced in [Sch96]. There the propagator in WKB approximation is derived by applying the stationary phase approximation

(SPA) to the path integral representation of the quantum mechanical propagator. The result is the van Vleck propagator in d dimensions

$$G_{WKB}(x,t;y,0) = \sum_{\alpha} \left(\frac{\imath}{2\pi\hbar}\right)^{d/2} \sqrt{\left|\det \frac{\partial^2 S_\alpha}{\partial x \partial y}\right|} e^{\imath(S_\alpha/\hbar \, - \, \mu_\alpha \pi/2)} \tag{4.1}$$

where α labels the classical paths connecting x and y in the time t and S_α is the corresponding classical action and μ_α is the number of negative eigenvalues of the matrix $\partial^2 S_\alpha / \partial x \partial y$ which corresponds to the number of focal points along the trajectory. As the propagator describes how the wave function at position y at time 0 influences the wave function at position x at time t it is a function of x, y and t and therefore we have to calculate the action also as the action of a classical path connecting two points within a certain time t. Therefore we need the action $S_\alpha(x,y,t)$. In some problems it is easier to express this action as a function of initial position x, final position y and energy E. Therefore we define the Fourier transform of this propagator

$$\tilde{G}(x,y;E) = \int_0^\infty \mathrm{d}t \, e^{\frac{\imath E t}{\hbar}} G(x,t;y,0). \tag{4.2}$$

Inserting eq. (4.1) into (4.2) and applying the SPA which again corresponds to $\hbar \to 0$ one obtains

$$\frac{\partial}{\partial t}\big(Et + S_\alpha(x,y;t)\big) = 0 \Leftrightarrow E = -\frac{\partial S_\alpha(x,y;t_{\alpha\sigma})}{\partial t}, \tag{4.3}$$

where σ indices the different solutions of this equation. We can see that by applying the SPA we get a Legendre transformation also known from classical mechanics or thermodynamics. It allows us to exchange a variable by the derivative by the same variable [Jel89]. In order to perform a Legendre transformation we need to invert eq. (4.3) to get $E(t)$ or $t(E)$. This is explained in more detail in appendix B. The transformation defines a new action

$$W(x,y;E) = S + Et. \tag{4.4}$$

From now one W will always denote the action as a function of energy E and S the action as a function of time t. One of the most important properties derives from the fact that S_α satisfies the Hamilton-Jacobi equation which is build in order to fulfil

$$E = H\left(\frac{\partial W}{\partial x}, x\right). \tag{4.5}$$

This allows us to calculate W for the path easily. This will be very important when applying the method to a specific problem. Now we will introduce all quantities into eq. (4.1) and perform the Fourier transform. Using $S_{\alpha\sigma} \equiv S(x,y,t_{\alpha\sigma})$ we obtain

$$\begin{aligned}\tilde{G}_{WKB}(x,y;E) = &\left(\frac{\imath}{2\pi\hbar}\right)^{d/2} \sum_{\alpha,\sigma} \sqrt{\left|\det \frac{\partial^2 S_{\alpha\sigma}}{\partial x \partial y}\right|} \\ &\times \exp\left(-\frac{\imath\mu_{\alpha\sigma}\pi}{2} + \frac{\imath S_{\alpha\sigma}}{\hbar} + \frac{\imath E t_{\alpha\sigma}}{\hbar}\right) \int_0^\infty \mathrm{d}t \, e^{\imath(\partial^2 S_{\alpha\sigma}/\partial t^2)(t-t_{\alpha\sigma})^2/2\hbar},\end{aligned} \tag{4.6}$$

where the Maslov index, energy and time have two indices. The first index is for the classical path (α) and the second index for the different stationary points in the time[1] (β). In order to obtain this equation we expanded S in t and truncated after the second order which is the standard procedure in SPA. The Legendre transformation and the corresponding choice of E and t ensures that the linear term vanishes. In this equation the determinant is still expressed by means of S. This is the wrong action and we have to express it by W. Therefore we have to go into the details of the transformation as we have to respect the boundary condition of the variation of the action in order to do this transformation. This is carried out in appendix B. There the general case is derived. We will already assume that the action W will not contain products containing x and E, which will be the case for Hamiltonians of type $H(p,q) = T(p) + V(q)$ where p are momenta and q are spatial coordinates. Introducing this into eq. (B.13) we get

$$-\frac{\det(\partial^2 S/\partial x \partial y)}{\partial^2 S/\partial t^2} \equiv \tilde{D} = \frac{\partial^2 W}{\partial x \partial E}\frac{\partial^2 W}{\partial y \partial E}, \tag{4.7}$$

where the left side of this equation is the definition of $\tilde{D}$ and the right side is the evaluation for the case mentioned above. The determinant $\tilde{D}$ represents the density of paths connecting x and y. This can be seen by having a look at the variational approach to classical mechanics. There it can be shown that this determinant is proportional to the inverse of the determinant of the Jacobi field which gives the sensitivity of the classical path to a variation of the initial momentum. If the path is stable to variations the determinant of Jacobi fields is small or zero and thus many different paths in a surrounding contribute; so $\tilde{D}$ is large. A more formal derivation of this interpretation is given in [Sch96, Haa10]. The integral in eq. (4.6) is a Fresnel integral. When evaluating this integral we have to be careful with singular points of $\partial^2 S/\partial t^2$ which arise in turning points of the classical path. Similar to the Maslov indices for focal points in the time dependent theory a classical turning point contributes a phase of $\pi/2$ in the energy dependent theory. Evaluating this and introducing $\tilde{D}$ we arrive at

$$\tilde{G}_{WKB}(x,y;E) = \left(\frac{\imath}{2\pi\hbar}\right)^{d/2-1/2} \sum_{\alpha,\sigma} \sqrt{|\tilde{D}_{\alpha\sigma}|}\exp\left(-\frac{\imath\mu_{\alpha\sigma}\pi}{2} + \frac{\imath W_{\alpha\sigma}}{\hbar}\right), \tag{4.8}$$

where α denotes the classical paths and σ the different times. At this point the two indices have lost their intuitive interpretation but still have to be respected as they are defined by eq. (4.3). The sum over α and σ denotes the sum over all paths connecting x and y with energy E. This summation can now be carried out by having a look at the types of trajectories. Following the standard representation we would introduce a particle moving in some trapping potential. Therefore one has to care about turning points for different types of trajectories with none, one or two turning points and some general treatment of this trajectories. In contrast to the particle in a trapping potential we are interested in a regime where the

[1] Here it is important that stationary does not mean stationary in time. It just means that some quantity does not change as a parameter is changed. In our case this means we have paths with fixed energy for which the time to get from x to y does not change when slightly varying the energy.

orbits are rotating orbits on a cylindrical phase space which is a non trapped movement. This means we do not have turning points and have to sum over paths connecting x and y and the same path plus full rotations. This means we first calculate the action of a path connecting x and y with energy E using

$$E = \frac{1}{2m}\left(\frac{\partial W}{\partial x}\right)^2 + V(x) \tag{4.9}$$

$$\Rightarrow W(x,y,E) = \int_x^y \sqrt{2m(E-V(u)}\mathrm{d}u. \tag{4.10}$$

In order to add full rotations to this path we define $J(E) \equiv W(0,2\pi,E)$ and obtain in this way the Greens function in the known form

$$\tilde{G}_{WKB}(x,y;E) = \sqrt{\frac{m/2}{\sqrt{E-V(x)}\sqrt{E-V(y)}}}\sum_{k=0}^{\infty}\exp\left(\frac{\imath W(x,y,E)}{\hbar}+\frac{\imath k J}{\hbar}\right) \tag{4.11}$$

by using $\partial^2 W/\partial u \partial E = 2m/\sqrt{E-V(u)}$ and by introducing the rotation number k and dropping a common phase. The summation over l can be done by means of geometric summation. This will lead to a factor which has poles at

$$J(E) = 2\pi n\hbar \tag{4.12}$$

which is the quantisation condition. In order to get the energy eigenfunction we take just the $W(x,y,E)$ part into account. This is the part of the propagator giving the explicit $x \to y$ transformation.

If we have the eigenenergies we obtain the energy eigenfunctions by fixing the value of the energy function at some arbitrary position. The value at all other points can be obtained by using the propagator. In the end the wave function needs to be normalised which fixes the value we chose initially. As we now want to give the equations we will use to derive our result we will now switch from $(x,y) \mapsto (\theta,\theta')$ and from $\epsilon \mapsto \hbar$. In the beginning we need to determine the relevant momentum I from the action W. Afterwards we can calculate all relevant quantities from this action and the momentum. The equations that need to be evaluated to obtain the energies E_n and the energy eigenstates $|u_n\rangle$ are

$$I \equiv \frac{\partial W}{\partial \theta} \tag{4.13a}$$

$$\int_0^{2\pi}\mathrm{d}\theta' I(E_n,\theta) = 2\pi n\epsilon \tag{4.13b}$$

$$-\frac{\det(\partial^2 S/\partial\theta\,\partial\theta')}{\partial^2 S/\partial t} = \frac{\partial^2 W}{\partial\theta\partial E}\frac{\partial^2 W}{\partial\theta'\partial E} \tag{4.13c}$$

$$\langle\theta|u_n\rangle = N\sqrt{\frac{\det(\partial^2 S/\partial\theta\,\partial\theta')}{\partial^2 S/\partial t}}\; e^{\frac{\imath}{\epsilon}\int^\theta \mathrm{d}\theta' I(E_n,\theta)}. \tag{4.13d}$$

Here we would like to emphasise that we need to chose E_n and W such that the wave function eq. (4.13d) fulfils the periodic boundary conditions[2]. In the end

[2]This will be important later when we calculate the wave function by approximating the action as it will block us from using a more terms in the approximation.

we adjust N such that the energy eigenfunction is normalised. Some caution is needed in our treatment of the angles. In eqs. (4.13) we did not write the starting angle θ'. As mentioned it is supposed to be fixed and we refer all quantities to this fixed value. As shown in appendix B for our type of Hamiltonian we can write our W as an integral and therefore we can refer to some arbitrary point without loss of generality. Nevertheless we have to be careful with derivatives by θ'. They cannot be neglected as they make a difference even if θ' is fixed.

In this section we reviewed the WKB approximation starting from the van Vleck propagator. This way we could show how the topology of the rotating orbits simplifies the equations of the WKB approximation. We intended to give some closer insight which allows us to see what happens if we switch from an euclidean phase space to a cylindrical phase space. We showed that we can apply the WKB method to the pendulum by not caring about turning points and just closing the integral of the action via the periodic variable. The non existence of turning points in particular stabilises the WKB approximation by avoiding singular points.

4.2 Fidelity Using Energy Eigenstates

In section 4.1 we reviewed the WKB method and gave a formula for the Greens function and also a procedure to obtain energy eigenvalues and the corresponding energy eigenstates. Now we will show how we can calculate fidelity using these two ingredients. This is nothing special for WKB and just relies on the existence of eigenenergies and their eigenstates. In order to obtain numerical data for the pendulum we calculate the eigenstates and eigenenergies numerically by diagonalising eq. (3.10) and calculate the fidelity as described in this section. Later in this chapter we will use the eigenenergies and states obtained by WKB to obtain an analytical expression for the fidelity.

In chapter 2 we defined the fidelity of the state $|\Psi_{k_{1/2},\beta,\epsilon}(t)\rangle$ as the overlap of the initial state, evolved with slightly different kicking strengths, with itself. The fidelity therefore reads

$$F(\beta, k_1, k_2, \epsilon, t) = \left|\langle\Psi_{k_2,\beta,\epsilon}(t)|\Psi_{k_1,\beta,\epsilon}(t)\rangle\right|^2. \tag{4.14}$$

The initial state $|\Psi^0_\beta\rangle \equiv |\Psi_{k_{1/2},\beta,\epsilon}(0)\rangle$ is by definition of fidelity independent of $k_{1/2}$.

We will now use that the energy eigenstates build a complete set of states and can be used to express the identity as the time evolution for the single energy eigenstates is trivial. Because this eigenstates depend on the kicking strength k we introduce a new notation. An energy eigenstate of a system with kicking strength k is $|n\rangle_k$ where n is the quantum number. We have to be careful as an angular momentum state will be denoted by $|m\rangle$ where m denotes the angular momentum. This notation has to be handled very carefully as only a subscript distinguishes two completely different quantities. Using this notation we can give the time evolution of a state easily

$$|\Psi_{k_{1/2},\beta,\epsilon}(t)\rangle = \sum_n |n\rangle_k \; {}_k\langle n|\Psi^0_{\beta,\epsilon}\rangle \mathrm{e}^{-\imath\frac{t}{\epsilon}E^k_n}, \tag{4.15}$$

where E_n^k are the eigenenergies. Introducing this notation to eq. (4.14) we obtain

$$F(\beta, k_1, k_2, \epsilon, t) = \left| \sum_{n,m} \langle \Psi^0_{\beta,\epsilon} | n \rangle_{k_2 \ k_2} \langle n | m \rangle_{k_1 \ k_1} \langle m | \Psi^0_{\beta,\epsilon} \rangle \ \mathrm{e}^{\imath \frac{t}{\epsilon} (E_n^{k_2} - E_m^{k_1})} \right|^2 . \tag{4.16}$$

This formulas can be interpreted in several ways. We can interpret $|n\rangle_{k_2 \ k_2}\langle n|m\rangle_{k_1 \ k_1}\langle m|$ as a transition from an eigenbasis to the system with kicking strength k_1 to one with k_2. In this representation the fidelity is a special scalar product with respect to a basis transformation. In another interpretation we can regard $\langle \Psi^0_{\epsilon,\beta} | n \rangle_{k_2 \ k_2} \langle n | m \rangle_{k_1 \ k_1} \langle m | \Psi^0_{\beta,\epsilon} \rangle$ as a coefficient in a Fourier like series. As it has two indices we might interpret these coefficients as a coefficient matrix which again allows us to interpret the fidelity as a scalar product of two oscillating vectors with respect to the coefficient matrix. The later interpretation will turn out to be the more fruitful one. The reason is that it separates the time dependency completely from the time independent parts.

4.3 Application to the Pendulum

In the last section we showed how one can obtain fidelity if one has the energy eigenstates for k_1 and k_2 and the corresponding eigenenergies. In this section we will calculate this quantities in WKB approximation. we will first calculate the action W. It will turn out that this is given by means of elliptic integrals. To calculate the energy eigenfunctions we need to find approximations which allow us to calculate W and E_n consistent in order to respect the periodic boundary conditions. To get a more detailed expression for the spectrum we can drop this restriction which allows us to give a better approximation for the spectrum. In section 4.4 we will use the simple energy eigenfunctions and the detailed energies to obtain the fidelity using eq. (4.16).

As already mentioned we are interested in the rotating regime which corresponds to $E > \tilde{k}$. To calculate the action $W(\theta, E)$ we evaluate eq. (4.5) for the pendulum Hamiltonian eq. (3.4). This leads to

$$E = H\left(\frac{\partial W}{\partial \theta}, \theta\right) = \frac{1}{2}\left(\frac{\partial W}{\partial \theta} + \bar{\beta}\right)^2 + \tilde{k}\cos\theta \tag{4.17}$$

$$\Rightarrow W(\theta, E) = \int_0^\theta \left\{ \sqrt{2(E - \tilde{k}\cos\theta')} - \bar{\beta} \right\} \mathrm{d}\theta'. \tag{4.18}$$

The second equation is an elliptic integral [Abr64]. In order to get the eigenenergies we need to find an E_n that fulfils

$$W(2\pi, E_n) = 2\pi n \epsilon. \tag{4.19}$$

The energy will appear in the argument and modulus of the elliptic integral [Ald80] or the Jacobi elliptic function which is the inverse function to the elliptic integral. The energy is given as a root of eq. (4.19) but cannot be given as a closed expression as argument and modulus of the elliptic integral have an E_n

dependence. In the rotating regime we have $E > \tilde{k}$. Therefore we expand the integrand in a Taylor series in $\tilde{k}/E$. This results in

$$W(\theta, E) = \int^{\theta} \left((\sqrt{2E} - \bar{\beta}) - \frac{\epsilon k}{\sqrt{2E}} \cos\theta' + \frac{\epsilon^2 k^2}{2(2E)^{3/2}} \cos^2\theta' + O(\epsilon^3) \right) \mathrm{d}\theta' \tag{4.20}$$

$$= (\sqrt{2E} - \bar{\beta})\theta - \frac{\epsilon k}{\sqrt{2E}} \sin\theta + \frac{\epsilon^2 k^2}{2(2E)^{3/2}} \left(\frac{\theta}{2} + \frac{1}{4} \sin 2\theta \right) + O(\epsilon^3). \tag{4.21}$$

Now we can insert this action into the quantisation condition eq. (4.13b) which leads to

$$2\pi n\epsilon = (\sqrt{2E} - \bar{\beta})2\pi - \frac{\epsilon^2 k^2}{2(2E)^{3/2}}\pi + O(\epsilon^3). \tag{4.22}$$

Multiplication with $(2E)^{3/2}$ reduces this expression to

$$0 = 2\pi(2E)^2 - 2\pi(2E)^{3/2}(\bar{\beta} + n\epsilon) - \frac{\epsilon^2 k^2}{2}\pi + O(\epsilon^3). \tag{4.23}$$

Neglecting the order ϵ^3 terms would leave us with a polynomial of fourth order. The solutions can still be given in closed form but are very complicated. Our approximation also produced three additional solutions which are non-physical as they are very different to the exact energy. In subsection 4.3.2 we will give an approximation which allows us to calculate the energies quite accurate. Nevertheless this energies are not the exact energies. This means that $W(E_n, \theta)$ is not fulfilling the periodic boundary conditions. Therefore we have to find an approximation which can be solved exactly in such a way that the eigenfunctions fulfil the boundary conditions. This will be carried out in subsection 4.3.1. To get a detailed spectrum we will include more terms and give a more precise result in subsection 4.3.2.

4.3.1 Energy Eigenfunctions

Taking too many terms into account in eq. (4.21) leads to problems finding exact solutions of the quantisation condition eq. (4.19) which is important to fulfil the periodic boundary conditions. In order to obtain the wave function we therefore have to truncate eq. (4.21) after the linear ϵ term. This leads to

$$W(E, \theta) = (\sqrt{2E} - \bar{\beta})\theta - \frac{\epsilon k}{\sqrt{2E}} \sin\theta \tag{4.24}$$

$$\Rightarrow \int_0^{2\pi} \frac{\partial W}{\partial \theta} \mathrm{d}\theta' = (\sqrt{2E} - \bar{\beta})2\pi = 2\pi\epsilon. \tag{4.25}$$

Including the next order leads to an equation that cannot be solved exactly which is necessary to fulfil the boundary condition of the wave function mentioned above. In this subsection we will therefore use the energies $E_n = \frac{1}{2}(n\epsilon + \beta)^2$. How to

obtain the energy wave function using Greens function was shown in section 4.1. The result, eq. (4.13d), reads

$$\langle\theta|n\rangle_k = N(\epsilon, n, \bar{\beta}, k)\sqrt{\frac{\partial^2 W}{\partial\theta\partial E}\frac{\partial^2 W}{\partial\theta'\partial E}}\exp\left(\frac{\imath}{\epsilon}W(E_n,\theta)\right), \tag{4.26}$$

where N is a normalisation constant that needs to be fixed in the end. We still need to calculate the square root. This can be done by using eq. (4.24):

$$\frac{\partial W}{\partial\theta} = \sqrt{2E} - \bar{\beta} - \frac{\epsilon k}{\sqrt{2E}}\cos\theta \tag{4.27}$$

$$\frac{\partial^2 W}{\partial\theta\partial E} = \frac{1}{\sqrt{2E}} + \frac{\epsilon k}{(2E)^{3/2}}\cos\theta. \tag{4.28}$$

Also using $\sqrt{1+\epsilon A} \approx 1 + \epsilon/2\ A$ we find

$$\sqrt{\frac{\partial^2 W}{\partial\theta\partial E}} \approx \frac{1}{\sqrt[4]{2E}}\left(1 + \frac{\epsilon k}{4E}\cos\theta\right). \tag{4.29}$$

Here we will do a very crucial approximation. We will neglect the angular dependency in this equation. As we will see later the result is not too bad. To see this we would like to make some remarks on this approximation. Keeping the cosine term we would end up with a contribution of order ϵ^2 to the normalisation as the linear term contains only trigonometric functions whereas the quadratic term carries the square of the cosine. The correction to the wave function would be of order ϵ. Later we will give the angular momentum representation of the energy eigenfunction. In eq. (4.41) we will show that these are proportional to the Bessel functions of first kind of order $n-m$ where n is the angular momentum and m is the energy quantum number. Including the cosine term would add Bessel functions of order $n - m \pm 1$ to the linear ϵ term of the energy eigenfunction. This means that the contribution is additionally suppressed. Later we will use a more sophisticated method for obtaining the energies. In contrast to the energy eigenfunctions small deviations will be amplified as the energies are multiplied by time. For the wave function the deviations are not amplified.

Neglecting the angular dependency only the action eq. (4.24) and the normalisation fix the energy eigenfunction in angular representation. The result is

$$\langle\theta|n\rangle_k = \frac{1}{\sqrt{2\pi}}e^{\imath n\theta}e^{-\imath\frac{k}{n\epsilon+\beta}\sin\theta}. \tag{4.30}$$

In this expression several basic ideas of our approximation appear. The energy eigenfunction is basically a free rotator state whose phase has a sine modulation. On the one hand this respects the modulation of the phase due to the energy variation, on the other hand we neglected the θ dependence of $\tilde{D}$ which results in the missing variation of amplitude, which would denote a change of velocity. As already mentioned, the correction would be of order ϵ and so we do not expect a large error.

4.3.2 Eigenenergies

In subsection 4.3.1 we truncated the expansion eq. (4.21) after the linear term in order to obtain a solution which satisfies the boundary conditions. In the calculation of the energies we are not restricted by this. Therefore we can tolerate approximative solutions to eq. (4.21). For calculating the eigenenergies we start at eq. (4.31) and neglect the higher orders

$$0 = 2\pi(2E)^2 - 2\pi(2E)^{3/2}(\bar{\beta} + n\epsilon) - \frac{\epsilon^2 k^2}{2}\pi. \tag{4.31}$$

As already mentioned this is a polynomial of fourth order in $\sqrt{2E}$ and can in principal be solved in closed form. This solutions are very complicated and we are only interested in the solution that is near to the solution of eq. (4.19). Another disadvantage of the closed solution is that it has to fail as soon as we want to include additional terms as there is no closed solution for a polynomial of fifth order. Because of that we need to find a different possibility to get eigenenergies.

In order to fix the problem of finding the physical solution we will have a look at the $\epsilon \to 0$ case. In this case eq. (4.31) has an unique solution. We will expand $\sqrt{2E}$ in orders of ϵ and solve the result order by order. Therefore we define

$$\sqrt{2E} = \xi_0 + \xi_1\epsilon + \xi_2\epsilon^2 + \dots, \tag{4.32}$$

where the $\xi_i = \xi_i(\bar{\beta}, \tilde{k})$ depend on $\bar{\beta}$ and $\tilde{k}$. In order to insert this result into eq. (4.31) we have to use the multinomial expansion in a version which is ordered by powers in ϵ. Using eq. (C.8) we obtain

$$\sqrt{2E}^3 = \xi_0^3 + 3\epsilon\xi_0^2\xi_1 + \epsilon^2(3\xi_0^2\xi_2 + 3\xi_0\xi_1) + \epsilon^3(\xi_1^3 + 6\xi_0\xi_1\xi_2 + 3\xi_0^2\xi_3) + O(\epsilon^4) \tag{4.33}$$

$$\sqrt{2E}^4 = \xi_0^4 + 4\epsilon\xi_0^3\xi_1 + \epsilon^2(4\xi_0^3\xi_2 + 6\xi_0^2\xi_1^2) + \epsilon^3(4\xi_0\xi_1^3 + 12\xi_0^2\xi_1\xi_2 + 4\xi_0^3\xi_3) + O(\epsilon^4). \tag{4.34}$$

Inserting this into eq. (4.31) we obtain after ordering by powers of ϵ

$$\begin{aligned} 0 =& \xi_0^4 - \bar{\beta}\xi_0^3 \\ &+ \epsilon\Big(4\xi_0^3\xi_1 - 3\bar{\beta}\xi_0^2\xi_1 + n\xi_0^3\Big) \\ &+ \epsilon^2\Big(4\xi_0^3\xi_2 + 6\xi_0^2\xi_1^2 + 3n\xi_0^2\xi_1 - 3\bar{\beta}(\xi_0^2\xi_2 + \xi_0\xi_1^2) - \frac{k^2}{2}\pi\Big) \\ &+ \epsilon^3\Big(4\xi_0^3\xi_2 + 6\xi_0^2\xi_1^2 + 3n(\xi_0^2\xi_2 + \xi_0\xi_1^2) - \bar{\beta}(\xi_1^3 + 6\xi_0\xi_1\xi_2) + 12\xi_0^2\xi_1\xi_2\Big) \\ &+ O(\epsilon^4). \end{aligned} \tag{4.35}$$

Now we can calculate the coefficients ξ_i successively. This is due to the fact that the order ϵ^i term only contains $\xi_0, \dots, \xi_i$, where ξ_i will appear linearly[3], and thus

[3] If we have a look at the derivation of eq. (C.8) we need to distribute the i epsilons onto the coefficients. ξ_i can only appear in the ϵ^i term if it absorbs all epsilons, so it cannot appear multiple times.

can be solved for ξ_i as long as $\xi_0, \ldots, \xi_{i-1}$ are known. As ξ_0 can be found easily we can solve all orders successively. In this way we find

$$\xi_0 = \bar{\beta} \tag{4.36a}$$
$$\xi_1 = n \tag{4.36b}$$
$$\xi_2 = \frac{k^2}{4\bar{\beta}^3} \tag{4.36c}$$
$$\xi_3 = -\frac{3k^2 n}{4\bar{\beta}^4}. \tag{4.36d}$$

Now using eq. (C.8) again we obtain

$$\sqrt{2E}^2 = \xi_0^2 + \epsilon\ 2\xi_0\xi_1 + \epsilon^2(2\xi_0\xi_2 + \xi_1^2) + \epsilon^3(2\xi_1\xi_2 + 2\xi_0\xi_3) + O(\epsilon^4) \tag{4.37}$$

Inserting the coefficients from eq. (4.36) we get the final expansion for the energy

$$E = \frac{\bar{\beta}^2}{2} + n\bar{\beta}\epsilon + \left(\frac{k^2}{4\bar{\beta}^2} + \frac{n^2}{2}\right)\epsilon^2 - \left(\frac{nk^2}{2\bar{\beta}^3}\right)\epsilon^3 + O(\epsilon^4). \tag{4.38}$$

As already indicated we can interpret this result as an extension of the free rotor which has the energy $(n\epsilon+\bar{\beta})^2/2$ in our system. This reflects that we are treating the pendulum as a perturbed rotor.

4.4 Fidelity of the Pendulum using WKB

To calculate the fidelity we will use eq. (4.16) and focus on angular momentum states. These are the states referred to when speaking of β-rotors. Due to comparison to the experiment we will use the $|0\rangle$ state as initial state. But at first we have to compute the angular momentum representation of the energy eigenstates using the angular representation of the energy eigenstates. The angular momentum states are defined as

$$\langle\theta|n\rangle = 1/\sqrt{2\pi}\ \mathrm{e}^{\imath n\theta}. \tag{4.39}$$

Using $\mathbb{1} = \int_0^{2\pi} |\theta\rangle\langle\theta|$ we can calculate the projection on the angular momentum state using the angular representation of the angular momentum state and the energy eigenstate

$$\langle m|n\rangle_k = \int_0^{2\pi} \mathrm{d}\theta \langle m|\theta\rangle\langle\theta|n\rangle_k \tag{4.40}$$
$$= \frac{1}{2\pi}\int_0^{2\pi} \mathrm{d}\theta\ \mathrm{e}^{-\imath m\theta}\mathrm{e}^{\imath n\theta}\mathrm{e}^{\imath\frac{k}{n\epsilon+\bar{\beta}}\sin\theta} \tag{4.41}$$
$$= J_{m-n}\left(\frac{k}{n\epsilon+\bar{\beta}}\right), \tag{4.42}$$

where $J_n(x)$ is the Bessel function of first kind and we used the Anger expansion given in appendix A. We can use the same procedure to obtain the transition matrix

$$
\begin{aligned}
{}_{k_2}\langle n|m\rangle_{k_1} &= \int_0^{2\pi} \mathrm{d}\theta \; {}_{k_2}\langle n|\theta\rangle\langle\theta|m\rangle_{k_1} && (4.43)\\
&= \frac{1}{2\pi}\int_0^{2\pi} \mathrm{d}\theta \mathrm{e}^{-\imath n\theta}\mathrm{e}^{\imath\frac{k_2}{n\epsilon+\bar{\beta}}\sin\theta}\mathrm{e}^{\imath m\theta}\mathrm{e}^{-\imath\frac{k_1}{m\epsilon+\bar{\beta}}\sin\theta} && (4.44)\\
&= \frac{1}{2\pi}\int_0^{2\pi} \mathrm{d}\theta \mathrm{e}^{\imath(m-n)\theta}\mathrm{e}^{\imath\left(\frac{k_2}{n\epsilon+\bar{\beta}}-\frac{k_1}{m\epsilon+\bar{\beta}}\right)\sin\theta} && (4.45)\\
&= J_{n-m}\left(\frac{k_2}{n\epsilon+\bar{\beta}}-\frac{k_1}{m\epsilon+\bar{\beta}}\right). && (4.46)
\end{aligned}
$$

We will put all this together in order to get the fidelity. As already discussed in the last section we use the more accurate energies for the time evolution. We will therefore keep $E_n^{k_{1,2}}$ and insert our energies from eq. (4.38) later. Inserting the WKB results into eq. (4.16) we get

$$
F(\beta,k_1,k_2,\epsilon,t) = \left|\sum_{n,m=-\infty}^{\infty} J_n\left(\frac{k_2}{n\epsilon+\bar{\beta}}\right)J_m\left(\frac{k_1}{m\epsilon+\bar{\beta}}\right)J_{m-n}\left(\frac{k_2}{n\epsilon+\bar{\beta}}-\frac{k_1}{m\epsilon+\bar{\beta}}\right)\mathrm{e}^{\imath\frac{t}{\epsilon}(E_n^{k_2}-E_m^{k_1})}\right|^2 \tag{4.47}
$$

This is the final formula for the fidelity of a single pendulum using the WKB method, whose properties we will discuss. We will see that the crude approximations in the representation of the energy eigenfunction and therefore also in the transition matrix are very god, and that the crucial dynamics lies in the spectral structure.

4.5 Properties of WKB Fidelity - Single Rotors

In this section we will discuss the properties of single rotors using the WKB approximation. In order to estimate the value of the solution we will do some benchmarks. The first benchmark is the $\epsilon \to 0$ limit. For this case an analytical theory exists [Abb09, Wim06]. After that we will compare the result using the WKB approximation to the numerical result for the pendulum. Basically the pendulum is exactly solvable by means of Mathieu functions, but we decided to stick to the numerical approximation of the pendulum instead of numerical estimation of the Mathieu functions. There are several reasons. One of the main reasons is that having a set of Mathieu functions for some k we might be able to get a representation of the initial state by means of Fourier series of the Mathieu function but if we want to compare two different k we have to calculate the

overlap of two Mathieu functions with different Mathieu parameters[4]. This is complicated and most probably just possible approximately. Another reason is the dependence on the fractional momentum β as already shown in chapter 3. This momentum implies an interesting structure of the spectrum which will also lead to more complicated dependencies in the Mathieu functions.

4.5.1 The $\epsilon \to 0$ Case

One of the most important benchmarks in this system is the $\epsilon \to 0$ case. In the case of the quantum kicked rotor there is a good theoretical understanding [Wim04]. In [Abb09] the pendulum approximation is used to develop a theory for near resonant rotors using the pendulum approximation. They also check the $\epsilon \to 0$ case. Their result for the fidelity of a resonantly kicked rotor in pendulum approximation is

$$F(k_1, k_2, t) = J_0\left(\frac{2\delta k}{\bar{\beta}} \sin\frac{\bar{\beta}t}{2}\right)^2. \tag{4.48}$$

We will now show that the WKB solution also reproduces this behaviour. Therefore we take the transformation matrix and the state vector in their integral representation eqs. (4.45) and (4.41). For small ϵ we can neglect the ϵ in the denominator of the exponent. As the energy difference in the exponent is divided by ϵ, only the term linear in ϵ in eq. (4.38) contributes to the difference of the energies in the phase factor of eq. (4.47). So we get $(E_n^{k_2} - E_m^{k_1})/\epsilon = \beta(n-m)$. Putting all together we get

$$\begin{aligned} F(k_1, k_2, t) = \Bigg| \sum_{n,m} \int_0^{2\pi} \mathrm{d}\theta \int_0^{2\pi} \mathrm{d}\theta' \int_0^{2\pi} \mathrm{d}\theta'' \mathrm{e}^{\imath \frac{t}{\epsilon}(E_n^{k_2} - E_m^{k_1})} \\ \times \langle \Psi_{\epsilon,\beta}(0)|\theta\rangle\langle\theta|n\rangle_{k_2\ k_2}\langle n|\theta'\rangle\langle\theta'|m\rangle_{k_1\ k_1}\langle m|\theta''\rangle\langle\theta''|\Psi_{\beta,\epsilon}(0)\rangle \Bigg|^2. \end{aligned} \tag{4.49}$$

This expression is equivalent to eq. (4.47) in the case of small ϵ. We decided to switch to the integral representation as we are able to use the sum in combination with the exponentials to obtain Dirac δ functions. There might also be an identity which makes it possible to start directly with eq. (4.47) but the way we proceed is much more intuitive. We insert the integral representations and rearrange the exponents:

$$\begin{aligned} &= \left| \sum_{n,m} \iiint \frac{\mathrm{d}\theta\mathrm{d}\theta'\mathrm{d}\theta''}{(2\pi)^3} \mathrm{e}^{\imath t\bar{\beta}(n-m)} \mathrm{e}^{\imath n\theta} \mathrm{e}^{-\imath\frac{k_2}{\bar{\beta}}\sin\theta} \mathrm{e}^{-\imath n\theta'} \mathrm{e}^{\imath\frac{k_2}{\bar{\beta}}\sin\theta'} \mathrm{e}^{\imath m\theta'} \mathrm{e}^{-\imath\frac{k_1}{\bar{\beta}}\sin\theta'} \mathrm{e}^{-\imath m\theta''} \mathrm{e}^{\imath\frac{k_1}{\bar{\beta}}\sin\theta''} \right|^2 \\ &= \left| \sum_{n,m} \iiint \frac{\mathrm{d}\theta\mathrm{d}\theta'\mathrm{d}\theta''}{(2\pi)^3} \mathrm{e}^{\imath n(\theta-\theta'+\bar{\beta}t)} \mathrm{e}^{-\imath\frac{k_2}{\bar{\beta}}\sin\theta} \mathrm{e}^{\imath\frac{k_2}{\bar{\beta}}\sin\theta'} \mathrm{e}^{\imath m(\theta''-\theta'-\bar{\beta}t)} \mathrm{e}^{-\imath\frac{k_1}{\bar{\beta}}\sin\theta'} \mathrm{e}^{\imath\frac{k_1}{\bar{\beta}}\sin\theta''} \right|^2 \end{aligned}$$

[4]The procedure does not give much hope to get a simple closed formula as we obtained using the WKB method. We decided therefore going the simple self made way instead of going the sophisticated one.

Now we do the summation and use $\sum_n \mathrm{e}^{\imath\theta n} = 2\pi\delta(\theta)$ to arrive at

$$F(k_1,k_2,t) = \Bigg| \iiint \frac{\mathrm{d}\theta\mathrm{d}\theta'\mathrm{d}\theta''}{2\pi} \times \delta(\theta-\theta'+\bar{\beta}t)\mathrm{e}^{-\imath\frac{k_2}{\beta}\sin\theta}\mathrm{e}^{\imath\frac{k_2}{\beta}\sin\theta'}\delta(\theta''-\theta'-\bar{\beta}t)\mathrm{e}^{\imath\frac{k_1}{\beta}\sin\theta'}\mathrm{e}^{-\imath\frac{k_1}{\beta}\sin\theta''}\Bigg|^2. \quad (4.50)$$

Due to the δ-functions the θ' and θ'' integrations lead to

$$\theta' = \theta - \bar{\beta}t \quad (4.51)$$

$$\theta'' = \theta' + \bar{\beta}t = \theta, \quad (4.52)$$

which brings us to

$$F(k_1,k_2,t) = \left| \int_0^{2\pi} \mathrm{d}\theta \frac{1}{2\pi}\mathrm{e}^{\imath\frac{k_2-k_1}{\beta}\sin(\theta-\bar{\beta}t)}\mathrm{e}^{-\imath\frac{k_2-k_1}{\beta}\sin\theta}\right|^2 \quad (4.53)$$

$$= \left| \frac{1}{2\pi}\int_0^{2\pi} \mathrm{d}\theta \mathrm{e}^{\imath\frac{\delta k}{\beta}2\cos\left(\theta-\frac{\bar{\beta}t}{2}\right)\sin\left(\frac{\bar{\beta}t}{2}\right)}\right|^2 \quad (4.54)$$

$$= J_0^2\left(\frac{2\delta k}{\bar{\beta}}\sin\left(\frac{\bar{\beta}t}{2}\right)\right), \quad (4.55)$$

where $\delta k \equiv k_2 - k_1$. This is exactly the result also derived in [Abb09]. Although the pendulum approximation has no meaning in the $\epsilon = 0$ case the leading contribution coincides with the result using a van Vleck propagator approach.

We have just checked that eq.(4.47) reproduces the expected result for $\epsilon \to 0$. In order to get more out of eq. (4.47) we need to discuss the different components. We will begin by discussing the properties of the coefficients and later have a look how the spectral structure influences the fidelity.

4.5.2 Dominating Matrix Elements

In this section we will describe the properties of the coefficients in eq. (4.47). We will split the terms in the sum in eq.(4.47) into an exponential and a coefficient[5]. As these coefficients have a dependency on n and m we introduce a coefficient matrix. We will refer to this interpretation when we talk about diagonal and off-diagonal terms. In order to understand the influence of the different terms in eq. (4.47) we will have a look to the entries of the coefficient matrix. Therefore we plotted the coefficients in fig. 4.1 as a function of β. In (a) all coefficients with $\max(|m|,|n|) < 10$ are plotted. By comparing with (b) we can see that the diagonal dominates the summation. For small β the $n,m = 0$ coefficient dominates. For growing β the neighbouring diagonal elements dominate. The off diagonal elements are suppressed.

[5] This is the coefficient we will talk about in this chapter.

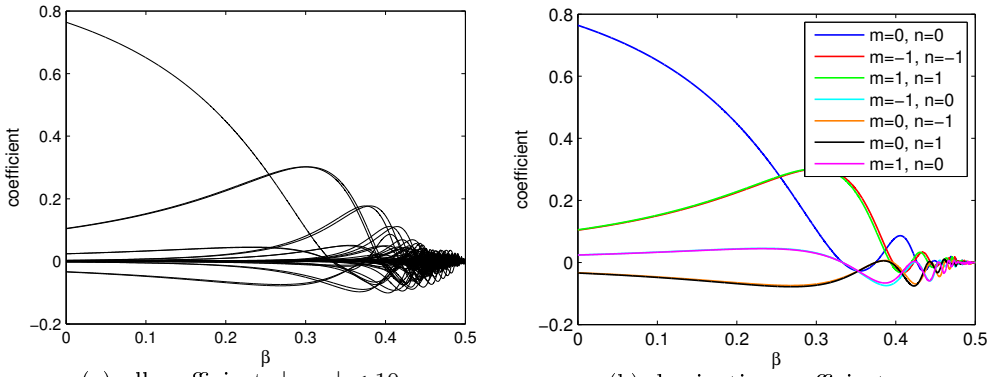

(a) all coefficients $|n, m| < 10$ (b) dominating coefficients

Figure 4.1: In this figure the coefficients of the complex exponentials from eq. (4.47) are shown for $\epsilon = 0.01$, $k_1 = 0.8\pi$, $k_2 = 0.8\pi$ and $\tau = 2\pi + \epsilon$. In (a) all coefficients with $\max(|m|, |n|) < 10$ are plotted as a function of β. In (b) the dominating coefficients are plotted. One can see that when β is small the central term with $n, m = 0$ dominates. With growing β the neighbouring diagonal elements dominate. The off diagonal elements are suppressed.

To understand this behaviour we need to recapitulate some properties of Bessel functions and have to remind ourselves of which $\bar{\beta}$ range the presented β range corresponds to. As described in chapter 3 the range of $\beta \in [0, 0.5]$ corresponds to $\bar{\beta} \in [-\pi, 0]$. For the interpretation this means that for β near zero we are in the regime of small argument of the Bessel functions and for β near to the resonance in the regime of larger argument. For Bessel functions with order different from zero we know that for small arguments we have [Abr64]

$$J_n(x) \propto \frac{2}{\sqrt{2\pi n}} \left(\frac{\mathrm{e}x}{2n}\right)^n, \tag{4.56}$$

And for large argument we know that they behave like

$$J_n(x) \approx \sqrt{\frac{2}{\pi x}} \cos\left(x - \frac{n\pi}{2} - \frac{\pi}{4}\right). \tag{4.57}$$

This means, that the Bessel functions have contributions only in an intermediate regime. This can be seen by considering for which values of the argument of the Bessel function leads to large values. This way the relevant regime for the argument of the Bessel function can be obtained. The lower boundary of the interval of importance is higher for larger orders. The coefficients in eq. (4.47) are products of Bessel functions of order n, m and $n-m$. In order to get large values the interval of contributions must have a maximal overlap because otherwise one Bessel function suppresses the contributions of the other. This means n, m should be similar and thus $n-m$ should be small. This is the reason why for small β the diagonal terms dominate. The off diagonal terms are suppressed by the Bessel function of order $n-m$, but for small argument in addition the $m = n \neq 0$ terms are also small. They grow when the argument is of similar magnitude as the order. Therefore they grow as β gets larger. Nevertheless they are suppressed more and more by the $n-m$ term as β grows. By this we can understand that

more and more coefficients contribute as we get closer to the resonant β although they decay in magnitude.

The case plotted in fig. 4.1 is already a case of big ϵ. In our numerics evaluation of eq. (4.47) we use coefficients with $\max(|m|, |n|) < 10$. This includes nearly all coefficients contributing up to $\beta \approx 0.4$.

4.5.3 Spectral Properties

In this section we will have a look at the quality of the approximation of the spectrum in eq. (4.38). Therefore we will compare it to the numerical result first. After that we will discuss the effect of the different orders in ϵ on the fidelity. Therefore we will also discuss a case with a very poor approximation in order to show where the decay in the pendulum fidelity originates.

To do the comparison with the numerical pendulum data we have to identify the energy levels from the numerics with those of the WKB theory. As already shown in chapter 3 due to β there can be nearly degeneracies. These degeneracies can be understood having a look at eq. (4.38). We can see that the dominating term is a n^2 term. This means that the energies are near to the parabola, as we would expect for the free rotor. So there can be terms which are nearly degenerate although the corresponding quantum numbers are very different. This corresponds to the degeneracy of left and right rotating states in the free rotor. As the numerics are done by diagonalising the matrices using algorithms of QL or QR type[6] [And99] we get the eigenvalues sorted by their value. This ordering is completely non-physical so we need to find some identification scheme to compare them.

We have to find a observable which allows us to identify the different energy levels. As already mentioned the dominating behaviour is the one of the rotor. There the degeneracy can be broken by distinguishing the momentum. If we calculate the momentum for the WKB energy eigenfunctions we see that ${}_k\langle n|\hat{I}|\psi_n\rangle_k = n\epsilon$. This means we could sort the WKB values by calculating the momentum. Therefore we also sort the numerical values by the momentum expectation value of the energy eigenfunctions. This is done in fig. 4.2. There we show the sorted momentum expectation values in black and the WKB result in red. We see that the states that are located on the island form a step in the momentum. They propagate with momentum $\bar{\beta}$ as this is the momentum offset, whilst island type states are not supposed to move as they are trapped on the island[7]. We see, therefore, that the WKB prediction just differs on the island. This is clear as the WKB method we used is made for rotating type states and therefore has to fail for oscillating states.

Another way to see this, is having a look at eq.(3.10). We can see that there are regimes where the diagonal dominate and regions where the off diagonal dominates. The entries on the diagonal are those of a rotor with momentum $n\epsilon +$

[6] This algorithms should not be mixed with the QR or QL decomposition. The QR algorithm is for example described in [Sch05a]. The algorithms have their name from their extensive use of the QR/QL decomposition but are themselves iterative algorithms for finding eigenvalues and vectors.

[7] This can be seen by having a look at harmonic eigenoscillator states. Their momentum expectation value is 0. Here β is an offset on the momentum and so the trapped states move with this momentum.

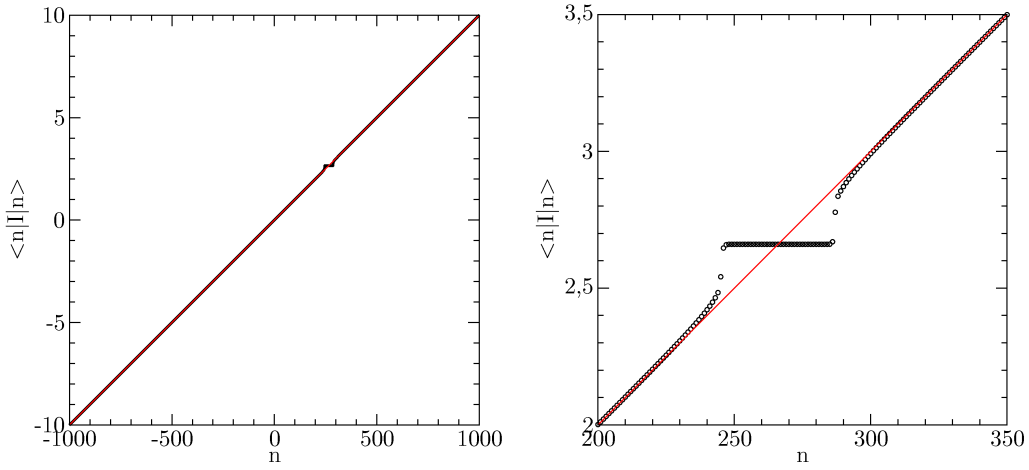

Figure 4.2: In this figure we want to illustrate the momentum structure of the pendulum energy eigenstates. We show the sorted momentum expectation values for $\epsilon = 0.01$, $k = 0.8\pi$ and $\beta \approx 0.07648$. In (a) the an overview is shown. In red we show the WKB expectation and in black the corresponding pendulum values, which are obtained using the numerical procedure described in chapter 3. In (b) we show the part which corresponds to the island in detail.

$\bar{\beta}$. This means that in the diagonal dominated regime m is still a good quantum number, whereas in regions with dominating side bands m is no good quantum number any more. This is an alternative motivation for the identification of energy eigenvalues we do. Having this identification we can now compare the energies.

This is done in fig. 4.3(a). The energy values follow the WKB prediction quite well. In fig. 4.3(b) the deviation near to $n = 0$ between the numerical energies and those in WKB approximation is shown in different orders of ϵ in eq. (4.38). We can see that we have to take up to $O(\epsilon^3)$ into account in order to match the qualitative features of the spectrum. All lower orders have systematic offsets or different slopes.

Next we will discuss some qualitative features of the fidelity of the pendulum by having a look at the different terms in eq. (4.38). In order to give a feeling what happens we will do a much cruder approximation which is not too bad for small times. We will have a look at the lowest order WKB solutions[8]

$$E_n = \frac{1}{2}(n\epsilon + \bar{\beta})^2 \tag{4.58}$$

$$\langle\theta|n\rangle_k = \frac{1}{\sqrt{2\pi}} \mathrm{e}^{\imath n\theta} \mathrm{e}^{-\imath \frac{k}{n\epsilon+\bar{\beta}} \sin\theta}. \tag{4.59}$$

[8]To be precise the formulation is not consistent. Squaring the first order is not the same as taking the square to second order. Nevertheless looking at eq. (4.63) we see that doing it the right way just contributes a common phase factor which does not change the result. Important is that the diagonal terms do not depend on n.

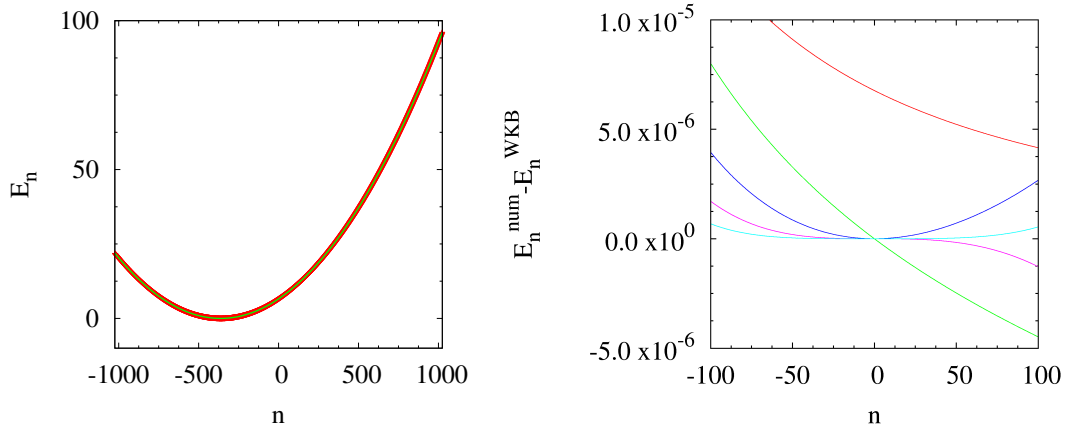

Figure 4.3: The numerical pendulum data is compared to the WKB result for $\beta \approx 0.07648$, $k = 0.8\pi$ and $\epsilon = 0.01$. The energy values are sorted by the corresponding $\langle\psi_n|\hat{I}|\psi_n\rangle$. This sorting has to be done because of of the (nearly) degeneracy due to the two sides of the minimum of the parabola in (a). There the pendulum spectrum (red) is shown and also the leading order in the WKB solution (black) is shown. One can see that the qualitative shape is met quite well. In (b) the difference of the WKB result eq. (4.38) to the numerical result is shown. Therefore we took the energy eq.(4.38) in different orders in ϵ. The red line is $O(\epsilon)$, the green line is $O(\epsilon^2)$, the blue line is $O(\epsilon^3)$, the magenta line is $O(\epsilon^4)$ and the cyan line is $O(\epsilon^5)$. It is obvious that only the solution with at least order ϵ^3 reproduces the characteristic features in the vicinity of $n = 0$.

Inserting this into eq. (4.16) we arrive at

$$F(k_1,k_2,\beta,t) = \left| \sum_{n,m} J_n\left(\frac{k_2}{n\epsilon+\bar{\beta}}\right) J_m\left(\frac{k_1}{m\epsilon+\bar{\beta}}\right) J_{n-m}\left(\frac{k_2}{n\epsilon+\bar{\beta}} - \frac{k_1}{m\epsilon+\bar{\beta}}\right) \mathrm{e}^{-\frac{\imath}{2}t\left((n^2-m^2)\epsilon-(n-m)\bar{\beta}\right)} \right|^2 \tag{4.60}$$

$$= \left| \sum_{n} J_n\left(\frac{k_2}{n\epsilon+\bar{\beta}}\right) J_n\left(\frac{k_1}{n\epsilon+\bar{\beta}}\right) J_0\left(\frac{k_2-k1}{n\epsilon+\bar{\beta}}\right) + \sum_{\substack{n,m \\ n\neq m}} J_n\left(\frac{k_2}{n\epsilon+\bar{\beta}}\right) J_m\left(\frac{k_1}{m\epsilon+\bar{\beta}}\right) J_{n-m}\left(\frac{k_2}{n\epsilon+\bar{\beta}} - \frac{k_1}{m\epsilon+\bar{\beta}}\right) \times \mathrm{e}^{-\frac{\imath}{2}t\left((n^2-m^2)\epsilon-(n-m)\bar{\beta}\right)} \right|^2 . \tag{4.61}$$

Here we can see that the first sum over n only does not depend on time which means that it leads to a non decaying component. This is shown in fig. 4.4(a). There a pendulum and the WKB approximation eq. (4.61) are compared. There

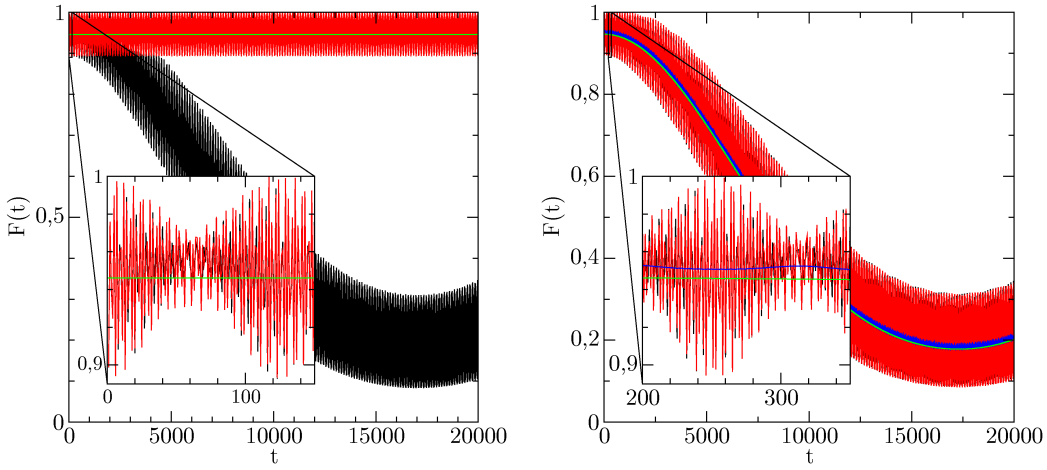

Figure 4.4: In this figure we compare the WKB result (red) to the numerical result for the pendulum (black). We show the $\beta \approx 0.7486$, $k_1 = 0.6\pi$, $k_2 = 0.8\pi$, $\epsilon = 0.05$ case. In (a) we show the fidelity with the simple spectrum of eq.(4.58). Obviously the oscillations are reproduced quite well but the decay is not included. In green the saturation value of the first term in eq. (4.61) is shown. It describes the offset quite well. In (b) the fidelity is calculated using the more detailed spectrum from eq. (4.38). It reproduces the oscillations and the decay well. In blue the running average over 50 kicks is shown. In green we plotted the contribution of the diagonal terms. As we can see it reproduces the averaged fidelity quite well.

are two characteristic features; the decay and the oscillations modulated on it. The oscillations are described well by the WKB solution where the decay is not covered. On the other hand the first sum in eq.(4.61) can be evaluated and describes the saturation value quite well.

In order to include the decay we have to include terms in the energy which do not vanish trivially as the diagonal $n = m$ terms in eq. (4.61). This means we need to include further terms in order to get rid of this behaviour. Therefore we have a look at eq. (4.38). The ϵ^2 term will not destroy the saturation as it is a common phase of all diagonal terms. It even has a part independent of n or m which contributes a phase to all terms and which means that the overlap is spinning in the complex plane[9]. The ϵ^3 term is the first term which really gives each diagonal term an unique phase evolution so that we cannot find a partial sum having a common phase.

We give the energy differences needed in the exponent in eq. (4.47). From eq. (4.38) we obtain

$$\Delta E_{n,m} \equiv E^n_{k_2} - E^m_{k_1} = \\ (n-m)\bar{\beta}\epsilon + \left(\frac{n^2-m^2}{2} + \frac{k_2^2-k_1^2}{4\bar{\beta}^2}\right)\epsilon^2 - \frac{k_2^2 n - k_1^2 m}{2\bar{\beta}^3}\epsilon^3 + O(\epsilon^4). \quad (4.62)$$

In order to see the structure more clearly, we rewrite the expression by introducing

[9] Nevertheless this term will be very important when building ensembles as it carries the strongest $\bar{\beta}$ dependency.

the distance to the diagonal d by $n = m + d$. This way we obtain

$$\Delta E_{m+d,m} = d\bar{\beta}\epsilon + \left(\frac{d^2 + 2dm}{2} + \frac{k_2^2 - k_1^2}{4\bar{\beta}^2}\right)\epsilon^2 - \frac{k_2^2 d + (k_2^2 - k_1^2)m}{2\bar{\beta}^3}\epsilon^3 + O(\epsilon^4). \quad (4.63)$$

We can see that most of the terms contain a factor d which means that they vanish on the diagonal. The leading order of the energy difference terms on the diagonal are of order ϵ^3 as the ϵ^2 term contains no m. The ϵ^2 term even has a contribution containing no m or d which means that it is a common phase for all terms. It will be important if we average over different $\bar{\beta}$ as it might not be sensitive to different m but it is to different $\bar{\beta}$. Nevertheless the diagonal elements contribute the smallest energies to the time evolution and therefore also the longest time scales.

Inserting eq. (4.63) into eq. (4.47) we obtain

$$F(\beta, k_1, k_2, \epsilon, t) = \left| \sum_{m=-\infty}^{\infty} J_m\left(\frac{k_2}{m\epsilon + \bar{\beta}}\right) J_m\left(\frac{k_1}{m\epsilon + \bar{\beta}}\right) J_0\left(\frac{k_2 - k_1}{m\epsilon + \bar{\beta}}\right) \mathrm{e}^{\imath \frac{t}{\epsilon} \Delta E_{m,m}} \right.$$
$$\left. \sum_{\substack{n,m=-\infty \\ n \neq m}}^{\infty} J_n\left(\frac{k_2}{n\epsilon + \bar{\beta}}\right) J_n\left(\frac{k_1}{m\epsilon + \bar{\beta}}\right) J_{m-n}\left(\frac{k_2}{n\epsilon + \bar{\beta}} - \frac{k_1}{m\epsilon + \bar{\beta}}\right) \mathrm{e}^{\imath \frac{t}{\epsilon} \Delta E_{n,m}} \right|^2. \quad (4.64)$$

We are interested to describe the long time behaviour. In fig. 4.4 we could see that the off-diagonal elements and the leading energy terms already give rise to the fast oscillations. As the diagonal carries the low energies we have to analyse their structure in order to understand the long time behaviour. The coefficients of the diagonal terms are shown in detail in fig. 4.5. These coefficients decay very fast for not too small $\bar{\beta}$ and k. The sign of the coefficient is invariant with respect to the change from $m \to -m$ in the argument of the Bessel functions as both Bessel functions on the left contribute the same sign and it therefore cancels. Nevertheless, for $\epsilon \neq 0$, the argument of the Bessel function does not have this property. However the difference due to this asymmetry is very small. In fig. 4.5(b) we plotted the effect due to the m dependency of the argument. To show this we plotted

$$\left| J_m\left(\frac{k_1}{\bar{\beta}}\right) J_m\left(\frac{k_1}{\bar{\beta}}\right) J_0\left(\frac{k_1 - k_2}{\bar{\beta}}\right) - J_m\left(\frac{k_1}{\bar{\beta} + \epsilon m}\right) J_m\left(\frac{k_1}{\bar{\beta} + \epsilon m}\right) J_0\left(\frac{k_1 - k_2}{\bar{\beta} + \epsilon m}\right) \right|. \quad (4.65)$$

This difference is very small and we can also see that for small m even the relative difference is small compared to fig. 4.5(a). Therefore we neglect this m dependence of the argument and only keep it in the order of the Bessel functions.

The coefficients in fig. 4.1 have a quadratic shape. For Bessel functions we can give the series representation of eq. (A.9). For small argument we just take the first term in this expansion. This means for large n using Stirling's approximation [Abr64],we get

$$J_n(x) \approx \frac{x^n}{2^n n!} \approx \frac{1}{\sqrt{2\pi n}} \left(\frac{\mathrm{e}x}{2n}\right)^n. \quad (4.66)$$

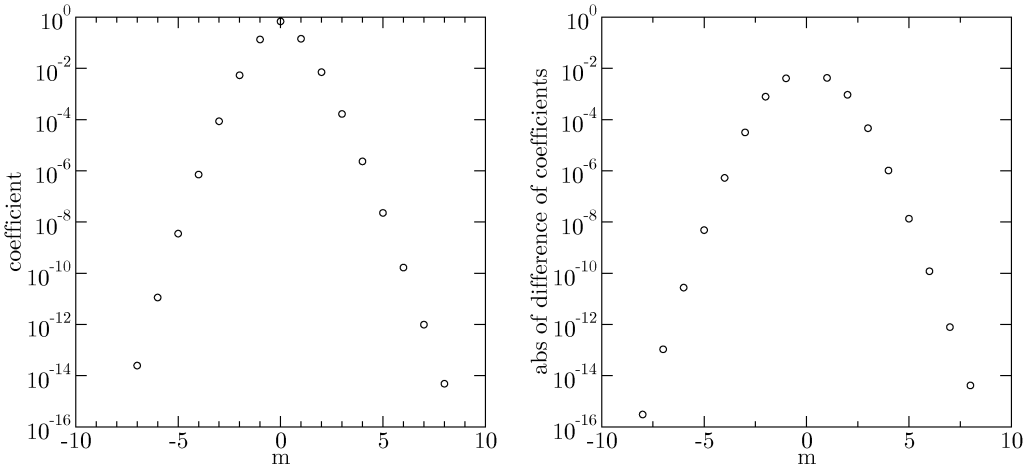

(a) strength of asymmetry and magnitude of coefficients

(b) difference of coefficients with and without n dependency in the argument of the Bessel functions

Figure 4.5: In this figure we show some of the properties of the diagonal coefficients. We show the $\beta \approx 0.7486$, $k_1 = 0.6\pi$, $k_2 = 0.8\pi$, $\epsilon = 0.05$ case. In (a) the coefficients of the diagonal terms in eq. (4.64) are plotted. We can see that they decay rapidly with growing order of the Bessel functions. Comparing the m with the $-m$ coefficients we see that there is just a weak asymmetry. This asymmetry is due to the m dependency of the argument of the Bessel functions. This is shown in (b). Here we see the absolute value of the difference of the coefficients with argument $k/\bar{\beta}$ and $k/(\bar{\beta} + \epsilon m)$, see eq. (4.65). We see that the difference is very small. Both figures are in semi-logarithmic scale. Especially for small m also the relative difference is small.

In our case the argument is much smaller as the order. The difference between the arguments for different k is also small compared to the order. Therefore we neglect the m dependence and assume that the arguments are equal. We will call this argument x. Applying this approximation we obtain

$$J_n(x)J_n(x)J_0(x) \propto \frac{1}{2\pi n}\Big(\frac{ex}{2n}\Big)^n\Big(\frac{ex}{2n}\Big)^n = \frac{1}{2\pi n}\Big(\frac{\mathrm{e}x}{2n}\Big)^{2n}. \tag{4.67}$$

Taking the logarithm and neglecting terms proportional to $\ln n$ we see that the dominating term is a n^2 term. We can see this scaling also in fig. 4.5(b). This ensures also that the coefficients on the diagonal drop very quickly.

We will now insert this approximations into eq. (4.64). This means we will neglect the m dependency in the denominator of the arguments of all Bessel functions.

$$F(k_1,k_2,\beta,t) \approx \left|\mathrm{e}^{\imath\frac{k_2^2-k_1^2}{4\bar{\beta}^2}\epsilon t}\sum_{m=-\infty}^{\infty} J_m\Big(\frac{k_1}{\bar{\beta}}\Big)J_m\Big(\frac{k_2}{\bar{\beta}}\Big)J_0\Big(\frac{k_2-k_1}{\bar{\beta}}\Big)\mathrm{e}^{-\imath\frac{k_2^2-k_1^2}{2\bar{\beta}^3}m\epsilon^2 t} + f_{\text{offdiag}}\right|^2 \tag{4.68}$$

$$\approx \Bigg| J_0\Big(\frac{k_1}{\bar\beta}\Big) J_0\Big(\frac{k_2}{\bar\beta}\Big) J_0\Big(\frac{k_2-k_1}{\bar\beta}\Big) + \sum_{m=1}^{\infty} J_m\Big(\frac{k_1}{\bar\beta}\Big) J_m\Big(\frac{k_2}{\bar\beta}\Big) J_0\Big(\frac{k_2-k_1}{\bar\beta}\Big) \Big(\mathrm{e}^{-\imath m \frac{k_1^2-k_2^2}{2\bar\beta^3}\epsilon^2 t} + \mathrm{e}^{\imath m \frac{k_1^2-k_2^2}{2\bar\beta^3}\epsilon^2 t} \Big) + \mathrm{e}^{\imath \frac{k_1^2-k_2^2}{4\bar\beta^2}\epsilon t} f_{\text{offdiag}} \Bigg|^2 \tag{4.69}$$

$$= \Bigg| J_0\Big(\frac{k_1}{\bar\beta}\Big) J_0\Big(\frac{k_2}{\bar\beta}\Big) J_0\Big(\frac{k_2-k_1}{\bar\beta}\Big) + 2\sum_{m=1}^{\infty} J_m\Big(\frac{k_1}{\bar\beta}\Big) J_m\Big(\frac{k_2}{\bar\beta}\Big) J_0\Big(\frac{k_2-k_1}{\bar\beta}\Big) \cos\Big(m\frac{k_1^2-k_2^2}{2\bar\beta^3}\epsilon^2 t\Big) + \mathrm{e}^{\imath \frac{k_1^2-k_2^2}{4\bar\beta^2}\epsilon t} f_{\text{offdiag}} \Bigg|^2 . \tag{4.70}$$

In the discussion we will use this approximation and the different terms very often. What we have just given is the basic idea of the approximation. Motivated by this idea we will give own names the different parts of the fidelity. The first idea is to separate the diagonal and the off diagonal contributions by $F = |f_{\text{diag}}^{\text{exact}} + f_{\text{offdiag}}|^2$. This leads to the definition of

$$f_{\text{diag}}^{\text{exact}} \equiv \mathrm{e}^{\imath \frac{k_2^2-k_1^2}{4\bar\beta^2}\epsilon t} \sum_{m=-\infty}^{\infty} J_m\Big(\frac{k_1}{m\epsilon+\bar\beta}\Big) J_m\Big(\frac{k_2}{m\epsilon+\bar\beta}\Big) J_0\Big(\frac{k_2-k_1}{m\epsilon+\bar\beta}\Big) \mathrm{e}^{-\imath \frac{k_2^2-k_1^2}{2\bar\beta^3} m\epsilon^2 t}. \tag{4.71}$$

The next step in the approximation was to neglect the m dependency of the argument which motivates the definition of

$$f_{\text{diag}} \equiv \mathrm{e}^{\imath \frac{k_2^2-k_1^2}{4\bar\beta^2}\epsilon t} \Bigg(J_0\Big(\frac{k_1}{\bar\beta}\Big) J_0\Big(\frac{k_2}{\bar\beta}\Big) J_0\Big(\frac{k_2-k_1}{\bar\beta}\Big) + 2\sum_{m=1}^{\infty} J_m\Big(\frac{k_1}{\bar\beta}\Big) J_m\Big(\frac{k_2}{\bar\beta}\Big) J_0\Big(\frac{k_2-k_1}{\bar\beta}\Big) \cos\Big(m\frac{k_1^2-k_2^2}{2\bar\beta^3}\epsilon^2 t\Big) \Bigg). \tag{4.72}$$

These approximation will be the starting point for the theory for ensembles. Therefore it is important to define a versatile vocabulary here.

In order to understand the value of this approximation we will first compare it to the result without the approximations, which is done in fig. 4.6. In fig. 4.6(a) we show f_{diag} including terms up to $m = 2$ and $f_{\text{diag}}^{\text{exact}}$. We can see that the first few terms inherit most of the characteristics and the differences are very small. In fig. 4.6(b) we compare the approximation from fig. 4.6(a) to the full WKB result and the pendulum. f_{diag} describes the long time behaviour of the WKB result very well which means that the long time behaviour is determined by the diagonal terms as already suspected. Unfortunately the WKB result misses the decay of amplitude seen in the pendulum case. This effect will be much stronger when being near the nonlinear resonance island. In chapter 5 we will discuss the behaviour in different regimes and in this discussion also some considerations how to explain this decay.

We have now a pretty good description for the fidelity of single rotors in comparison to the pendulum. Now we can go on and see what we can find out on the fidelity of ensembles of rotors.

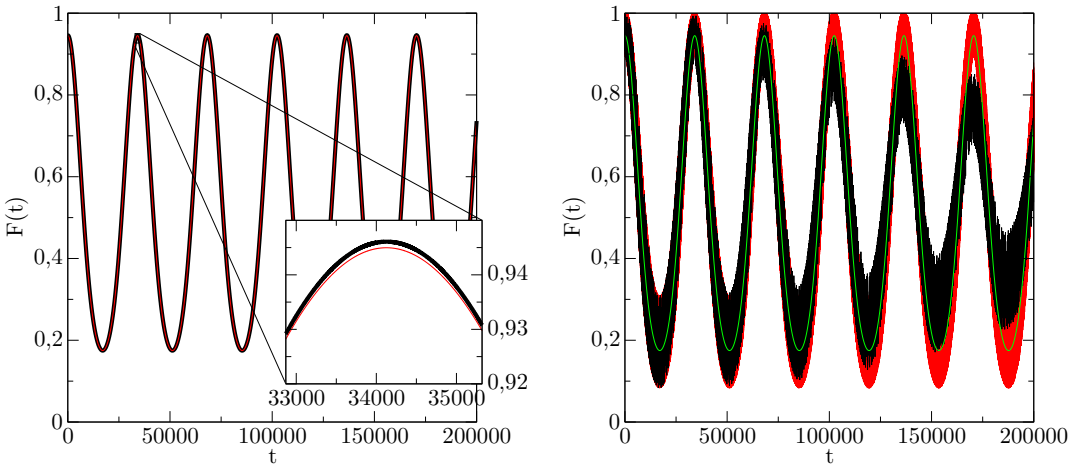

(a) comparison of approximation to full result

(b) comparison to full WKB and pendulum

Figure 4.6: In this figure we compare eq. (4.70) to the full WKB result, the full diagonal result $f_{\text{diag}}^{\text{exact}}$ and the pendulum result. We show the $k_1 = 0.6\pi$, $k_2 = 0.8\pi$, $\epsilon = 0.05$ and $\beta \approx 0.07648$ case. In (a) we compare f_{diag} (red) to the $f_{\text{diag}}^{\text{exact}}$ (black). In f_{diag} we included the terms up to $m = 2$. In the inset we can see that the difference is very small. In (b) we show the full WKB result (red), the pendulum result (black), and $|f_{\text{diag}}|^2$ (green),. The diagonal result approximates the long-time behaviour of the WKB result very well which unfortunately misses some decay of amplitude compared to the pendulum result.

4.6 Properties of WKB Fidelity - Ensembles

As mentioned in chapter 2 one cannot prepare single rotors but rather ensembles of rotors in the experimental set ups. Therefore we need to understand the effects due to building an ensemble. Unfortunately we could not arrive at a closed theory for these ensembles. Therefore we will give some rather weak results for the fidelity of pendulums. As we will mention in chapter 5 there are also some problems in the QKR-pendulum correspondence.

We will use a special set of parameters, which will be introduced and justified in the plots in chapter 5. To build an analytical formula we will take eq. (4.72) and use it to build an ensemble. But first we would like to give an idea of the mechanism which leads to the decay.

In subsection 4.5.3 we showed how $\Delta E_{n,m}$ influences the fidelity on the corresponding time scale. Therefore we focused on the dynamics of single rotors. Now we will focus onto the dynamics of an average over several rotors. As introduced in chapter 2 the average is defined as

$$F(k_1, k_2, \epsilon, t) = \left| \int_{\beta_1}^{\beta_2} f(\beta, k_1, k_2, \epsilon, t) \mathrm{d}\beta \right|^2, \tag{4.73}$$

where f is the overlap and $\beta_{1/2}$ are the boundaries of the averaging interval. When discussing single rotors we focused on the interplay of $\Delta E_{n,m}$ with the coefficients by focusing on the dependence on n and m. In ensembles also different β contribute to the result. We will see that the averaging introduces a decay of

fidelity. This decay can be understood by the oscillations that are generated when varying β. In order to understand the approximations we do, it is important to understand how averaging of a fast oscillating function leads to a decay.

One example of this mechanism was already used in section 4.1. There we used the stationary phase approximation to introduce the Legendre transformation. The stationary phase approximation is used when dealing with integrals over oscillating terms. One example of such an expression is

$$F(\lambda) = \int_{\infty}^{\infty} \mathrm{d}t \mathrm{e}^{\imath\lambda f(t)}. \tag{4.74}$$

By expanding the exponent in a Taylor series around an isolated extremal point we arrive at an expression whose leading term is quadratic. Truncating after this term we can integrate the resulting Fresnel integral and we obtain

$$F(\lambda) = \int_{-\infty}^{\infty} \mathrm{d}t \mathrm{e}^{\imath\lambda f(t)} \approx \sqrt{\frac{2\pi\imath}{\lambda f''(t_0)}} \mathrm{e}^{\imath\lambda f(t_0)}. \tag{4.75}$$

This example from [Sch96] shows that fast oscillating functions behave like Dirac δ-functions. In this case the oscillating function extracts the point of stationary phase. The same mechanism is also used in the theory of Dirac series. These are series of functions whose integral is 1 and which converge to 0 nearly everywhere. This series can be used to derive the Dirac δ-distribution [Arf08]. Two well known examples for such series are the sinc representation and the Fresnel representation. In this examples a $\sin(t/\epsilon)/t$ and an $\mathrm{e}^{\imath t^2/\epsilon}\sqrt{\epsilon}$ term are used to obtain the Dirac property in the limit $\epsilon \to 0$.

To show how oscillations can lead to a δ-function like behaviour we have a look at

$$\int_a^b \mathrm{e}^{\imath t x} \mathrm{d}x = \frac{1}{\imath t}\, \mathrm{e}^{\imath \frac{b+a}{2} t}\, 2\imath \sin\Big(\frac{b-a}{2} t\Big). \tag{4.76}$$

In the limit $t \to \infty$ we observe a $1/t$ decay. If we assume $t = 1/\epsilon$ and $a \approx b$ this is an approximation of the sinc representation. This example shall show how integrals over oscillating functions decay when increasing the oscillation frequency as long as the integration interval does not contain a point of stationary phase.

This is the mechanism we will use in the following. At first we will identify the important terms. Then we will do some approximations which allow us to arrive at an analytical approximative expression for the fidelity.

Diagonal Approximation

We showed that a strong dependence on β in the exponent leads to a decay. The exponent is given by $t\Delta E_{n,m}/\epsilon$. In the regime where $\bar{\beta}$ is not too close to zero the first term in eq. (4.63) has the strongest effect. This means that the off-diagonal terms have a very fast decay due to the averaging procedure. To check this we compare $|f_{\mathrm{diag}}^{\mathrm{exact}}|^2$ to the fidelity of the pendulum. This is shown in fig. 4.7. We can see that on longer time scales the decay of the fidelity of the pendulum is well

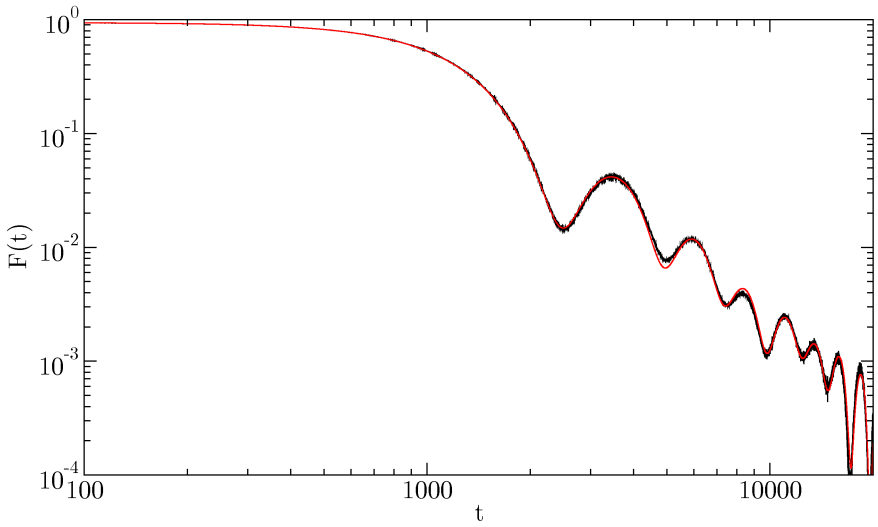

Figure 4.7: In this figure we compare the ensemble using f_{diag} to the fidelity of the pendulum. We used $k_1 = 0.6\pi$, $k_2 = 0.8\pi$, $\epsilon = 0.05$, and $\beta \in [0.035, 0.135]$. For the diagonal WKB ensemble we used 10000 rotors and for the pendulum we used ≈ 70000 rotors. We can see that the diagonal approximation describes the pendulum data very well.

described by the diagonal terms of the WKB result. On the other hand we can see that the off-diagonal terms have hardly any influence for longer time scales.

First we will also do the approximations shown in the last section. This means we neglect the m dependency of the argument of the Bessel functions. We will therefore recall the definition of f_{diag} and introduce a new notation

$$f_{\text{diag}} \equiv \mathrm{e}^{\imath \frac{k_2^2 - k_1^2}{4\bar{\beta}^2} \epsilon t} \left(c_{00} + 2 \sum_{m=1}^{\infty} c_{mm} \cos\left(m \frac{k_1^2 - k_2^2}{2\bar{\beta}^3} \epsilon^2 t \right) \right) \tag{4.77a}$$

$$c_{mn} \equiv J_m\left(\frac{k_1}{\bar{\beta}}\right) J_n\left(\frac{k_2}{\bar{\beta}}\right) J_0\left(\frac{k_2 - k_1}{\bar{\beta}}\right) \tag{4.77b}$$

A difference to single rotors is that we also need to consider the $\bar{\beta}$ dependence of the coefficients. As we can see in fig. 4.1, far away from the island[10] the $\bar{\beta}$ dependency is very weak. Therefore we neglect this dependence and assume that the coefficients are constant. We fix their value at the arithmetical mean of the integration boundaries. Thiis choice is arbitrary and might not be the best. It is made to simplify the equations which will arise in the following calculations.

Neglecting the $\bar{\beta}$ dependence in the argument of the Bessel function reduces the calculation of the ensemble to the structure of the exponent. So we have to focus on its $\bar{\beta}$ dependence. We can see that the exponent has a $1/\bar{\beta}^2$ and a $1/\bar{\beta}^3$ dependence. In the example above we showed how to integrate a phase factor with linear dependence on the phase. Integrals of the form

$$P_\alpha(x) = \int_a^b \mathrm{e}^{\imath x z^\alpha} \mathrm{d}z \tag{4.78}$$

[10] For the parameters in fig. 4.1 the island has a diameter of ≈ 0.2 in units of β. This means the rotors with $\beta < 0.4$ are of rotating type and the others are of oscillating, and therefore island, type.

cannot be expressed by means of simple function. We showed that we can give a simple expression in for $\alpha = 1$ but already for $\alpha = 2$ we need Fresnel integrals. We do not know any simple solutions for $\alpha < 1$. As only linear exponents can be integrated in a simple way we need to linearise the phase. This can be done by means of Taylor expansion. We expand the exponent at the middle of the integration interval. This leads to the following approximations and definitions

$$\frac{1}{\bar{\beta}^2} \approx \frac{1}{\tilde{\beta}^2} - \frac{2}{\tilde{\beta}^3}\delta\bar{\beta} \qquad \frac{1}{\bar{\beta}^3} \approx \frac{1}{\tilde{\beta}^3} - \frac{3}{\tilde{\beta}^4}\delta\bar{\beta} \qquad \tilde{\beta} = \frac{\bar{\beta}_1 + \bar{\beta}_2}{2} \qquad \bar{\beta} = \tilde{\beta} + \delta\bar{\beta}, \tag{4.79}$$

where $\bar{\beta}_1$ and $\bar{\beta}_2$ are the boundaries of the averaging interval. Introducing this approximation into eq. (4.77a) we obtain

$$f_{\text{diag}}^{\text{app}} \equiv \mathrm{e}^{\imath\frac{k_2^2-k_1^2}{4}\left(\frac{1}{\tilde{\beta}^2}-\frac{2}{\tilde{\beta}^3}\delta\beta\right)\epsilon t}\left(c_{00} + 2\sum_{m=1}^{\infty} c_{mm}\cos\left(m\frac{k_1^2-k_2^2}{2}\left(\frac{1}{\tilde{\beta}^3}-\frac{3}{\tilde{\beta}^4}\delta\beta\right)\epsilon^2 t\right)\right). \tag{4.80}$$

This expression can be integrated. We will show here as an example the integration of the c_{00} term. This will explain the general procedure. After writing the cosine as a sum of complex exponentials the same method can be used for the other terms too. As the calculations are lengthy and not very enlightening we refer to appendix D. Defining $\delta_{k^2} \equiv k_2^2 - k_1^2$ and $\delta \equiv \bar{\beta}_2 - \bar{\beta}_1$ we can give the contribution of the c_{00} term by

$$\int_{\beta_1}^{\beta_2} \mathrm{e}^{\imath\frac{k_2^2-k_1^2}{4\bar{\beta}^2}\epsilon t}\mathrm{d}\bar{\beta} \approx \int_{-\delta/2}^{\delta/2} \mathrm{e}^{\imath\frac{\delta_{k^2}}{4}\left(\frac{1}{\tilde{\beta}^2}-\frac{2}{\tilde{\beta}^3}\delta\beta\right)\epsilon t}\mathrm{d}\delta\bar{\beta} \tag{4.81}$$

$$= \frac{1}{\epsilon t}\frac{2\tilde{\beta}^3}{\delta_{k^2}}\mathrm{e}^{\imath\frac{\delta_{k^2}}{4\tilde{\beta}^2}\epsilon t}\sin\left(\frac{\delta_{k^2}}{4\tilde{\beta}^3}\delta\ \epsilon t\right). \tag{4.82}$$

In appendix D we defined $I(k_1, k_2, m, \epsilon, \tilde{\beta}, t)$ which allows us to give the complete integral as

$$\int_{\beta_1}^{\beta_2} f_{diag}^{app}\mathrm{d}\bar{\beta} \approx \frac{2\tilde{\beta}^3}{\delta_{k^2}\epsilon t}\mathrm{e}^{\imath\frac{\delta_{k^2}\epsilon t}{2\tilde{\beta}^3}}\left(c_{00}\sin\left(\frac{\delta_{k^2}}{4\tilde{\beta}^3}\delta\epsilon t\right) + \sum_{m=1}^{2} c_{mm} I(k_1, k_2, m, \epsilon, \tilde{\beta}, t)\right). \tag{4.83}$$

This is the final formula for ensembles in diagonal approximation. The result is shown in fig. 4.8. There the same data from fig. 4.7 and the theoretical result of eq. (4.83) are plotted. We can see that the result reproduces some of the qualitative features. It reproduces the period of the oscillations and the decay behaviour approximately. The period of $f_{\text{diag}}^{\text{app}}$ is a little bit too long and eq. (4.83) overestimates the minima.

The deviation can be understood by reconsidering the approximations we did. To get a feeling of what approximation has which effect we plotted the different stages of approximation in fig. 4.9. Neglecting the m dependency does hardly change anything. This is expected as we already showed in fig. 4.5(a) that the error is very small. The negligence of the $\bar{\beta}$ dependency has a much larger effect.

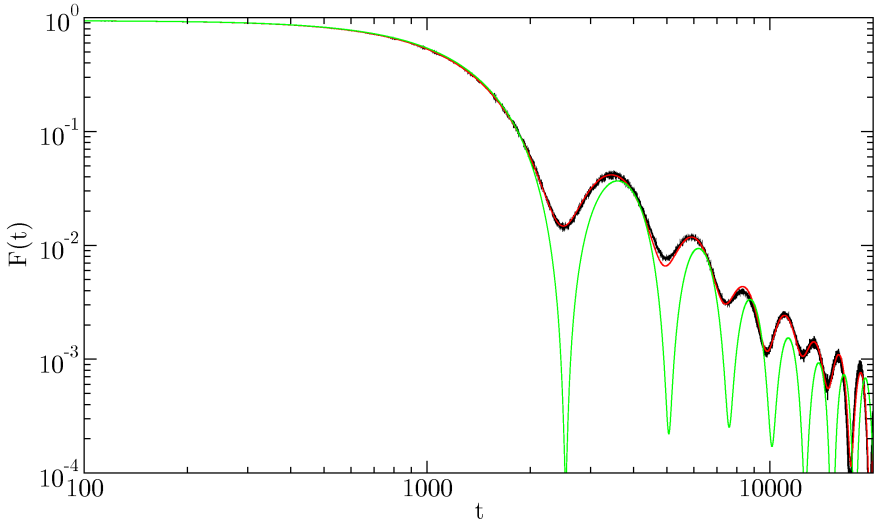

Figure 4.8: This figure shows the same setting as fig. 4.7 but also includes the theoretical result (green) from eq. (4.83). We can see that the theoretical curve describes the decay pretty well and it also describes the oscillationsapproximately.

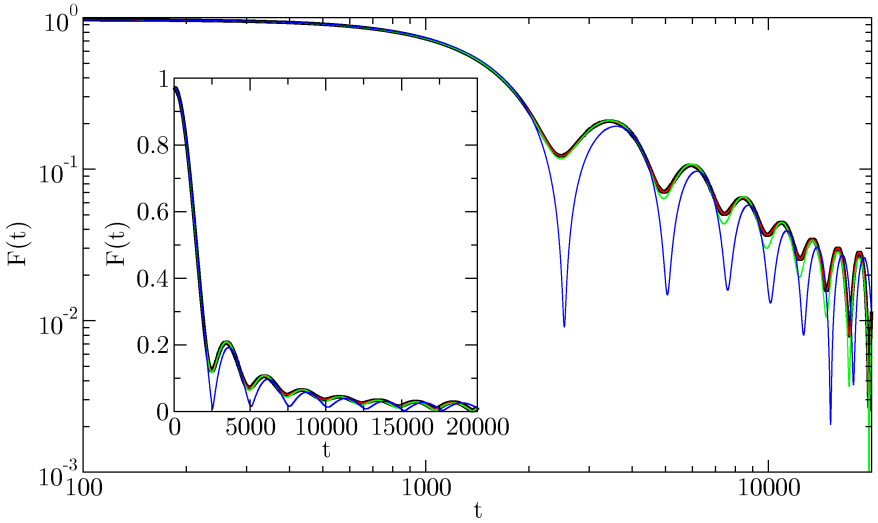

Figure 4.9: In this figure the different stages of the approximation leading to eq. (4.83) are shown. As usual we show the case of $k_1 = 0.6\pi$, $k_2 = 0.8\pi$, $\epsilon = 0.05$, and $\beta \in [0.035, 0.135]$. The figure contains an ensemble using $f_{\text{diag}}^{\text{exact}}$ (black), the same but with neglected m dependence in the arguments of the Bessel functions (f_{diag}) (red), the result with neglected m dependence and introduction of $\tilde{\beta}$ to the arguments of the Bessel functions (green), and in the end the result from eq. (4.83), where also the phase dependence is simplified ($f_{\text{diag}}^{\text{app}}$) (blue). We can see that the first approximations are small and the largest deviation is due to the simple phase approximation. In the inset the same data is shown on a linear scale. Comparing these to the logarithmic scaling we can see that the absolute correspondence is not as good as the logarithmic plot pretends. Nevertheless we can deduce the essential features of the decay

This can be understood as by doing this approximation we match two coefficients perfectly to obtain a cosine in eq. (4.77a). In the exact WKB result[11] there would not be a perfect match and therefore we would still see the small difference in the minimum. The fidelity does not decay to zero as we still have the $1/\bar{\beta}^{\alpha}$ in the exponent. This prevents a perfect match. Therefore the green line overestimates the minimum only slightly. By removing the non linear $\bar{\beta}$ dependency in the exponent we generate a perfect match of the phases. By enforcing this match we were able to introduce the sine in eq. (4.82) and eq. (D.5). This is also the reason why we fixed $\tilde{\beta}$ to be the arithmetical mean of the integration boundaries. The price we pay is an overestimation of the minima.

In the inset of fig. 4.9 we can see that the position of the maxima gets worse for longer times but the hight of the maxima is met quite well. As already mentioned we chose $\tilde{\beta}$ in order to get the sine in eq. (4.82) and eq. (D.5). This choice might be bad for approximating a function which is a sum of a $1/\bar{\beta}^2$ and a $1/\bar{\beta}$ term. A linear approximation has to miss the skewness of such a function. Therefore we probably have chosen not the best $\tilde{\beta}$ for the description of the period of the oscillations in fig. 4.9. A linear approximation reproducing the average value and the average slope would be better but would be more arbitrary, as it is no expansion of the exponent, and the formulas would be more complicated.

4.7 Summary

In this chapter we introduced an approximative theory for the pendulum using the WKB approximation. We had to use approximations of different quality in order to be able to get a closed picture. Especially the evaluation of the wave function was only possible in leading order in a consistent way. For the spectrum we were able to give a procedure that reproduces the spectrum in high precision. Nevertheless we have to keep in mind that this approximation can only be valid in the rotator like regime and has to fail near the island. In the picture of the WKB spectrum one is able to develop a better understanding of the behaviour observed in fig. 3.2. Although we are able to understand the structure of the dependence of the rotator like states on β by the WKB spectrum we cannot explain avoided crossings in our semi-classical theory. In the picture of WKB we expect real crossings whereas from the point of view of quantum mechanics we did not find a reason why the crossing should not be avoided and in the lower lying levels avoided crossings can be seen. In chapter 3 we also pointed out the similarity to the band model in which at the one border a gap exists in first order perturbation theory. We did not follow this question although it would be interesting to understand why and how the WKB approximation is getting unstable near this crossings.

We could give an approximative result for the fidelity of small ensembles. However this approximation is very crude and we do not have a very strict estimation of the error. This theory is surely a first shot as presented here. One

[11] We still use the WKB approximation as an approximation and would like to emphasise that "exact" in this context means not doing the approximations we introduced.

could try to obtain a more detailed picture of the error by studying the influence of the neglected terms in the exponent. We think that one might try to include the second order as it can be treated by means of Fresnel integrals and so there might be some approximations that might give some insight. We decided not to follow this idea as we felt that it was more important to look whether this approximation helps in the understanding of the QKR data.

Until now we only focused on the comparison to the pendulum data and a regime where we expect our approximations to hold. We still need see in which regime our approximations are feasible. Therefore we will compare to numerical calculations in chapter 5. There we will also go back to the system of the quantum kicked rotor that was neglected in this chapter.

Chapter 5

Numerical Results

Until now we have just checked the correspondence of pendulum and QKR by using Husimi functions. We also derived a theory for pendulums and ensembles of pendulums. These results were checked shortly against numerical data. We did not yet discuss the behaviour in different regimes. This is what we will do in this chapter. We describe the qualitative properties of the phase space. After that we will describe the fidelity qualitatively in order to define characteristics. Using these characteristics we will compare the three approaches to each other. After discussing the properties of single rotors we will switch to sums of two rotors and go on with ensembles. In this section we will continue the discussion of the analytical result from section 4.6. We will define several characteristics of the decay of fidelity and show in which regime which approximation is valid.

5.1 Different Regimes of the QKR

To do numerics we need to define the range of the parameters of interest. Some of the parameters will be determined by practical needs, as for example phase space structures, others can be chosen freely. We fixed the kicking strength to values that are comparable to the experimental ones used in [Wu09]. We chose $k_1 = 0.6\pi$ and $k_2 = 0.8\pi$. The other parameters can now be determined by several other needs. One of the most important ones is that we need the ϵ-classical phase space to be near integrable which means that $\tilde{k} \lessapprox 0.1$. In order to fulfil this need we choose the ϵ range of interest to be $\epsilon \in [0.1, 0.001]$ and fix the ϵ-classical phase space in this way.

As the ϵ-classical phase space is defined now we have to chose the regions in which we want to place the rotors. As we determined the parameters in a way that the phase space is always near integrable we do not have stochastic regions in the phase space[1]. The only structures we have to respect besides near trivial[2] tori are resonances leading to islands. The most dominating resonance structure is the first order resonance at $J = 0$ and $\vartheta = 0$ which was analysed in [Abb09].

[1] At least not on the scale of the Planck cell.

[2] Near trivial tori is meant to be in the sense of Hamilton-Jacobi theory. There one chooses the canonical variables so that the trajectories are flat. So are the rotator like orbits in the case $\tilde{k} = 0$.

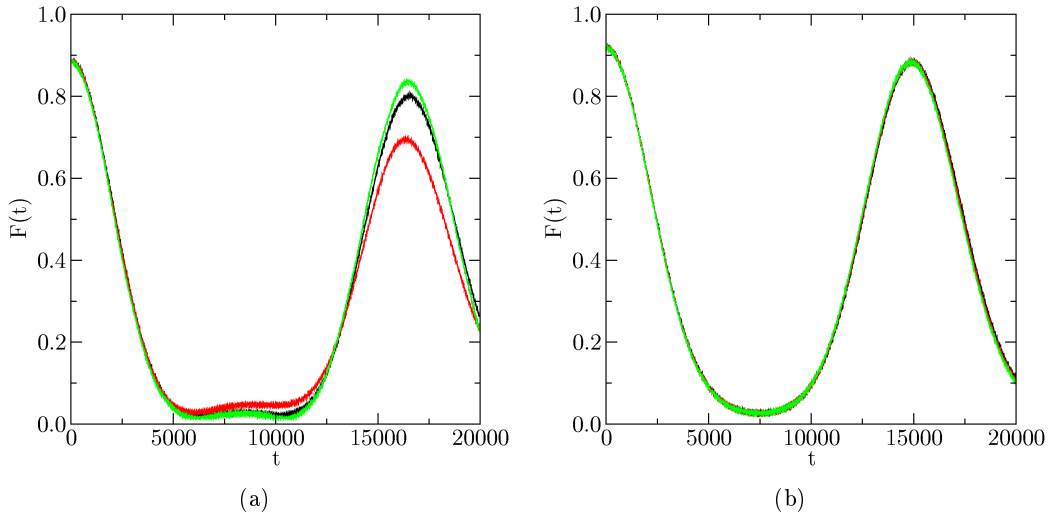

Figure 5.1: We plotted rotors with $\beta \approx 0.177$, $\epsilon = 0.05$, $k_1 = 0.6\pi$ and $k_2 = 0.8\pi$. This β value corresponds to a initial state representing $J \approx -2.02$ which is on to the third order resonance in fig. 5.2. To see the behaviour clearer we build the running average over 100 kicks. The ascending order of the rotors is green, red and black, where the spacing is ≈ 0.0003. In (a) we show QKR data and in (b) we show pendulum data. We can see that the revival behaves smooth in the pendulum case and has a dip in the QKR data. This is due to the higher order resonance.

Abb *et al.* analysed the main resonance by using the harmonic oscillator approximation. They found a rapid decay and revivals. Their argument, however, should also be valid in states that are dominated by higher order resonances. In order to understand in what way higher resonances influence the fidelity, we placed in fig. 5.1 some rotors near to the third order resonance at $J \approx 2$. We show three rotors with a spacing of about $\Delta\beta \approx 0.0003$ and can see that in the case of the QKR the middle rotors shows a different behaviour in contrast to the neighbouring ones. This behaviour cannot be seen in the case of the pendulum as the pendulum might have also rational winding numbers but has no islands near to such periodic points in phase space. The influence is not as large as in the case of the main resonance because the higher order resonance only covers the rotors in parts due to its wave shape in phase space. Nevertheless, we notice that there is an influence on the fidelity that leads to a qualitative difference that lies in the qualitative difference of the trajectories. As we are not able to understand the influence in detail we will try to use only rotator like orbits for our description.

In order to avoid higher order resonances we have to have a close look at the ϵ-classical phase space. In fig. 5.2 we show the ϵ-classical phase space for the case of $\epsilon = 0.1$, which is already our worst case, in the sense that it will be the largest ϵ we use in this thesis. It is enough to show only half the phase space as the other half can be obtained by point mirroring at $J = 0$ and $\vartheta = \pi$ what can be seen easily by inserting this transformation into eq. (2.4). On the scale of fig. 5.2 we observe the primary resonance at $J = 0$, the second order resonance at $J = -\pi$ and the third order resonance at $J \approx -2$.

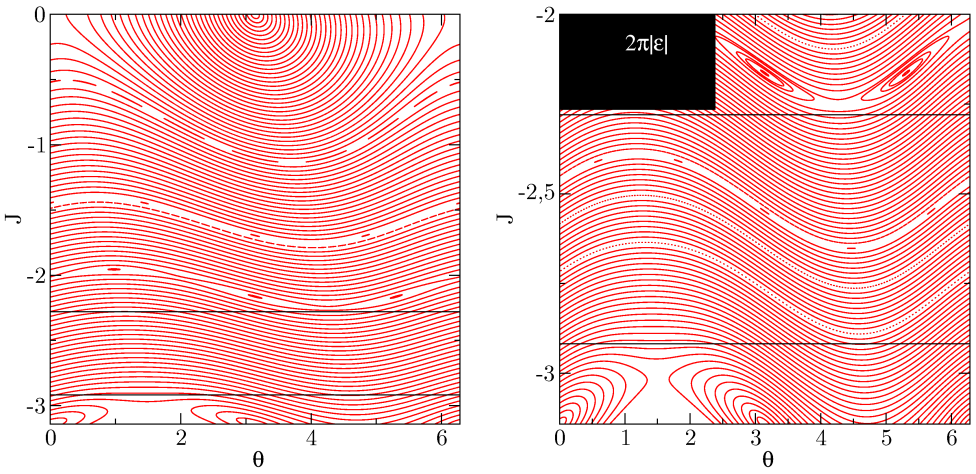

(a) Overview over the complete phase space (b) Details of the subensemble we chose

Figure 5.2: We show the $\epsilon = 0.1$ and $k = 0.8\pi$ phase space. In (a) the half of the phase space is shown. The black frame is a region which satisfies the requirements indicated in the text. This region does not contain higher order resonances or the existing resonances are small compared to the Planck cell volume $2\pi|\epsilon|$. In (b) a detailed plot is given. The solid black box represents the phase space cell and the black frame the subensemble also indicated in (a).

The size of the main resonance can be estimated by the pendulum approximation [Lic92] by calculating the width of the island of the pendulum. This way we obtain for half the diameter of the island

$$\Delta J_{\text{half}} = \sqrt{\tilde{k}}. \tag{5.1}$$

This estimate is also valid for higher order resonances as these can be mapped to primary resonances using canonical perturbation theory [Lic85]. We will, however, not use this for higher order resonances. To decide whether a resonance may influence the dynamics we need to compare its size to the volume a state needs in phase space. This volume is the Planck cell and is given in ϵ-classical approximation by $2\pi|\epsilon|$[Gia91]. This means that the Planck cell grows like ϵ and the island like $\sqrt{\epsilon}$ but also that the Planck cell shrinks faster than the principal island. This way we are able to place states on the island even in the case $\epsilon \to 0$ and can observe the behaviour of the island. Nevertheless, the phase space volume off the resonance island shrinks and so is its influence onto an ensemble covering the complete phase space cell.

In order to define ranges for β in which we want to test our theory we have to find stripes in the ϵ-classical phase space in which there is no higher order resonance and the trajectories are of rotor type. We will therefore focus on the spaces in between the resonances. In fig 5.2(b) we show the stripe between the second and the third order resonance in detail. By comparison with the Planck cell we see that the resonances are large enough to carry a quantum state and have to be avoided. The stripe that is marked corresponds to β-values

$$\beta \in [0.035, 0.135]. \tag{5.2}$$

This β-values are obtained by using eq. (3.6) under the assumption of a $I = 0$ state. This is important to mention as J, I and β are no equivalent quantities. The quasi-momentum is a conserved quantity and therefore does not change in time. The physical momentum is I which is not continuous when treated quantum mechanically. The procedure we use here to fix β values are only valid for initial states.

The stripe we have just defined is very far from the island and will therefore be called the far regime. In order to analyse the dependence we need to find also stripes near to the island and in between. The space between the third order and primary resonance is a candidate and is shown in fig. 5.3 for several values of ϵ. The space without large higher resonances is smaller than in the case far from the island. We can define another stripe which we call the intermediate regime by

$$\beta \in [0.20, 0.30]. \tag{5.3}$$

This regime is reasonable even for $\epsilon = 0.1$, but it contains the fourth order resonance which is small compared to the Planck cell for large enough ϵ. If we restrict ϵ further we can define a stripe that avoids this fourth order resonance for $\epsilon \leq 0.05$ by

$$\beta \in [0.27, 0.37], \tag{5.4}$$

which will be called the near regime. This regime needs to be handled with care as it is only valid for small enough ϵ.

The regimes we have just defined will be our testing ground in the rest of this chapter. We will now check whether these regimes we just defined also influence the behaviour of the fidelity. Now we will have a look at fidelities and analyse qualitative changes as we scan the various regimes.

5.2 Single Rotors

We will start the numerical analysis of the fidelity with the most simple case; the single rotor. We will use the term rotor for QKR the rotor in pendulum approximation and the rotor in WKB approximation. Which method was used to obtain the data will be said where the results are shown. We try to emphasise this way that we treat the QKR in different approximations, which means we will not treat a pendulum but a rotor in pendulum approximation.

Before we can compare the different approaches to each other we will need to define the characteristics of the fidelity of a rotor we will use to evaluate the quality of the approximation. Defining this characteristics will be the basis of our further discussion of the fidelity as these properties will be our vocabulary we use. Unfortunately the pendulum approximation has a systematic deviation which will be discussed in section 5.2.2 so that it is impossible to define a strict measure for the quality of the approximation. The discussion therefore will be rather qualitative and because of that we need to define the terms and subjects of the discussion carefully. We will start with the discussion of these properties and the pairwise comparison of the approaches.

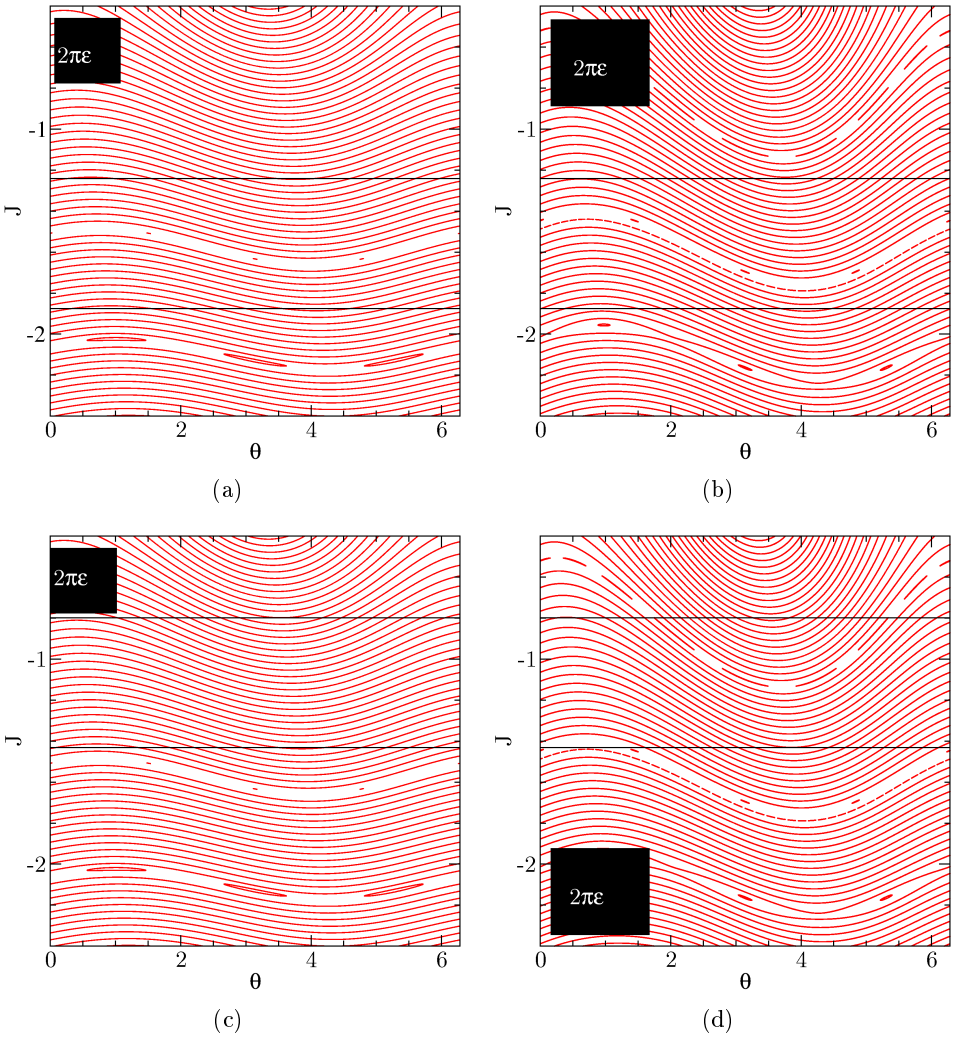

Figure 5.3: We show the case of $k_1 = 0.6\pi$ and $k_2 = 0.8\pi$. In (a) and (c) we show the phase space for $\epsilon = 0.05$ and in (b) and (d) for $\epsilon = 0.1$. In (c) and (d) we indicated the stripe corresponding to $\beta \in [0.27, 0.37]$ and in (a) and (b) we indicated $\beta \in [0.20, 0.30]$. The black boxes indicate the Planck cell.

To explain the behaviour we will utilise the WKB result to show in what way the correspondence breaks down. The behaviour of this approximation was already discussed in chapter 4. We will now use its properties to see how the approximations fail and which properties are not described by the pendulum approximation or the WKB result. It will also help to understand why and how the approximations fail.

5.2.1 Qualitative Description

Before we treat the rotors in different approximations in different regimes we first have to describe the rotors qualitatively. This is very important as we will also define several characteristics of the fidelity we will describe. We have a look at a rotor which is in the overlap of near and intermediate regime as this can be regarded as the most moderate regime. In order to keep the time scales short[3] we decided to take a rather large ϵ. Such an example is given in fig. 5.4. We see immediately that there are several distinct time scales. In fig. 5.4(a) we can see that there are some long time oscillations with fast oscillations modulated on it. The fast oscillations look like noise on this scale. Averaging over 100 kicks kills this fast oscillations and shows the long time behaviour quite clearly. In fig. 5.4(c) we show the beginning of the first oscillation and can see that the fast oscillations again have a structure. The fast oscillations from (a) turn out to be an still fast oscillating function with an oscillating envelope function. So we can distinguish three time scales:

- the long time oscillations which have the largest amplitude and could be regarded as collapse and revivals,
- the envelope oscillations,
- the fast oscillations modulated on the envelope.

These three characteristics will be our criteria for the quality of the approximations. Later we will however stop distinguishing the last two and just divide in long time oscillations and fast oscillations.

For the description of the characteristics of the fidelity we focused on a case that is rather near to the island in contrast to the examples discussed in chapter 4 which were far from the island. We did only compare the WKB result to the pendulum in fig. 4.6 and not to the QKR. This is done in fig. 5.5. We can see that the correspondence between the pendulum and the QKR is poor whereas the correspondence between pendulum and WKB is better. This discrepancy can be understood qualitatively and will be the subject of the next subsection where we will focus on the quality of the approximation when going to a different regime.

5.2.2 Quality of the Approximations

We will now focus on the properties of the results in different approximation in more detail. As we already noticed in the description of the qualitative properties

[3] A larger ϵ leads to a stronger perturbation which results in a more rapid decay of fidelity.

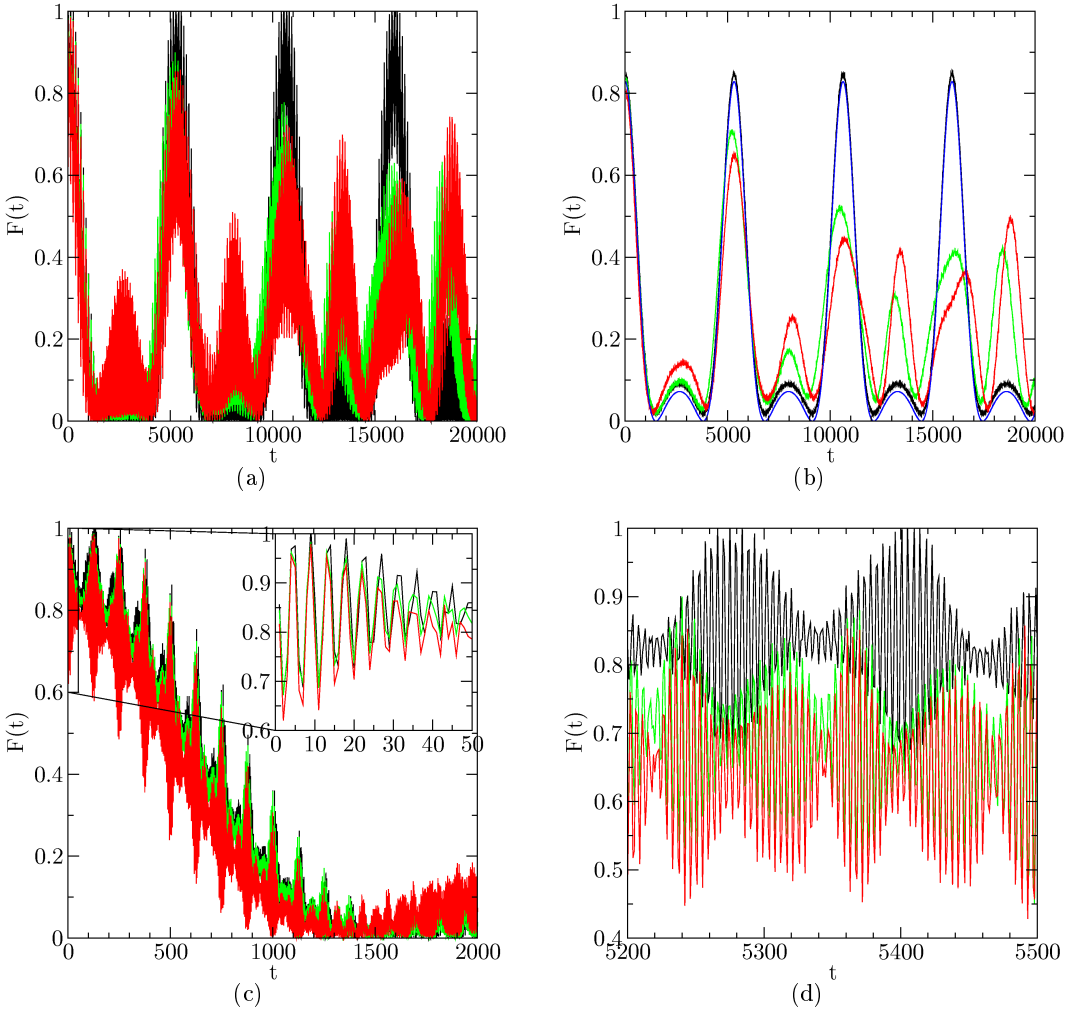

Figure 5.4: In this figure we show the fidelity of a single rotor with $\epsilon = 0.05$, $k_1 = 0.6\pi$, $k_2 = 0.8\pi$ and $\beta \approx 0.27031$. The black lines is the WKB result, the green line is the pendulum data and the red line the QKR. In (a) we show an overview. To show the details we averaged the data from (a) over 100 kicks to kill fast oscillations in (b). We also added the result from eq. (4.70) in blue. In (c) we show the initial decay in detail. The inset shows the detail of the fast oscillation. In (d) a detail in the second revival is shown.

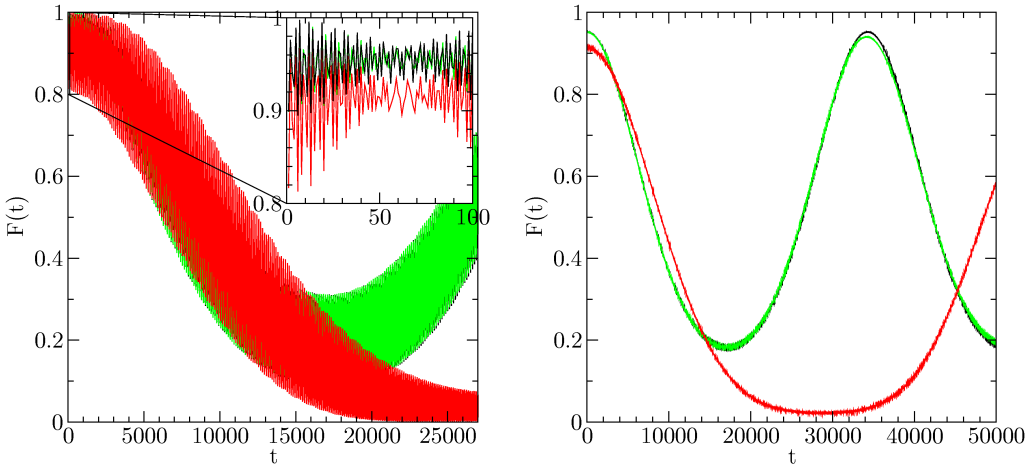

Figure 5.5: Here we show a rotor for $\epsilon = 0.05$, $k_1 = 0.6\pi$, $k_2 = 0.8\pi$ and $\beta \approx 0.07648$. The QKR data is shown in red, the pendulum data in green and the WKB result in black. In (a) we show the mentioned data. In (b) we show the same data as in (a) averaged over 100 kicks. We can see that, although the fast oscillations coincide quite well, the long time oscillation is not described by the pendulum approximation.

the quality of the approximation differs between rotors near and far from the island. In this section we focus on understanding the different characteristics by looking at the spectral properties and the coefficients. To get a better picture we need to discuss the transition more accurately.

To discuss this breakdown of the correspondence in a more systematic way we will compare rotors in different regimes. In fig. 5.6 we plotted three different rotors using QKR, WKB and pendulum. To see the long time characteristics better we averaged over 100 kicks.

We will now compare the results pairwise in order to work out the value of the different approximations. We will begin with the comparison of pendulum and WKB result which is more or less the continuation of the brief discussion in section 4.3. After that we will compare the pendulum to the QKR and explain in what way the pendulum approximation may help to describe the QKR.

WKB and Pendulum

In chapter 4 we already compared the WKB and pendulum data shortly. There we used an rotor which is in the regime far from the island. We saw a very good correspondence there. The case of a rotor far from the island is a case of good agreement between pendulum and WKB as can be seen in fig. 5.6. In this section we need to understand why and how this correspondence breaks down when approaching the island and which characteristics of the fidelity are nevertheless described. We will repeat the interpretation of the pendulum as an perturbed rotor and show how the approximations influence different quantities. In order to prepare the discussion of the properties described by the WKB result we will

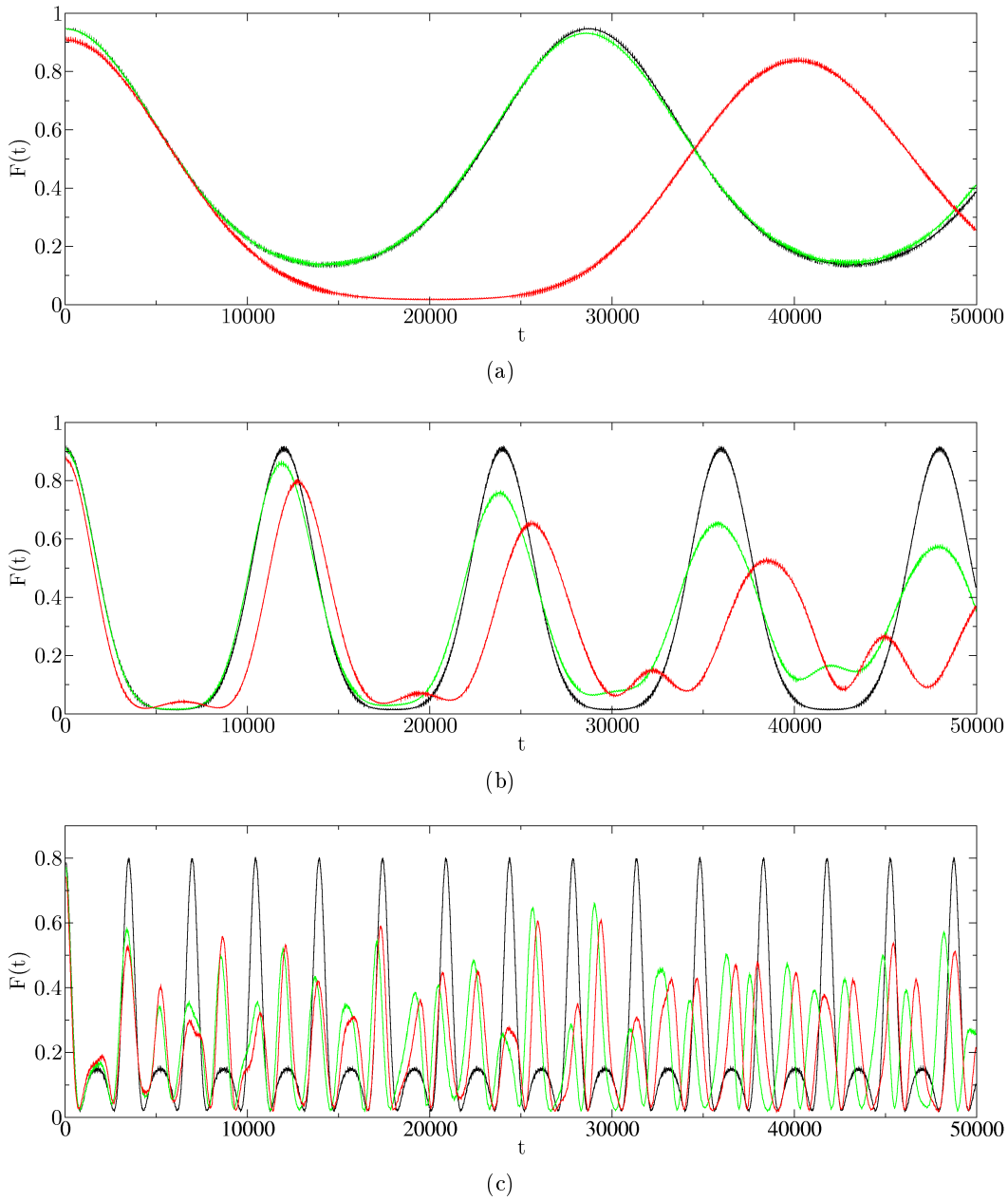

Figure 5.6: In this figure the fidelity using WKB (black) and the pendulum (green) are compared to the QKR (red). We show the $\epsilon = 0.05$, $k_1 = 0.6\pi$ and $k_2 = 0.8\pi$ case. In (a) we show $\beta = 0.1$, in (b) $\beta = 0.2$ and in (c) $\beta = 0.3$. The data is averaged over 100 kicks to kill fast oscillations.

give a description of the correspondence between WKB and pendulum data in different β ranges.

In the discussion of the WKB result in section 4.3 we chose some rotor deep in the rotating regime of the pendulum phase space. This is important for the approximations to be valid as we already showed that the WKB result can be understood essentially as perturbation of the free rotor. In this interpretation the kicking term is a perturbation to the free rotor and the quality of the approximation is governed by $\tilde{k}/E$ as this determines the quality of the Taylor expansion in eq. (4.21). This is also what we see in fig. 5.6. We can see that we have a nearly perfect correspondence in fig. 5.6(a) which breaks down as we go closer to the island.

Another hint for the interpretation of the WKB result as an perturbation of the free rotor is the structure of the energy eq. (4.38). There we can see that the expansion is also an expansion in powers of $1/\bar{\beta}$. This terms explode as we approach the island[4]. This is a sign that the approximations for the energy break down.

Before we continue the discussion we will first use the example in fig. 5.4 to describe the features and problems of the WKB result closer. We will therefore compare the characteristics defined in subsection 5.2.1. In fig. 5.4(c) we can see that the fast oscillations and the envelope of the pendulum is described well by the WKB result. This correspondence breaks down for larger times as can be seen in (d). In in the long time behaviour we observe a variation of the hight of the revivals in the pendulum data in fig. 5.4(b). This variation in hight is not described by the WKB result. Although the variation in the hight of the revivals are not described the period of the revivals is described perfectly.

When focusing onto the behaviour in different regimes we can see that between the main revivals in fig. 5.6(a) smaller bumps appear in fig. 5.6(a) to fig. 5.6(c) when approaching the island. In the discussion of fig. 5.4(b) we found that the hight of the revivals varies in the pendulum data. This variation gets stronger near the island. The WKB result however does not show such a behaviour but describes the appearance of the bump between the principal revivals. To understand this behaviour we will now use the results from chapter 4.

We have just seen that the WKB result reproduces the fast oscillations only initially. Nevertheless the long time behaviour is described well. To understand this behaviour we will have a closer look at eq. (4.63) in order to identify the terms that lead to this fast oscillations. In section 4.3 we discussed shortly that the contributions with $d = 0$ are of order ϵ^2 whereas the other energy differences are of order ϵ or 1 and therefore much larger which corresponds to shorter time scales. That the long time behaviour is due to the diagonal terms can be seen when comparing f_{diag} to the averaged WKB data in fig. 5.4(b) where the WKB data in diagonal approximation describes the averaged WKB data very well which means that the fast oscillations are due to the off diagonal terms.

The revivals can be associated to special terms in eq. (4.63) where $d = 0$. Therefore we use the WKB result in diagonal approximation eq. (4.70) for the

[4]Reminder: The island corresponds to $\bar{\beta} = 0$ in contrast to β where the principal nonlinear island corresponds to $\beta = 0.5$. This is discussed in detail chapter 3.

discussion. Calculating the periods of the cosine terms we can identify the main revival in fig. 5.4(b) with the $m = 1$ term. As all other frequencies of the cosine are integer multiples of the $m = 1$ frequency the bump between the principal revivals can be associated to the $m = 2$ term. Which frequency component is present how strong is given by the behaviour of the coefficients c_{mm} in eq. (4.77a). The behaviour of this coefficients is described in the discussion of fig. 4.1. There we found out that the components with higher m contribute more when approaching the island. This corresponds to the occurrence of higher order contribution in fig. 5.6 when going from (a) to (c) which corresponds approaching the island.

On the one hand we see higher frequency components and the principal revival in the WKB result but on the other hand the height of the revivals varies in the pendulum data in contrast to the WKB result. This decay of the principal revival and the rise of the higher frequency component in fig. 5.4(b) can be understood as a beating phenomenon. In order to describe this phenomenon as beating one needs to introduce small energy differences between the terms with $m = -m'$. One idea would be to take the next order in ϵ in eq. (4.63) into account that contributes such an energy difference. Introducing this term we observe a beating in the hight of the revivals and an amplification of the higher order contributions. The order of the hight is the same as the one observed in the pendulum data but the temporal sequence of the heights is not described. The next order correction to the energy therefore cannot explain this decay in the hight of the revivals. Another idea would be to take further terms in the expansion of the action into account in eq. (4.21). However, the accuracy we use here proved to be sufficient enough for our purpose.

The behaviour of the revivals depends crucially on the magnitude of the coefficient, which controls how strong the contribution is, and the exact spectral structure, which controls the beating behaviour. It is very difficult to separate these two contributions in detail as the behaviour arises in their interplay. This is problematic as we used two different accuracies in our approximations in chapter 4.

QKR and Pendulum

In chapter 4 we focused on the WKB approximation as an approximation for the pendulum which itself is an approximation to the QKR. We still need to discuss this correspondence. It is obvious from fig. 5.5 that this correspondence is not perfect in all regimes and is therefore problematic and we have to notice that there are β-rotors whose description is not very good. Having a look at fig. 5.6 we can see that the correspondence becomes worse when we go away from the island. The most striking mismatch is in the period of the long time oscillation, whereas we can see that this time scale is described pretty well near the island but scales incorrectly when going away from the island. Unfortunately, this scaling is what determines the decay when building ensembles as we have seen already in section 4.6. Despite this mismatch the pendulum describes the amplitude of the long time behaviour very well and also reproduces the appearance of higher frequency components in fig. 5.6(b). Having a look at fig. 5.4(d) we can see that

the pendulum describes the envelope even on longer time scales at least if the large oscillation scale is described well.

The pendulum shows an impressive accuracy on the long time scale as long as the rotor is near the island. Comparing fig. 5.4(c) and fig. 5.4(d) we see that the pendulum describes the envelope oscillation for a long time whereas the correspondence to the WKB result breaks down. In fig. 5.4(b) we can see that the variation of the height of the revivals already discussed above coincides between pendulum data and QKR data. This behaviour is also relatively stable when varying β as can be seen in fig. 5.6(b) and fig. 5.6(c). The most obvious problem is the failure in describing the time scales. We can see that when leaving the island the QKR shows longer time scales than the pendulum.

We can obtain a qualitative understanding of this problems by comparing the phase space. To understand this we need to recall the different structure of the phase space of the pendulum and the KR. The phase space of the pendulum is the cylinder whereas the phase space of the KR is the torus as the the momentum is also periodic. This is discussed in detail in chapter 3 and can easily be seen in fig. 3.1. As the pendulum lacks this periodicity it is not periodic at the border of the phase space cell and therefore has to differ there from the kicked rotor. This gives a qualitative motivation why the correspondence breaks down at the border of the phase space cell.

The amplitude of the fidelity also deviates and this difference is still present in the $\epsilon \to 0$ limit. In order to understand this we need to compare the result for resonant rotors to the resonant limit of the ϵ-classical theory. In [Wim06] a result for the fidelity of resonant QKR is given as

$$F_{\bar{\beta}}(t) = \left| J_0\left(\frac{\sin(t\bar{\beta}/2)}{\sin(\bar{\beta}/2)} \delta k \right) \right|^2 \tag{5.5}$$

on the one hand, but on the other hand we showed in chapter 4 in correspondence with [Abb09] that the pendulum approximation leads to

$$F_{\bar{\beta}}(t) = \left| J_0\left(\frac{2\delta k}{\bar{\beta}} \sin\left(\frac{\bar{\beta} t}{2} \right) \right) \right|^2 \tag{5.6}$$

in the resonant limit. This results can be understood as approximations to each other by approximating the denominator of the argument of the Bessel function linearly. To understand the effect of this approximation we need to understand the structure of the term better. The argument is an oscillating function whose period is defined by the numerator and whose amplitude is defined by the denominator so that the oscillation of the argument is centred around zero. This function is the argument of a Bessel function of zeroth order which is one for vanishing argument and decays with an oscillating behaviour [Abr64]. This means the fidelity is an oscillating function around some average value which is determined by the amplitude of the oscillations of the argument. In order to compare an offset we averaged the fidelity over 8000 kicks. In fig. 5.7 we show this averaged fidelity F_{av} for different β and for the pendulum and the QKR. We can see that even in the resonant case the results are better near the island. The mismatch of initial amplitude can therefore be described already in the resonant picture.

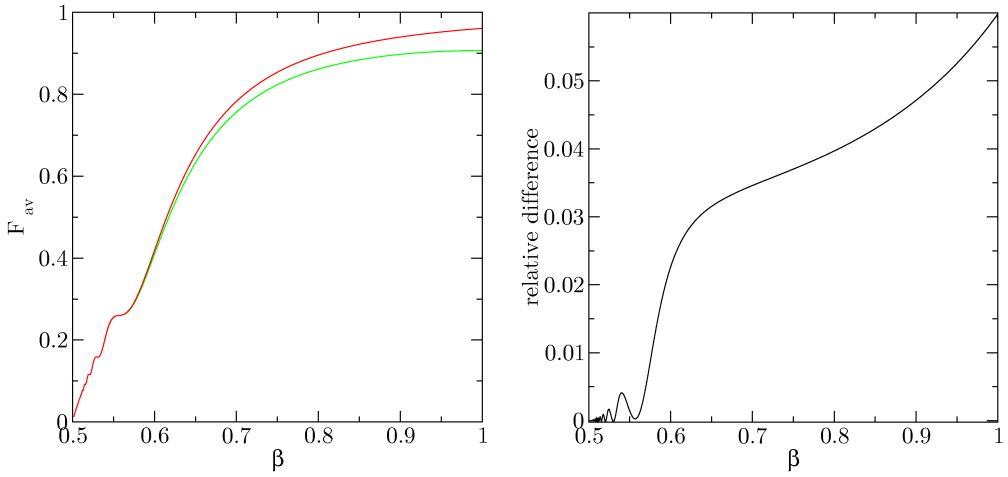

(a) (b)

Figure 5.7: To illustrate the difference between eq. (5.5) and eq. (5.6) we averaged over 8000 kicks to kill the oscillation and obtain the mean value. In (a) we show the averaged fidelity of the QKR (green) and the pendulum (red). In (b) we show the relative difference of the Pendulum to the QKR.

The initial oscillations and the offset are described by the resonant result for the QKR. The detuning leads to a decay as was pointed out in [Wim06]. In this thesis we aim to describe this decay. Taking the results by [Abb09] into account it is clear that the decay from this saturation value and the saturation itself must come from the rotator like orbits. On the one hand the harmonic oscillator approximation describes island states well [Abb09] but on the other hand the island states cannot describe the saturation in the limit $\epsilon \to 0$ and therefore also cannot describe the decay of the fidelity starting at this saturation value. The comparison of the results for the resonant case shows clearly that there is a lack of correspondence between pendulum and QKR, which corresponds to the different results for the resonant rotor in [Abb09] and [Wim06]. Therefore we cannot expect this discrepancy to disappear in the resonant case but we can hope to at least describe other properties.

5.3 Two Rotors

Before averaging over an interval in β we first focus on the average over two overlaps. This will give us a feeling of the properties of the fidelity which are important to describe the behaviour of the average of a continuous ensemble. It also allows us to see whether the QKR has just a wrong coefficient or whether it inhibits a different scaling law in general. As our ensemble average is defined as the average of the overlap we need to add the overlaps

$$f = \tfrac{1}{2}\big(f_{\beta_1} + f_{\beta_2}\big), \tag{5.7}$$

where f is the overlap and so the fidelity is obtained by $F = |f|^2$. In this section we also need to consider the phase of the overlap and not just its absolute value

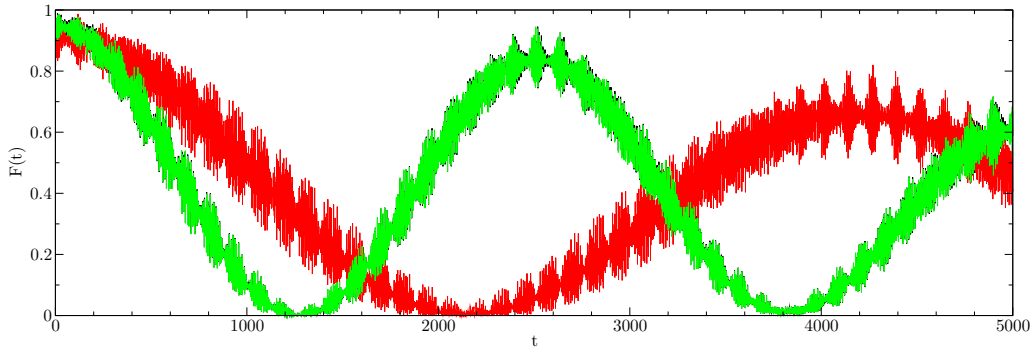

Figure 5.8: In this figure we show the absolute value of the sum of two rotors. We show WKB (black), pendulum (green) and QKR (red) data for $\beta_1 = 0.03$, $\beta_2 = 0.13$, $k_1 = 0.6\pi$, $k_2 = 0.8\pi$ and $\epsilon = 0.05$. The corresponding time for the first decay is $T_1 = 1275.9.6$ according to eq. (5.9). We can see that the WKB and pendulum data agree well but both deviate from the QKR data.

as we did for single rotors.

A closer look at the WKB result for the pendulum shows that we could simplify it by separating a common phase factor in eq. (4.72). This means that the fidelity rotates in the complex plane with a frequency which scales like $\bar{\beta}^{-2}$. This is the dominating frequency scale as the other frequencies are of order ϵ^2. When adding two overlaps we expect some beating between these two rotors. The beating frequency can be obtained by considering just the c_{00} term. Building the average of two rotors with $\bar{\beta}_{1/2}$ we obtain by neglecting the $\bar{\beta}$ dependence in c_{00}

$$f \approx c_{00}\left(\mathrm{e}^{\imath\frac{\delta_{k^2}}{4\bar{\beta}_1^2}\epsilon t} + \mathrm{e}^{\imath\frac{\delta_{k^2}}{4\bar{\beta}_2^2}\epsilon t}\right) = \tfrac{1}{2}c_{00}\mathrm{e}^{\imath\frac{\delta_{k^2}}{8}\frac{\bar{\beta}_2^2+\bar{\beta}_1^2}{\bar{\beta}_1^2\bar{\beta}_2^2}\epsilon t}\cos\left(\frac{\delta_{k^2}}{8}\frac{\bar{\beta}_2^2-\bar{\beta}_1^2}{\bar{\beta}_1^2\bar{\beta}_2^2}\epsilon t\right), \tag{5.8}$$

where $\delta_{k^2} \equiv k_2^2 - k_1^2$ was defined in chapter 4. One characteristic of the fidelity is the first oscillation that decays nearly until zero. As a characteristic quantity we can define the time to the first minimum T_1. Because the fidelity F is defined as the square of f, the time to the first minimum corresponds to the time to the first zero of the cosine and therefore to the fourth of the period of the cosine. This way we obtain

$$T_1 \equiv \frac{4\pi}{\delta_{k^2}\epsilon}\frac{\bar{\beta}_1^2\bar{\beta}_2^2}{\bar{\beta}_1^2 - \bar{\beta}_2^2}. \tag{5.9}$$

In fig. 5.8 we show such an ensemble. As we can see the pendulum does not describes the QKR data. On the other hand this is not too surprising as we already discussed that the $\bar{\beta}$ scaling is described very poorly by the pendulum approximation. This beating time is very sensitive to this scaling.

In order to check the scaling of the beating we have to compare pairs of rotors. When dealing with pairs of rotors we can construct pairs which have a common property. This way we can check whether they fulfil this property without reproducing the right absolute time scale. We will construct pairs of rotors having the same T_1. Therefore we fix one pair of rotors whose quasimomentum we call $\bar{\beta}_{1/2}$ and fix the one rotor of the other pair to have quasimomentum $\bar{\beta}_1'$ and calculate the second quasi momentum $\bar{\beta}_2'$. As the other parameters are the same we

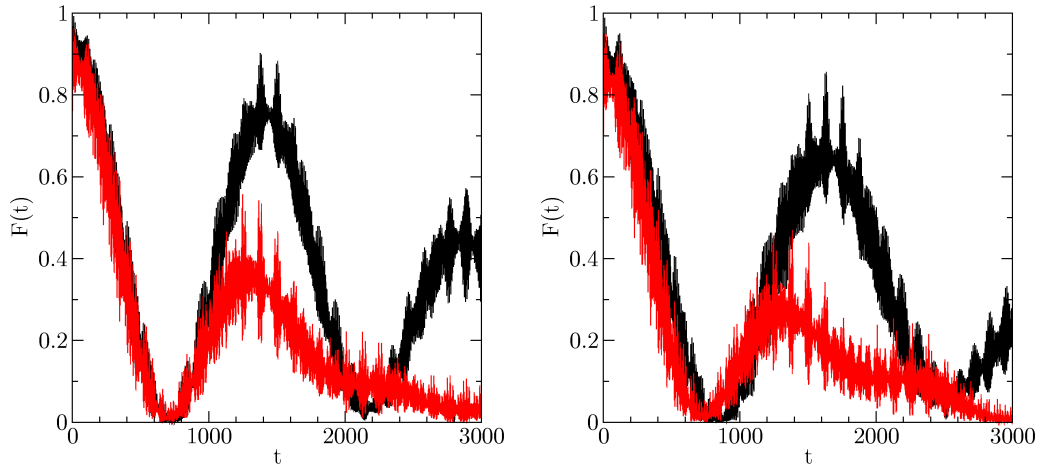

(a) Pendulum data (b) QKR data

Figure 5.9: In this figure we show pairs of rotors which are chosen according to eq. (5.11). The ensembles shown are $\beta_1 = 0.2$, $\beta_2 = 0.25$, $\beta'_1 = 0.25$ and $\beta'_2 = 0.28$. We show the dashed ensemble in black and the undashed ensemble in red. In (a) we show pendulum data and in (b) QKR data.

obtained

$$\frac{1}{\bar{\beta}_1^2} - \frac{1}{\bar{\beta}_2^2} = \frac{1}{\bar{\beta'}_1^2} - \frac{1}{\bar{\beta'}_2^2}. \tag{5.10}$$

Solving this equation for $\bar{\beta}'_2$ we obtain

$$\bar{\beta'}_2 = \pm \frac{|\bar{\beta}_1 \bar{\beta}_2 \bar{\beta'}_1|}{\sqrt{\bar{\beta}_1^2 + \bar{\beta}_2^2 + \bar{\beta'}_1^2(\bar{\beta}_1^2 + \bar{\beta}_2^2)}}. \tag{5.11}$$

This equation is build just by using the right scaling in $\bar{\beta}$. By testing its validity we can test for the right scaling even if the absolute values do not match.

In fig. 5.9 we show such a pair of rotors. We can see that the initial decay of the rotor pairs coincides for the pendulum but only coincides approximately in the case of the QKR. In the QKR data we can see that the fidelity deviates qualitatively after the first decay. This means that our model describes the pendulum again pretty well but can only be a very weak model for the QKR system. In this regime we can only hope to find the qualitative behaviour of the initial decay and a scaling factor in the time. This can be seen in the black plot in fig. 5.9(b). A second minimum is reached at about $t = 2100$ which corresponds to approximately three times the time of the first minimum. We have about the same ratio for the pendulum in fig. 5.9(a). So we can hope to find a description for the qualitative shape up to a finite some time scaling factor.

5.4 Continuous Ensembles

In the last section we studied how two overlaps interfere. In chapter 2 we showed that we have to average the overlap over a whole interval in order to describe

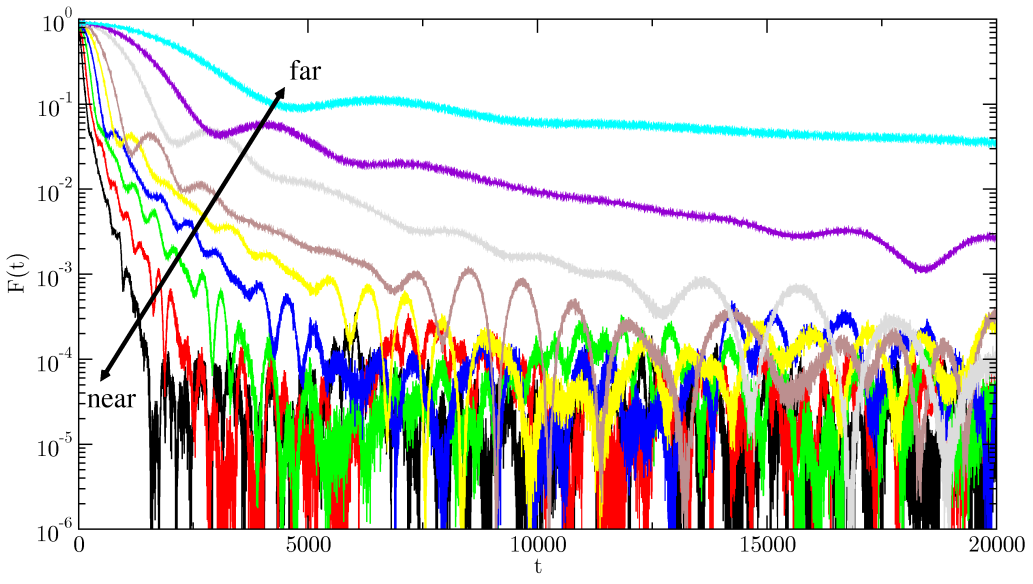

(a)

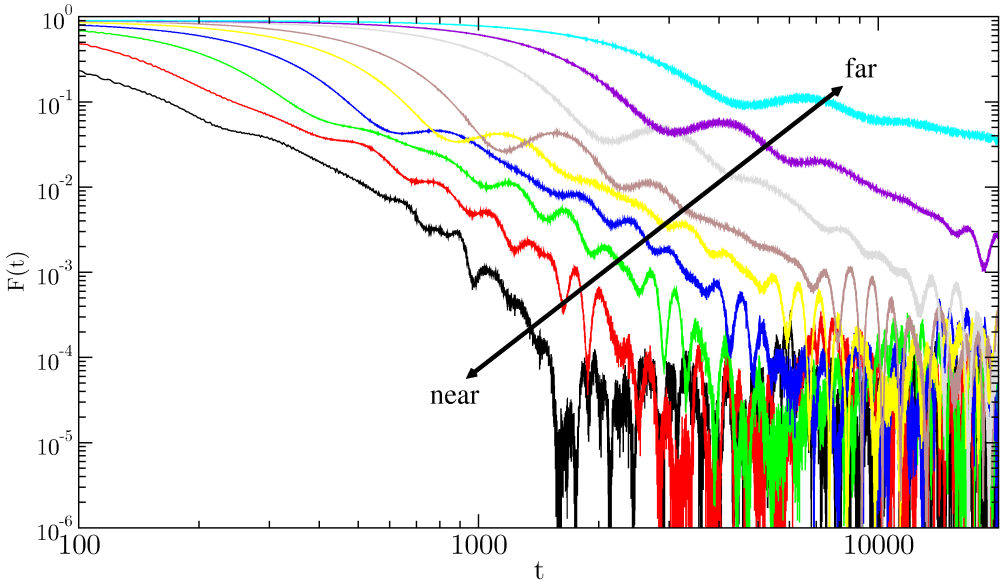

(b)

Figure 5.10: To give an idea of the influence of the regime we show different QKR ensembles containing ≈ 10000 rotors with $\beta_2 - \beta_1 = 0.1$ and $0.03 < \beta_1 < 0.27$. The other parameters are $\epsilon = 0.05$, $k_1 = 0.6\pi$ and $k_2 = 0.8\pi$. In (a) we show the data in semi-logarithmic scaling and in (b) in logarithmic scaling. The arrows indicates which ensemble is near and which is far the island.

the behaviour of a cloud of atoms. We saw in the last section that not only the relative phases of the single coefficients in the expansion of a single rotor plays a role but also the β dependence of the common phase. In section 4.6 we could see that this mechanism is the main contribution to the decay. As our theory is made for small ensembles we will focus on ensembles not covering the complete phase space cell. As we just treat ensembles covering only a part of the phase space cell we also have to say which part we cover. The importance of this questions and the effect of this choice is illustrated in fig. 5.10. There we can see that the region in phase space has a large impact on the behaviour. The aim of this chapter will be to understand this behaviour qualitatively and also to show which aspects of this behaviour can be understood in which approximation. A special focus will be on the quality of the approximations and regimes of their validity.

We begin by saying a few things on the numerical implementation. Afterwards we will compare the different approximations. We will start with the comparison of the pendulum and the WKB result for ensembles and continue the discussion of the analytical result from section 4.6 but now in different regimes. The discussion of the validity of the pendulum approximation in the context of ensembles will follow and we will end with a summary of this chapter.

5.4.1 Numerical Implementation

As our numerical procedure gives us the fidelity iteratively we cannot integrate in every time step over the β interval. We generated 50000 random numbers using RAN2 from [**?**] and averaged over the corresponding fidelities. The code was ported to FORTRAN 90 and double precision by hand. We produced a set of random numbers for the the interval $\beta \in [0.035, 0.135]$ and shifted this values for other regimes. If we needed larger stripes of very flexible data we used a set of values in $\beta \in [0, 0.5]$. We saved the resulting overlap in small sub ensembles and were able to build various ensembles afterwards this way.

The choice of the βs has to be handled with care. Not only the way we choose but also the question how many we chose is important to obtain a reliable approximation to a continuous strip in β. We want to obtain a result that describes a continuous ensemble best. this is done this by approximating the continuous ensemble by a finite ensemble. This leads to a finite spacing in the energies and therefore the difference between the finite and the infinite ensemble will show after some time connected to this spacing[5]. On the other hand we found out that equal spaced rotors lead to artificial revivals. These can be avoid by choosing random rotors which in exchange leads to some noisy behaviour.

5.4.2 Pendulum and WKB

First we will compare the pendulum data to the WKB data in order to analyse the correspondence for ensembles. In fig. 5.11 we show the pendulum and WKB data for the three regimes defined in section 5.1 and the differences between

[5]This argument is similar to those in [Izr90] where they used the finite energy spacing to describe the break of diffusive growth.

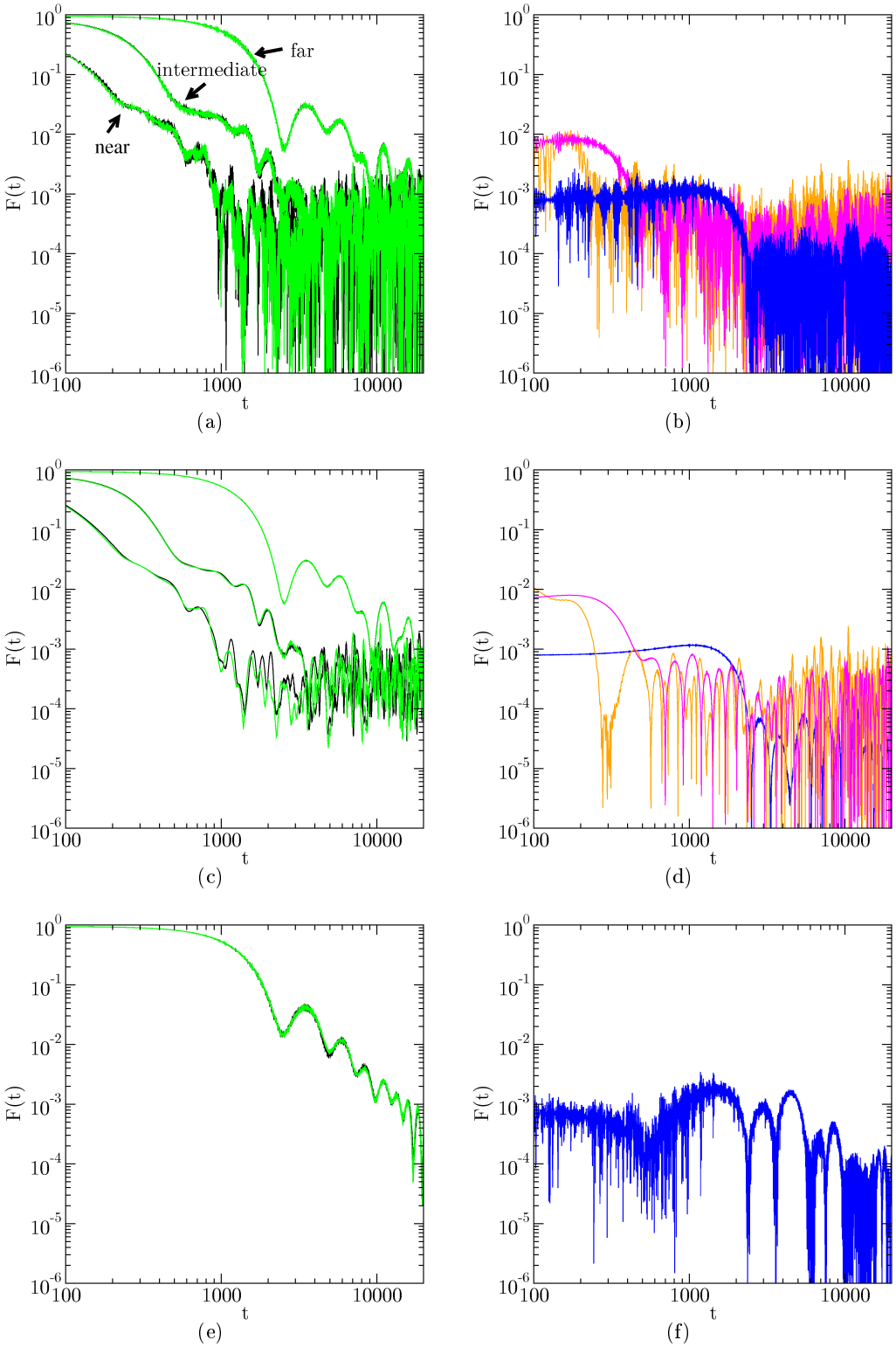

Figure 5.11: In this figure we show ensembles for $k_1 = 0.6\pi$, $k_2 = 0.8\pi$ and $\epsilon = 0.05$ using the WKB (black) and the pendulum (green) data. In (a) to (d) we show ensembles of 500 rotors and in (e) and (f) we show an ensembles of ≈ 7000 rotors for the pendulum data and 10000 rotors for the WKB data. In the left column we show the data and in the right column we show the absolute value of the difference between pendulum and WKB data. We show the ensembles (from left to right, also indicate by arrows in (a)) for the near (orange), the intermediate (magenta) and the far (blue) regime. In (c) we show the data from (a) averaged over 100 kicks and in (d) the difference of the time averaged fidelities in (c).

them. In order to show the long time behaviour more clearly we also show the data averaged over 100 kicks and the difference of these averaged fidelities. In the discussion of single rotors we found out that the fast oscillations are not described well by the WKB result. That the ensemble also shares this problem can be seen in fig. 5.11(b) as the fast oscillations are of the same order as the fast oscillations in the difference between the WKB result and the pendulum data. By averaging we can get rid of the fast oscillations. In the case without the fast oscillations the correspondence is much better as can be seen in fig. 5.11(d). The deviation is much smoother here. Nevertheless the WKB result does not describe the pendulum data in the saturation like part of the fidelity decay. As soon as the data is smoother the WKB result describes the pendulum very well in the non saturated regime.

In order to get a feeling on how big the ensembles need to be we focus on fig. 5.11(e). There we show the same data as in the far from island ensembles in fig. 5.11(a) but with much larger ensembles. For numerical reasons we only have ≈ 7000 rotors for the pendulum data and 10000 rotors for the WKB data. By comparing to the small ensemble we see that the numerics have not converged at 500 rotors. Nevertheless the correspondence to the WKB data hold although the ensembles contain a different amount of rotors.

As the numerics for the pendulum are very time consuming[6] we cannot build ensembles much larger than 500. Unfortunately we need larger ensembles in order to obtain an ensemble that describes the continuous ensemble. When we need big ensembles we will therefore assume that WKB and pendulum are equivalent despite the differences in the case of single rotors. This is feasible as the correspondence for ensembles is much better than for single rotors.

5.4.3 WKB and Analytical Result

In chapter 4 we gave an analytic formula for the fidelity of an ensemble of rotors and compared it shortly to pendulum data. Now we will continue this comparison in more regimes. In fig. 5.10 we showed a variety of QKR ensembles placed in different regions in the phase space cell and their decay behaviour. In order to see the effect of the regime in the phase space onto the quality of the approximation we depict a few ensembles and present them separately. In fig. 5.12 and fig. 5.13 we show data for WKB, QKR ensembles and the analytical result eq. (4.83) for two different ϵ and different ranges of β. For now we will focus at the WKB and the analytical data and discuss the QKR data in the next section.

We see that the analytical result produces a slightly too long period and overestimates the minima, as already discussed in section 4.6. This behaviour can be seen very nicely in fig. 5.12. If we increase ϵ we can see that the analytical result deviates from the WKB result. In fig. 5.13(a) and fig. 5.13(c) the analytical result describes the WKB data still well but it starts to fail in fig. 5.13(b).

After some initial fast decay the WKB data shows some decay with an oscillation. This behaviour is illustrated best in fig. 5.15. In order to show the

[6] In order to obtain reliable numerical results we need to choose the matrices big enough to cover the island. For such big matrices the calculation of eigenvectors and eigenvalues takes quite some time.

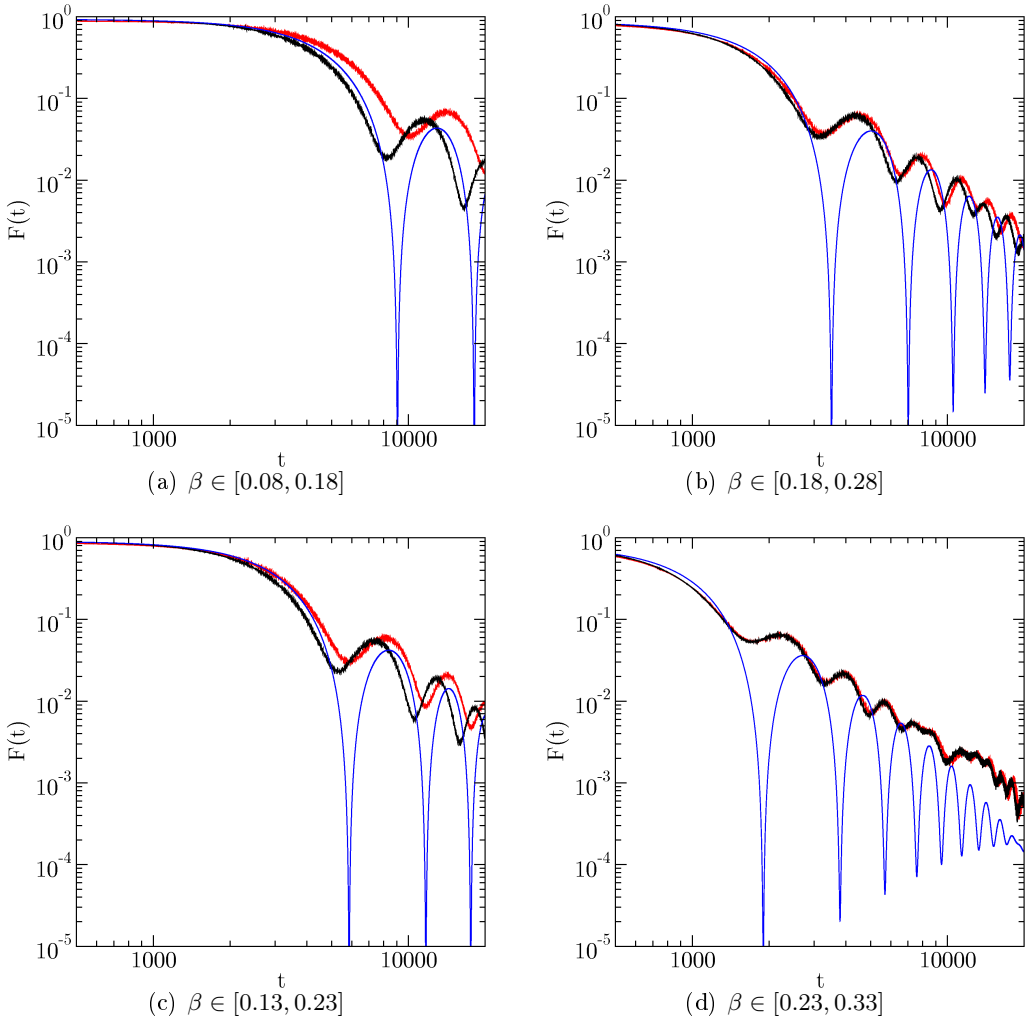

(a) $\beta \in [0.08, 0.18]$ (b) $\beta \in [0.18, 0.28]$

(c) $\beta \in [0.13, 0.23]$ (d) $\beta \in [0.23, 0.33]$

Figure 5.12: In this figure we show data for WKB (black) and QKR (red) ensembles containing ≈ 11000 rotors with $\epsilon = 0.01$, $k_1 = 0.6\pi$ and $k_2 = 0.8\pi$. The corresponding analytical result eq.(4.83) is shown in blue.

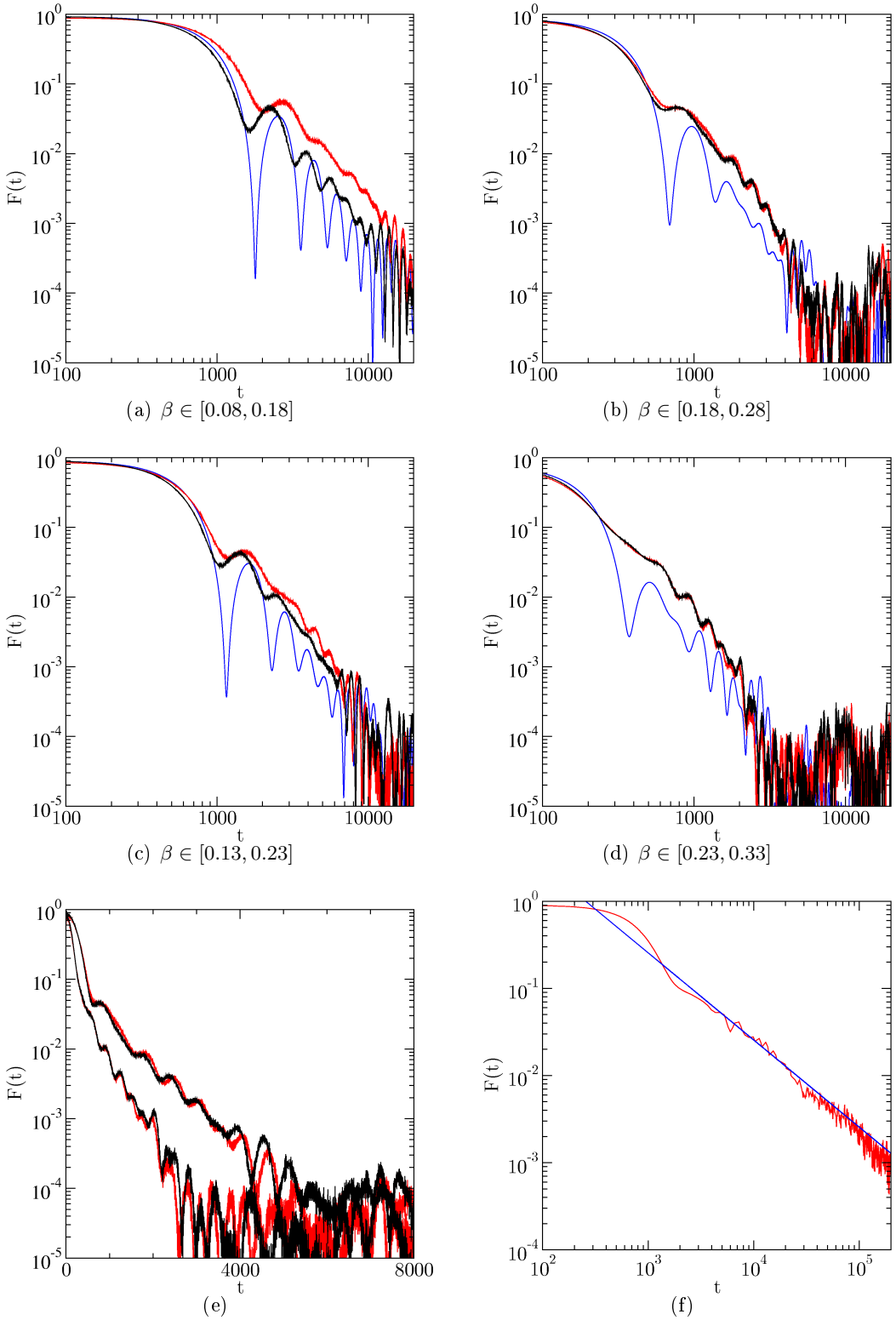

Figure 5.13: In this figure we show data for WKB (black) and QKR (red) ensembles containing ≈ 11000 rotors with $\epsilon = 0.05$, $k_1 = 0.6\pi$ and $k_2 = 0.8\pi$. The corresponding analytical result eq.(4.83) is shown in blue. In (e) we show the data from (c) and (d) in semi-logarithmic scaling. In (f) we show QKR data for an ensemble with $\beta \in [0.035, 0.135]$ containing 10000 rotors for a long time. The blue line is a $1/t$ functional fit.

behaviour, in this figure the data is smoothed by averaging over 100 kicks. This way we can see that as the fidelity decays an oscillation becomes visible that seems to dominate the longer time behaviour. Comparing[7] fig. 5.13(d) and fig. 5.15 we can see that we cannot decide whether the WKB decays exponentially or algebraic. On the one hand the oscillation hides the interesting region when the decay crosses over into the saturation like regime and on the other hand the decay is not long enough to decide the kind of the decay. Nevertheless, we can observe in fig. 5.13(a), fig. 5.13(b) and fig. 5.12 that the fidelity in WKB approximation can be approximated well by a power law until intermediate times. As soon as the fidelity decays further this algebraic behaviour breaks down and therefore can just be regarded to be a crude approximation for the initial behaviour. This breakdown happens sooner near the island due to the faster decay of fidelity in general there.

As the analytical result is strict $1/t^2$ (see eq. (4.83)) the correspondence between the analytical result and the WKB result has to fail near the island as the WKB decay shows clear non algebraic behaviour. The failure of the approximation can be understood as the linear approximation of eq. (4.63) we used in the derivation in section 4.6 gets worse when approaching the island which corresponds to the pole of the $1/\bar{\beta}^2$ and $1/\bar{\beta}^3$ term. Due to the strict $1/t^2$ behaviour of the analytical result the oscillations that generate some saturation behaviour in the WKB data cannot be reproduced and the analytical result can only be expected to be valid on short time scales. However, the period of the remaining oscillation matches to the initial oscillations that are described well by the analytical result.

Unfortunately, we could not derive a mathematical estimation of the error. This means we can just consider numerical evaluation to check the validity of the analytical result. Comparison to the WKB result shows that the decay and the oscillations modulated on it are described although the shape is not met perfectly. The description of the decay breaks down as the ensembles approach the island. This happens faster for larger ϵ. Even in the regime near the island some features are described. The analytical result is only valid on not too long time scales.

5.4.4 WKB and QKR

In the last section we compared the QKR data to the analytical result. We still need to understand the correspondence between pendulum and QKR. As the pendulum is numerically very extensive and we need big ensembles in order obtain results that are reliable on longer time scales we have to find another way to obtain data for the pendulum. As we saw in subsection 5.4.2 when building ensembles the WKB result describes the pendulum good enough for our needs. Therefore we will discuss the correspondence between WKB result and QKR data instead of the pendulum.

In the decay of fidelity we can identify three temporal regimes. In order to define these regimes we will continue the discussion of the behaviour we already

[7] We are aware that the ensembles shown are not the same but the qualitative behaviour is the same and the argument is valid nevertheless.

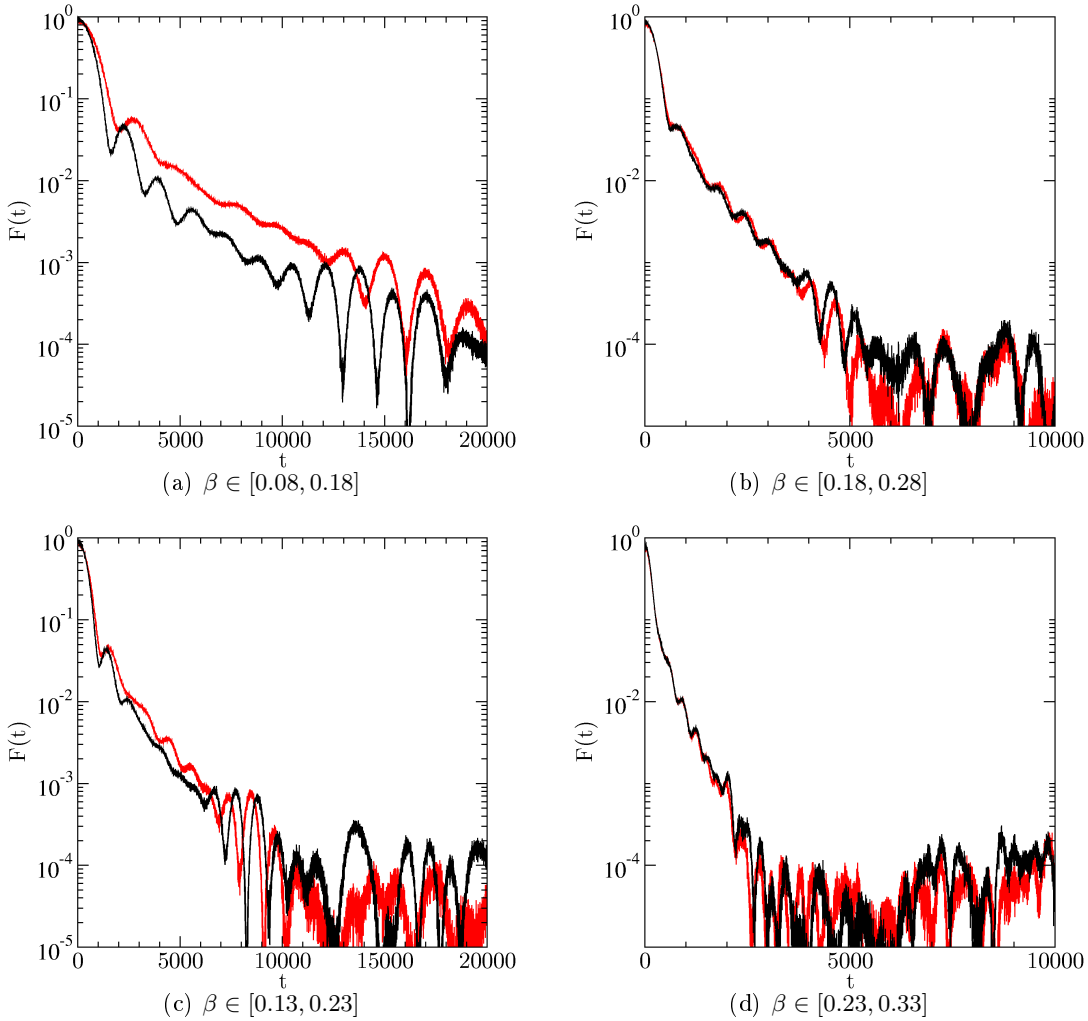

Figure 5.14: In this figure we show we show fig. 5.13(a) to fig. 5.13(d) in semi-logarithmic scaling.

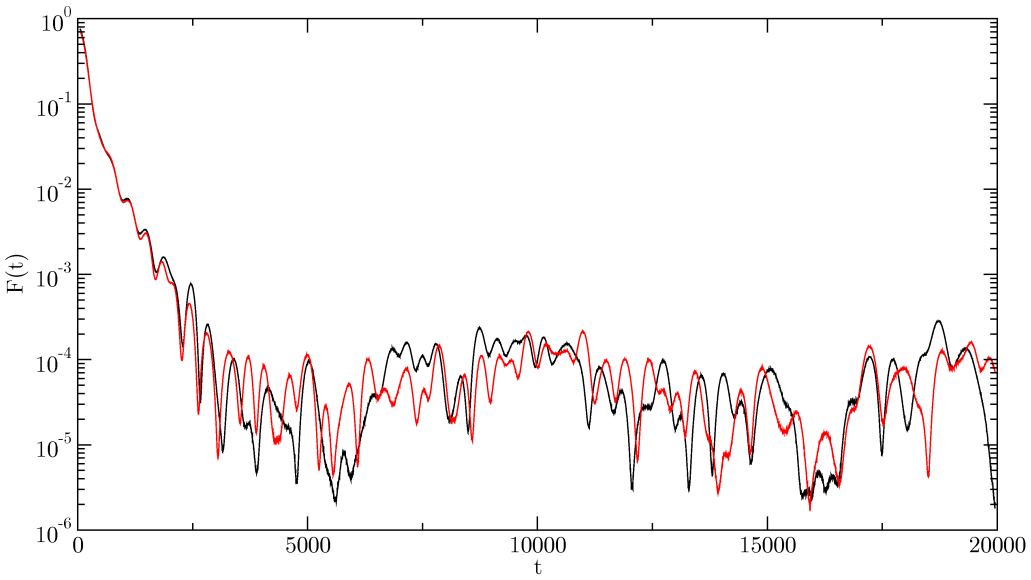

Figure 5.15: In this figure we show an ensemble containing $\approx$ 10000 rotors with $\epsilon = 0.05$, $k_1 = 0.6\pi$, $k_2 = 0.8\pi$ and $\beta \in [0.2; 0.3]$. in order to show the oscillatory behaviour at long times we averaged the data over 100 kicks. The KR data is shown in red and the WKB data is shown in black.

started in the last subsection. The regimes can be seen best in the intermediate ensembles in fig. 5.14:

- An initial fast decay could be approximated by a Gaussian decay. On the other hand also the analytical result describes the behaviour well by using a $\sin(t)/t$ function. This can also be interpreted as approximations to each other and therefore we cannot really give a strict criterion to decide how this initial decay can be described.

- A intermediate decay. After the initial drop the fidelity decays over a quite long time. Onto this decay process an oscillation is added which is dominating as soon as the value of the fidelity decays to the order of the oscillation amplitude which therefore defines the crossover to the next regime. This oscillation on the one hand limits the duration of the decay and on the other hand hides the behaviour in the vicinity to the crossover to saturation. These reasons make it impossible to identify an exponential or algebraic decay. Not only is the duration of the decay to short to justify algebraic behaviour but the region where one would see a difference is also blurred by the oscillation.

- A remaining oscillation that behaves like some saturation. In the introduction of the decay regime we mentioned that there is an oscillation superimposed. It seems that the amplitude of this oscillation saturates and therefore remains as the fidelity decays to the scale of this oscillation. This oscillation can be seen nicely in fig. 5.15. Nevertheless in this regime also other time

scales are visible and we cannot exclude further decay due to the limited time shown.

The visibility of this regimes depends on the range of β. It seems that the amplitude of the remaining amplitude only shows a weak β dependence and therefore the onset of the remaining oscillation or saturation depends on the decay rate of the fidelity in the decay regime. As can be seen in fig. 5.10 this decay is faster near the island. This corresponds to the idea of the KR as a perturbation of the pendulum and the pendulum approximation shows that the perturbation is strongest near the island. So we expect a stronger decay due to this perturbation.

For the second regime it is difficult to identify the decay behaviour. In order to specify the type of the decay one needs to plot the decay logarithmically and semi-logarithmically. This is done in fig. 5.13 and fig. 5.14. In the case far from the island we can find regions in which the behaviour can be approximated by a power law but these regions are much to short to clearly identify a power law. On the other hand the behaviour cannot be described by an exponential decay either. The oscillations make it difficult to distinguish between exponential and algebraic decay as they contribute significantly in the region where a difference between exponential and algebraic decay would show up. We therefore cannot apply this scheme to describe the decay. Despite the oscillation we have the impression that the WKB data shows a bending behaviour in the semi-logarithmic plots and therefore is less likely to be exponential than the QKR data, but the oscillations nevertheless avoid a clear classification.

The correspondence of WKB and QKR also depends of the regime of β. In fig. 5.13 we can see that the correspondence breaks down most significantly far from the island. There the time scale of the decay seems to be stretched in the QKR data. This deviation, however, starts rather abrupt as can be seen by comparing fig. 5.14(b), fig. 5.13(c) and fig. 5.13(a) or their semi logarithmic counterparts in fig. 5.14. The deviation between the two ensembles near to the island is small whereas the difference between the two outer figures is much larger. The nearer we are to the island the better the correspondence gets for the decay. Nevertheless in the remaining oscillations some of the frequencies are seen to agree but the overall correspondence is lost.

Motivated by the analytical result one might be tempted to search for algebraic behaviour. However, this picture is somehow misleading and the picture of exponential decay allows us to understand a few things better. For the rotors far from the island we observed an algebraic behaviour for quite a long time but not for a too large range in the fidelity[8] itself. In fig. 5.13(f) we show the fidelity of an ensemble up to long times far from the island. We can see that it shows an algebraic behaviour on the scale we show. Unfortunately this decay behaviour is $1/t$ which is in direct contradiction to the prediction of a t^{-2} decay from our analytical theory. In order to compare to the WKB result we plotted the QKR data and the WKB data in fig. 5.16 in logarithmic and linear scaling. We can see

[8] At $F \approx 10^{-3}$ usually the problems appear. In fig. 5.13(f) and fig. 5.16 we the fidelity for an ensemble of QKRs is still larger.

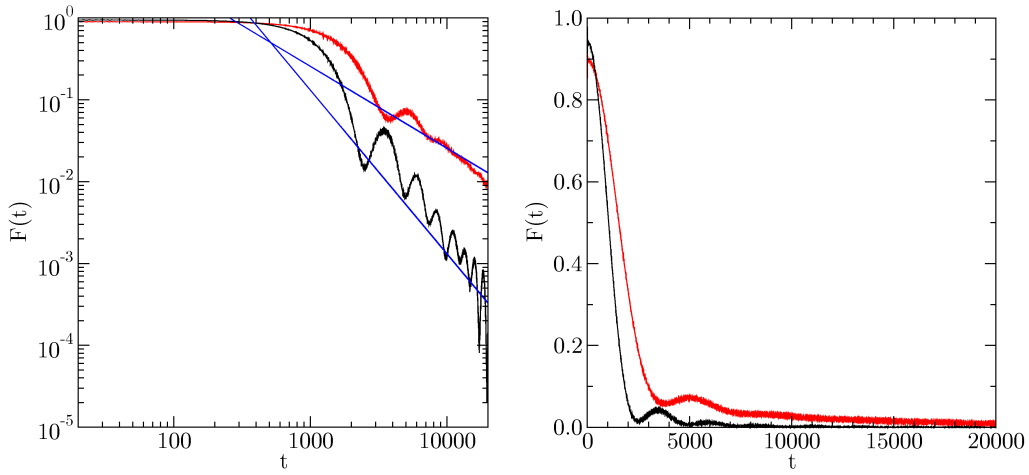

Figure 5.16: In this figure we show an ensemble of 10000 rotors for $\epsilon = 0.04$, $k_1 = 0.6\pi$, $k_2 = 0.8\pi$ and $\beta \in [0.035, 0.135]$. The QKR data is shown in red and the WKB data in black. In (a) we show the data in logarithmic and in (b) in linear scaling. To guide the eye we added a $1/t^2$ and a $1/t$ decay in blue. We can see that the WKB result is described by the $1/t^2$ until some intermediate time whereas the QKR data is more likely described by an unclear exponent.

that the WKB fulfils the prediction by the analytical theory well, whereas the QKR data seems to follow a power law with some non integer exponent. This emphasises that the algebraic behaviour may be just an approximation to an unknown asymptotic decay law. Considering fig. 5.10(a) we see that an exponential interpretation of the decay would lead to a growing decay time when leaving the island. This leads also in the logarithmic scaling to a bending of the fidelity and therefore would look like an algebraic behaviour but with a modified exponent. This explains why in the crossover region one observes strange exponents in fig. 5.13(f) and fig. 5.16.

5.4.5 Summary

In the end we are left with the question what we learned from the numerical observations. Therefore we have to distinguish the observations for single rotors and ensembles of rotors.

For single rotors we saw that the WKB result and the pendulum approximation correspond quite well, especially the main oscillatory time scale does so. This time scale is described well in a wide range where the amplitude and higher frequency components of the fidelity signal are missed when approaching the island. The pendulum describes the QKR when initial conditions are chosen near to the island. Leaving the vicinity of the island the correspondence becomes worse. Especially the β dependence of the main oscillation frequency is mis-estimated.

This wrong scaling was further analysed by building a sum of two rotors. This way we observed a beating phenomenon that can be described using the dominating term in WKB approximation. Also in this case we observe a mismatch

in time scales between pendulum and QKR. By comparing pairs of overlaps we could show that the pendulum locally can be a qualitative approximation to the QKR evolution.

Going from two rotors to a continuum of rotors we could not continue using the pendulum numerics as the calculations were to extensive. Instead we could use the WKB numerics as it describes the pendulum sufficient well. We compared the fidelity in several regimes and found out that the ensemble shares the problems of the approximation for single pendulums. Another problem is the type of the decay. On the one hand the decay is too short and on the other hand a remaining oscillation – leading to a saturation – hides the interesting behaviour. For a not too long time the WKB result can be regarded as a good approximation for the QKR.

We continued the discussion for the analytical result derived in section 4.6. We could show how this approximation breaks down when approaching the island. We could see that it nevertheless explains some special properties of the WKB. There is also a regime in which the analytical result describes the WKB solution and this describes the QKR result. Unfortunately, the long time decay is strictly $1/t^2$ for the analytical result and therefore it cannot explain the decay of the QKR. The just mentioned problems remain an open question for future studies.

Chapter 6

Conclusion and Outlook

6.1 Summary

In the calculation of the fidelity of a quantum state integrable states on the one hand are problematic as they cannot be described by universal properties and on the other hand such states allow explicit use of classical methods that by definition require regular structure. We focused at the kicked rotor as one of the cornerstones of non-linear dynamics and quantum chaos. Near to a resonance the system can be described by a pseudo-classical limit (dubbed also ϵ-classics). In this limit Abb *et al.* were able to calculate the fidelity using the island structure of the phase space [Abb09].

In this thesis we continued this approach and tried to find a description of the rotors belonging to some rotator type orbit. In order to describe these rotors we introduced the pendulum approximation. To obtain an analytical solution of the pendulum fidelity we used the WKB method in chapter 4. As the pendulum is already quite complicated and can be solved only by means of elliptic functions we had to do some further approximations. These approximations were discussed in section 4.3. In the end we could also give an approximate but analytical expression for ensembles of rotors using the WKB approximation for the pendulum. All these approximations were compared numerically to each other in chapter 5.

To understand the dynamics we first analysed the spectrum and the dynamics of the pendulum in chapter 3. Our focus was on two topics: We wanted to understand the effect of the quasimomentum as some intrinsic momentum offset onto the spectrum and we wanted to see whether we could reproduce the behaviour of the QKR using the pendulum Hamiltonian. We observed a part of the spectrum with a nearly equally spaced, β independent behaviour and another part with a parabolic net structure. We could explain this behaviour in a semi-classical way by considering island type tori which show β independent behaviour and rotator like tori which are shifted when varying β. This is also what the result of the WKB calculations in section 4.3 showed.

The pendulum approximation was derived in the ϵ-classical approximation. We know that the pendulum approximation works quite well in the classical phase space when the kicking is not too strong. It also reproduces the two different topologies of trajectories. Nevertheless, this does not guarantee that it

also reproduces the quantum behaviour. We compared the evolution of an initial state between QKR and pendulum using ϵ-classical Husimi functions. We saw that the pendulum approximation reproduced the dynamics of the QKR[1] for initial β-rotors quite well for short times. For long time behaviour we cannot say anything by using the Husimi function as the wave function becomes non-classical very quickly.

To describe the pendulum we used the WKB approximation in section 4.3. We approximated the action in a power series. For the calculation of energy eigenfunctions we had to fulfil a periodic boundary condition which forced us to take only the first order term into account. For the calculation of the eigenenergies we were able to give a more accurate result. We showed that the main characteristics of the pendulum can be understood by the spectral structure. To show this, we selected the dominating terms using the wave function and identified their temporal behaviour focusing on the spectrum. We showed that the long time oscillations can be described by the slowest oscillating terms.

In order to build the fidelity of an ensemble we checked whether the dominating terms we identified describe the fidelity. We showed that the slow components dominate the long time behaviour also in the case of ensembles. For building the ensemble, we integrated the WKB result restricted to the diagonal elements in section 4.6. To do this we had to approximate the spectrum linearly. In this way we could obtain an analytical approximation that describes the fidelity qualitatively. The analytical result predicts an strict $1/t^2$ decay of the fidelity. We could understand the shortages of the approximation.

To test these predictions we did extensive numerical checks in chapter 5. We compared single pendulums, averages of two overlaps and ensembles in the different approximations. For single rotors we showed that the WKB approximation gets worse near the island and the approximation of the pendulum to the QKR gets worse when leaving the island. In the case of WKB and pendulum, the mismatch arises in the underestimation of higher frequency components or beating phenomena. Nevertheless the main energy scales are reproduced quite well. Comparing the pendulum and the QKR we found that the pendulum does not well reproduce the time-scales of the QKR. The QKR has much longer time scales at the border of the phase space cell as the pendulum. Nevertheless, the fast oscillatory behaviour is described quite well initially. We showed that the mismatch of the amplitude can be understood when interpreting the near resonant results as deviation of the resonant behaviour. Even in the resonant behaviour a deviation could be shown by comparison to the previous results [Wim06] and [Abb09]. The mismatch of time scales could be motivated by comparing phase spaces.

Using pairs of rotors we could show that the decay behaviour is related to some common phase factor that does not influence the fidelity of single rotors but can lead to beating when comparing different rotors. By comparing different pairs of rotors we could show that the scaling behaviour of the quantum kicked rotor can locally be described by the pendulum approximation. Nevertheless we have the same breakdown of time scales that we also observed in the single rotors

[1] We did not use some ϵ-classical Floquet operator. We used the Floquet operator that was defined on the original space but analysed it using coherent states in the ϵ-classical phase space.

and the scaling factor is similar.

In the case of continuous ensembles the results are inconclusive. We had to master two tasks independently. On the one hand, we had to understand where which approximation fails and, on the other hand, we had to understand the decay behaviour of pendulum, WKB and QKR ensembles. The discussion of the quality of the approximation is very important as we cannot calculate big ensembles using the pendulum as their evaluation is very time consuming. We showed that the correspondence between the WKB result and the pendulum data is surprisingly good even in the regime where the approximation is not perfect for single rotors. This allowed us to use the numerical WKB result which can be evaluated easily for comparison to the QKR. The comparison of the analytical result to the pendulum data showed that the analytical result approximates the data very well far from the island and for not too large ϵ. When approaching the island the result breaks down quite fast. The analytical result shows a strict algebraic behaviour in contrast to the WKB ensembles and QKR ensembles. They show an initial fast decay which is followed by an intermediate decay on which an oscillation is added. This oscillation leads to a seemingly saturation like behaviour in contrast to the analytical result.

We have a description for the pendulum in which we can describe some features even using an analytical approximation. The correspondence breaks down near the island. The correspondence between QKR and pendulum breaks down far from the island. The regime where both approximations are valid is narrow. The WKB result is only able to describe the decay qualitatively for not too long times. At long times also the pendulum approximation breaks down.

6.2 Outlook and Open Questions

Our treatment of the QKR in pendulum approximation could not give a closed picture of the fidelity decay. We saw in chapter 5 that the breakdown of the approximations is only understood in a very qualitative way. There is no strict estimate of the errors. There are three steps of approximation: the approximation of the WKB result for the pendulum, the approximation of the pendulum to the QKR and the approximation for the exponent when deriving the analytical result.

One of the major problems in the derivation of the eigenfunctions for the pendulum in chapter 4 was that we had to truncate the approximation very soon because we needed to be able to solve the resulting equation consistently. We chose to make an expansion in powers of $\tilde{k}/E$ where $\tilde{k}$ is the ϵ-classical kicking strength and E is the energy. Maybe there is another type of expansion that allows the calculation of the energy with a higher precision. This would result in better wave functions and a better matrix. On the other hand one might try to introduce the exact solution of the pendulum and use some expansion of them. This might improve the theory near to the island. Such an approach might lead to an expression that is easier to integrate when building ensembles.

The correspondence between pendulum and the QKR is nevertheless still problematic on the classical level. We were not able to obtain a strict estimation of the

errors in this case. Having a better understanding of this approximation might help to understand the deviation in the time scales. Including higher order terms into the expansion makes the time independent pendulum approximation time dependent. We do not know how to treat such a problem semi-classically. Maybe it is possible to derive an effective model on the classical level.

In the derivation of the analytical result some consideration to the approximation of the integral would be helpful. We made the crudest approximation one can imagine in section 4.6. The integration can only be carried out directly in linear approximation in the exponent. Higher orders would lead to Fresnel integrals. One could try to introduce these functions into the solution in order to see where they contribute. We also thought about a different linear approximation. Our choice of the Taylor expansion was somehow arbitrary. Another idea was to choose a linear approximation reproducing the average slope and average value. This might solve the problem of the wrong time scale. Nevertheless it will make the formulas more complicated and the problem of missing higher orders is still present. A different expansion for the energy difference might help to include higher orders and therefore the skewness of the energy differences as a function of β in the calculations.

Besides the control of the approximations the comparison with other works of numerical data would be interesting. Other publications in this field deal mainly with coherent initial states [Wei05, San03, Hau05]. Our observations were mostly in momentum eigenstates for the sake of simplicity in the calculations. Using coherent states would introduce additional square terms that one might be able to control. On the other hand there exist theories for the fidelity of coherent states [Gor06].

There is also a theory for fidelity based on correlation functions [Gor06]. One could numerically evaluate these correlations in order to see whether it helps identifying the type of exponential decay numerically observed in the QKR system. Even if we might not be able to calculate these correlation analytically, such consideration might give an idea what determines this decay. The evaluation of the correlations for the pendulum could help to decide whether the unclear decay behaviour is due to a crossover between two regimes of decay.

In fig. 5.10 we showed ensembles of same width centred around different β values. We noticed that the functional form of all the fidelity decays is similar. Therefore we tried to rescale the time for each ensemble individually in order to see whether they show universal behaviour. The result of this rescaling is shown in fig. 6.1. We can see that in intermediate times the fidelities show some universal behaviour. We did not yet find a theoretical explanation but we think that this is a sign for some interesting future work.

However, these possibilities are rather technical ideas to continue this work. In our treatment of the rotator like orbits we found out that a simple treatment using the pendulum will not give a convincing description of the decay behaviour of the QKR. Therefore it is more promising to go back to states on the island and add gravity. By adding the gravity the rotational tori are destroyed and the

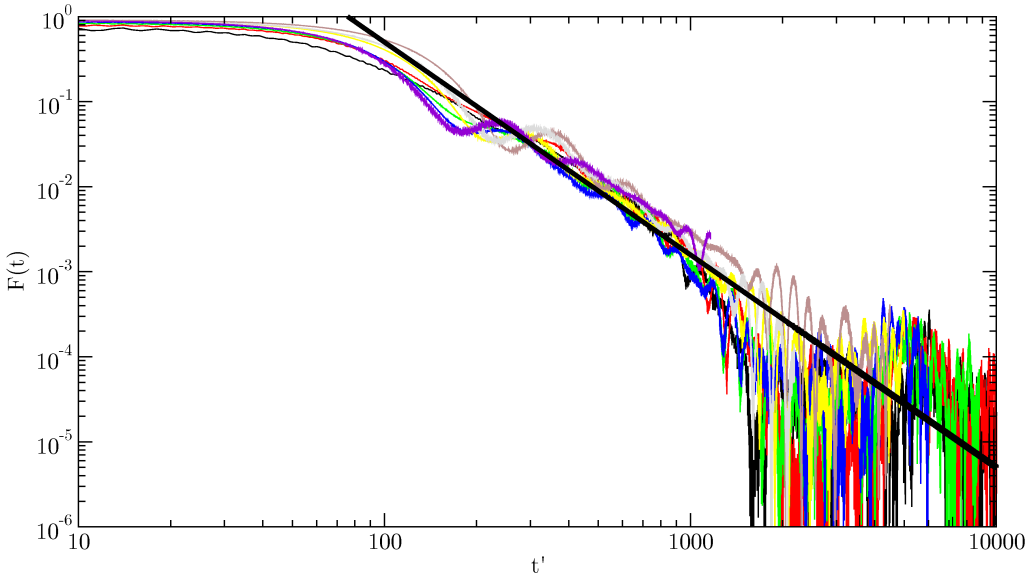

Figure 6.1: In this figure we show the same data as in fig. 5.10, where we presented different ensembles with $\delta\beta = 0.1$, $\epsilon = 0.5$, $k_1 = 0.6\pi$ and $k_2 = 0.8\pi$, but with rescaled times. The rescaled time $t' \equiv \alpha t$ where $0.1 < \alpha < 0.75$ was chosen for each ensemble individually. We want to show that the intermediate behaviour seems to be universal. The thick black line is an $t^{5/2}$ function.

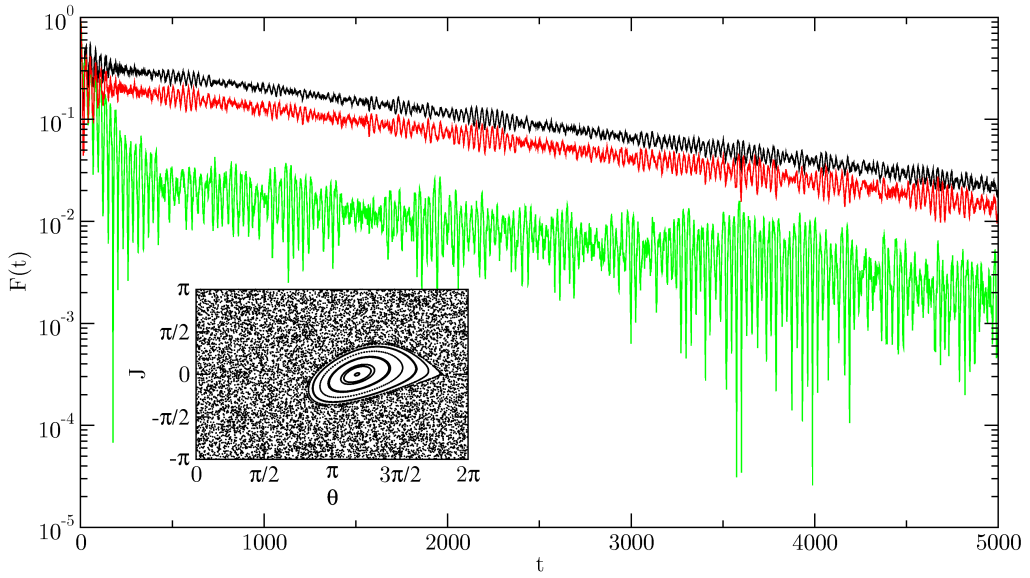

Figure 6.2: We show the fidelity for states in a QKR system with gravity with $\beta = 0.4898$, $\epsilon = -0.42319$, $\tau = 6.28319$, $\eta = 0.09253$, $k_1 = 0.7\pi$ and $k_2 = 0.8\pi$ (for a definition of the gravity parameter η and a derivation of the Hamiltonian see [Fis03]). We show different initial states. The black data is a coherent state centred on the island an with optimal squeezing, the red data is a coherent state centred on the island but squeezed in order to have an overlap with the chaotic sea. For comparison we also show a angular momentum eigenstate covered partially by the resonance island. In the inset we show the ϵ-classical phase space.

phase space develops chaotic regions, whereas the island is deformed but survives for moderate parameters. In this mixed phase space a state on the island couples to the chaotic sea.

Fidelity is one possibility to study the stability of such states and the influence of the chaotic environment on them. In [Wim04] the influence of the mixed phase space on the fidelity decay of a initial angular momentum eigenstate was studied numerically. It was found that the fidelity decay of a momentum eigenstate can be separated into two regimes. In the beginning a rapid decay followed by a slow exponential decay was observed. A central result from [Wim04] is shown in green in fig. 6.2. A first interpretation was that the initial decay is due to the part of the wave function overlapping with the chaotic sea and that the slow decay is due to tunnelling to the chaotic environment.

We tried to test his surmise by placing a coherent state on the island. The result is shown in fig. 6.2. We can see that such a state shows the same slow exponential decay as an initial angular momentum state. This essentially affirms the surmise by of [Wim04]. It would be interesting to understand how tunnelling out of a nonlinear resonance island effects the fidelity. Besides the here presented results on the gravity-free case, the question how fidelity evolves for the system of fig. 6.2 opens a new interesting field of study [Dub].

Appendices

Appendix A

Bessel Formulas

One of the constant visitors in the field of calculations around the quantum kicked rotor are the Bessel functions. One of the main reasons is the Anger expansion which is basically an integral representation of the Bessel functions of first kind. It allows to express the kick operator in the angular momentum representation using the Bessel functions. On the other hand the same reason makes them also a perfect tool in the pendulum calculations. Therefore we will give several formulas and identities that help handling them.

Some Expansions

Jacobi-Anger Expansion

The following formulas are eqs. (9.1.42) and (9.1.43) from [Abr64]. They relate the Bessel functions of first kind to the trigonometric functions.

$$\cos(z\sin\theta) = J_0(z) + 2\sum_{k=1}^{\infty} J_{2k}(z)\cos(2k\theta) \tag{A.1}$$

$$\sin(z\sin\theta) = 2\sum_{k=0}^{\infty} J_{2k+1}(z)\sin((2k+1)\theta). \tag{A.2}$$

Using these two equations to rewrite $\mathrm{e}^{\imath z\sin\theta} = \cos(z\sin\theta) + \imath\sin(z\sin\theta)$ we arrive after resorting the indices and rewriting the sine and cosine in terms of complex exponential functions at

$$\mathrm{e}^{\imath z\sin\theta} = \sum_{k=-\infty}^{\infty} J_k(z)\mathrm{e}^{\imath k\theta} \tag{A.3a}$$

$$= \sum_{k=-\infty}^{\infty} (-1)^k J_k(z)\mathrm{e}^{-\imath k\theta} \tag{A.3b}$$

By shifting θ we find as an analogous eqs. (9.1.44) and (9.1.45) from [Abr64]

$$\cos(z\cos\theta) = J_0(z) + 2\sum_{k=1}^{\infty}(-1)^k J_{2k}(z)\cos(2k\theta) \tag{A.4}$$

$$\sin(z\cos\theta) = 2\sum_{k=1}^{\infty}(-1)^k J_{2k+1}(z)\cos((2k+1)\theta) \tag{A.5}$$

the corresponding expansion of $\mathrm{e}^{\imath z\cos\theta}$

$$\mathrm{e}^{\imath z\cos\theta} = \sum_{k=-\infty}^{\infty} \imath^k J_k(z)\mathrm{e}^{\imath k\theta} \tag{A.6a}$$

$$= \sum_{k=-\infty}^{\infty} \imath^k J_k(z)\mathrm{e}^{-\imath k\theta}. \tag{A.6b}$$

Some Representations

A very helpful integral representation can be achieved by using the Jacobi-Anger expansion.

$$\int_0^{2\pi} \mathrm{e}^{\imath n\theta}\mathrm{e}^{\imath z\sin\theta} = 2\pi(-1)^n\ J_n(z) \tag{A.7}$$

$$\int_0^{2\pi} \mathrm{e}^{\imath n\theta}\mathrm{e}^{\imath z\cos\theta} = 2\pi\ \imath^n\ J_n(z). \tag{A.8}$$

they can be derived by inserting eq. (A.3) and eq. (A.6) and carry out the integration.

Asymptotic Expansion

In [Arf08] an expansion for the Bessel functions of integer order is derived:

$$J_n(x) = \sum_{s=0}^{\infty} \frac{(-1)^s}{s!(n+s)!}\left(\frac{x}{2}\right)^{n+2s}. \tag{A.9}$$

For large order and the rest fixed we have eq.(9.3.1) in [Abr64]:

$$J_n(x) \propto \frac{1}{\sqrt{2\pi n}}\left(\frac{ex}{2n}\right)^n. \tag{A.10}$$

Appendix B

Density of Trajectories

In chapter 4 we reviewed the derivation of WKB by applying a Fourier transformation to the van Vleck propagator. In the van Vleck propagator there is a term representing the density of states. This density gives us a measure of the trajectories starting in the vicinity of x and ending in the vicinity of y within the fixed time t. This density of trajectories is given as

$$D \equiv \det \left| \frac{\partial^2 S(x,y,t)}{\partial x \partial y} \right|, \tag{B.1}$$

where the time is fixed. The problem is to express this determinant by means of energy instead of time. In chapter 4 therefore a Legendre transformation is done. This yields

$$E = -\frac{\partial S(x,y,t)}{\partial t} \tag{B.2}$$

$$W(x,y,E) = S(x,y,t(E)) + Et(E) \tag{B.3}$$

$$S(x,y,t) = W(x,y,E(t)) - E(t)t, \tag{B.4}$$

where the first equation determines $t(x,y,E)$ and vice versa.

In order to introduce this transformation to D we have to remind ourselves that the term comes from the variation of the classical action by x and y at given time t. If we want to express D by means of W we need to take into account that the energy must not be constant when varying x and y at fixed t. In addition there are some identities for the derivatives [Sch96]

$$\frac{\partial W(x,y,E)}{\partial E} = t \tag{B.5}$$

$$\frac{\partial S(x,y,t)}{\partial u} = \frac{\partial W(x,y,E)}{\partial u}, \tag{B.6}$$

where the derivative with respect to u means derivation with respect to x or y where all other quantities (including E and t) are kept fixed. As the variation is at fixed time, the derivative of the time by x or y must vanish. This means [Gut90]

$$\frac{\partial t}{\partial u} = 0 = \frac{\partial^2 W(x,y,E)}{\partial u \partial E} + \frac{\partial^2 W(x,y,E)}{\partial E^2} \frac{\partial E}{\partial u}, \tag{B.7}$$

which directly gives

$$\frac{\partial E}{\partial u} = \frac{\partial^2 W(x,y,E)}{\partial u \partial E}\left(\frac{\partial^2 W(x,y,E)}{\partial E^2}\right)^{-1}. \tag{B.8}$$

Introducing this into D we arrive at

$$\left.\frac{\partial^2 S(x,y,t)}{\partial x \partial y}\right|_t = \frac{\partial}{\partial x}\left(\left.\frac{\partial W(x,y,E)}{\partial y}\right|_E + \left.\frac{\partial W(x,y,E)}{\partial E}\right|_E \left.\frac{\partial E}{\partial y}\right|_t - \left.\frac{\partial E}{\partial y}\right|_t t\right) \tag{B.9}$$

$$= \left.\frac{\partial^2 W(x,y,E)}{\partial x \partial y}\right|_E + \left.\frac{\partial^2 W(x,y,E)}{\partial E \partial x}\right|_E \left.\frac{\partial E}{\partial y}\right|_t + \underbrace{\left.\frac{\partial W(x,y,E)}{\partial E}\right|_E}_{=t} \left.\frac{\partial^2 E}{\partial x \partial y}\right|_t - \left.\frac{\partial^2 E}{\partial x \partial y}\right|_t t \tag{B.10}$$

$$= \left.\frac{\partial^2 W(x,y,E)}{\partial x \partial y}\right|_E + \left.\frac{\partial^2 W(x,y,E)}{\partial E \partial x}\right|_E \frac{\partial^2 W(x,y,E)}{\partial y \partial E}\left(\frac{\partial^2 W(x,y,E)}{\partial E^2}\right)^{-1} \tag{B.11}$$

As $t(E)$ and $E(t)$ are inverse to each other we find for the derivatives $\partial_t E = (\partial_E t)^{-1}$. Inserting eqs. (B.2) and (B.5) we obtain

$$\frac{\partial^2 S}{\partial t^2} = -\left(\frac{\partial^2 W}{\partial E^2}\right)^{-1}. \tag{B.12}$$

Putting all these formulas together we find

$$-\frac{\det(\partial^2 S/\partial x \partial y)}{\partial^2 S/\partial t^2} = \det\begin{bmatrix} \frac{\partial^2 W}{\partial x \partial y} & \frac{\partial^2 W}{\partial x \partial E} \\ \frac{\partial^2 W}{\partial y \partial E} & \frac{\partial^2 W}{\partial E^2} \end{bmatrix} \equiv \tilde{D}. \tag{B.13}$$

In chapter 4 a specialised version of this is used. There we noticed just shortly that we will deal with Hamltonians which have a spatial potential and a kinetic term which just depends on the momentum quadratically. This means we can write the action W as an integral

$$W(x,y,E) = \int_x^y \sqrt{2mE - V(u)}\mathrm{d}u. \tag{B.14}$$

This means that we can write the result as a sum of primitives. One consequence is that there are no terms containing a product of x and y and therefore the left upper entry in the matrix in eq. (B.13) will vanish. So we get the expression used in chapter 4

$$\tilde{D} = -\frac{\partial^2 W}{\partial y \partial E}\frac{\partial^2 W}{\partial x \partial E} \tag{B.15}$$

Appendix C

Multinomial Expansion

From standard calculus we know the binomial theorem to expand $(a+b)^n$. If we would like to calculate a sum to some integer power we need the multinomial theorem. This gives

$$\left(\sum_{i=1}^{m} a_i\right)^n = \sum_{\substack{1\leqslant k_1,\ldots,k_m\leqslant m \\ n=k_1+\ldots+k_m}} \binom{n}{k_1,\ldots,k_m} a_1^{k_1}\ldots a_m^{k_m}, \tag{C.1}$$

where the multinomial coefficients are defined as

$$\binom{n}{k_1,\ldots,k_m} = \frac{n!}{k_1!\ldots k_m!}. \tag{C.2}$$

We want to use this theorem to get the power series of a Taylor expansion to an integer power. This means that we are interested in the case $a_i = A_{i-1}\epsilon^{i-1}$ which corresponds to $(\sum_{i=0}^{m-1} A_i\epsilon^i)^n$ witch is equal to $(\sum_{i=1}^{m} A_{i-1}\epsilon^{i-1})^n$. Inserting this in eq.(C.1) We get

$$\left(\sum_{i=1}^{m} A_{i-1}\epsilon^{i-1}\right)^n = \sum_{\substack{1\leqslant k_1,\ldots,k_m\leqslant m \\ n=k_1+\ldots+k_m}} \binom{n}{k_1,\ldots,k_m} A_0^{k_1}\cdots A_{m-1}^{k_m}\epsilon^{1\cdot k_1+2\cdot k_3+\ldots+(m-1)\cdot k_m}. \tag{C.3}$$

We are now interested in the contributions in the different orders in ϵ. Therefore we assume $m > n$. This is no real restriction as A_i is at least of order ϵ^i and the case of $m < n$ can be included by choosing $\forall i > m : A_i = 0$.

We now need to collect all terms to a certain power of ϵ. If we are interested in the order ϵ^l we have to find all combinations of $k_2\ldots k_m$ so that $k_2 + 2\cdot k_2 + \ldots + (m-1)\cdot k_m = l$ where $\sum_i k_i < l$. This means we have to collect all terms which contribute some ϵ with the corresponding exponent. As all terms have the same number of factors we still have to choose $k_1 = n - \sum_i k_i$ which means filling up with terms contributing no ϵ.

We do this for the different orders in ϵ seperately. In the course of this we hope that the procedure gets clear.

$O(1)$

This means we just have contributions by k_1 because all other k_i would lead to an power in ϵ. This means

$$k_1 = n \wedge \forall i > 1 : k_i = 0. \tag{C.4}$$

$O(\epsilon)$

Here the case is still simple as only one ϵ appears. This means

$$k_2 = 1 \wedge (\forall i > 2 : k_i = 0) \wedge k_1 = n - 1. \tag{C.5}$$

$O(\epsilon^2)$

This is the first non trivial case. But we know that there are only two different types of k_i involved. So we have already two different types of terms:

$$k_3 = 1 \wedge k_1 = n - 1 \wedge (\forall i \neq 3 \vee i \neq 1 : k_i = 0) \tag{C.6a}$$
$$k_2 = 2 \wedge k_1 = n - 2 \wedge (\forall i \neq 2 \vee i \neq 1 : k_i = 0). \tag{C.6b}$$

$O(\epsilon^3)$

In this case we need to list all combinations with the right resulting power in ϵ:

$$k_4 = 1 \wedge k_1 = n - 1 \wedge (\forall i \neq 4 \vee i \neq 1 : k_i = 0) \tag{C.7a}$$
$$k_3 = 1 \wedge k_2 = 1 \wedge k_1 = n - 2 \wedge (\forall i \neq 3 \vee i \neq 2 \vee i \neq 1 : k_i = 0). \tag{C.7b}$$
$$k_2 = 3 \wedge k_1 = n - 3 \wedge (\forall i \neq 2 \vee i \neq 1 : k_i = 0). \tag{C.7c}$$

If we go on like this we will find the contribution in every order in ϵ we desire. As we need only the order ϵ^4 as motivated in section 4.3.2 we will stop here and build the final formula. We hope we made clear how to proceed in order to get higher orders.

After we now found out which index combinations contribute in which order we now have to calculate the corresponding multinomial coefficients from eq.(C.2). Doing this we arrive at our final formula

$$\left(\sum_{i=0}^{\infty} A_i \epsilon^i\right)^n = A_0^n + \epsilon\ n\ A_0^{n-1} A_1 + \epsilon^2 \left(n\ A_0^{n-1} A_2 + \frac{n(n-1)}{2}\ A_0^{n-2} A_1^2\right)$$
$$\epsilon^2 \left(\frac{n(n-1)(n-2)}{6}\ A_0^{n-3} A_1^3 + n(n-1)\ A_0^{n-2} A_1 A_2 + n\ A_0^{n-1} A_3\right) + O(\epsilon^4). \tag{C.8}$$

Appendix D

Integrating the Oscillation in the Diagonal Approximation

In chapter 4.6 We show an integral that shows the decay of fidelity. We showed it for the most simple case of the c_{00} term. The terms connected to the cosine terms in eq. (4.80) are more complicated. Therefore we rewrite the cosine in complex exponential functions

$$\begin{aligned}&\int_{-\delta/2}^{\delta/2} \mathrm{e}^{\imath\frac{k_2^2-k_1^2}{4}\left(\frac{1}{\tilde{\beta}^2}-\frac{2}{\tilde{\beta}^3}\delta\bar{\beta}\right)\epsilon t}\cos\left(m\frac{k_1^2-k_2^2}{2}\left(\frac{1}{\tilde{\beta}^3}-\frac{3}{\tilde{\beta}^4}\delta\bar{\beta}\right)\epsilon^2 t\right)\mathrm{d}\delta\bar{\beta}\\ &\quad=\mathrm{e}^{\imath\frac{\delta(k^2)}{4\tilde{\beta}^2}\epsilon t}\int_{-\delta/2}^{\delta/2}\mathrm{e}^{-\imath\frac{\delta(k^2)\epsilon t}{2\tilde{\beta}^3}\delta\bar{\beta}}\frac{1}{2}\left(\mathrm{e}^{\imath m\frac{\delta(k^2)\epsilon^2 t}{2}\left(\frac{1}{\tilde{\beta}^3}-\frac{3}{\tilde{\beta}^4}\delta\bar{\beta}\right)}+\mathrm{e}^{-\imath m\frac{\delta(k^2)\epsilon^2 t}{2}\left(\frac{1}{\tilde{\beta}^3}-\frac{3}{\tilde{\beta}^4}\delta\bar{\beta}\right)}\right)\delta\bar{\beta}\end{aligned} \tag{D.1}$$

We will focus on one of the summands as the different sign in the exponent can be absorbed in m. Therefore we rewrite

$$\begin{aligned}&\mathrm{e}^{\imath\frac{\delta(k^2)\epsilon t}{4\tilde{\beta}^2}}\int_{-\delta/2}^{\delta/2}\mathrm{e}^{-\imath\frac{\delta(k^2)\epsilon t}{2\tilde{\beta}^3}\delta\bar{\beta}}\frac{1}{2}\mathrm{e}^{\imath m\frac{\delta(k^2)\epsilon^2 t}{2}\left(\frac{1}{\tilde{\beta}^3}-\frac{3}{\tilde{\beta}^4}\delta\bar{\beta}\right)}=\\ &\qquad\qquad\frac{1}{2}\,\mathrm{e}^{\imath\frac{\delta(k^2)\epsilon t}{4\tilde{\beta}^2}\left(1+\frac{2m\epsilon}{\tilde{\beta}}\right)}\int_{-\delta/2}^{\delta/2}\mathrm{e}^{-\imath\frac{\delta(k^2)\epsilon t}{2\tilde{\beta}^3}\left(1+\frac{3m\epsilon}{\tilde{\beta}}\right)\delta\bar{\beta}}\end{aligned} \tag{D.2}$$

and carry out the integration

$$=\mathrm{e}^{\imath\frac{\delta(k^2)\epsilon t}{4\tilde{\beta}^2}\left(1+\frac{2m\epsilon}{\tilde{\beta}}\right)}\frac{2\tilde{\beta}^3}{\delta(k^2)\epsilon t(1+\frac{3m\epsilon}{\tilde{\beta}})}\sin\left(\frac{\delta(k^2)\epsilon t}{4\tilde{\beta}^3}\left(1+\frac{3m\epsilon}{\tilde{\beta}}\right)\delta\right). \tag{D.3}$$

Applying this on eq.(D.1) we find

$$\int_{-\delta/2}^{\delta/2} \mathrm{e}^{\imath\frac{k_2^2-k_1^2}{4}\left(\frac{1}{\tilde\beta^2}-\frac{2}{\tilde\beta^3}\delta\bar\beta\right)\epsilon t}\cos\left(m\frac{k_1^2-k_2^2}{2}\left(\frac{1}{\tilde\beta^3}-\frac{3}{\tilde\beta^4}\delta\bar\beta\right)\epsilon^2 t\right)\mathrm{d}\delta\bar\beta$$
$$= \frac{2\tilde\beta^3}{\delta(k^2)\epsilon t}\mathrm{e}^{\imath\frac{\delta(k^2)\epsilon t}{4\tilde\beta^2}}\left[\mathrm{e}^{\imath\frac{\delta(k^2)m\epsilon^2 t}{2\tilde\beta^3}}\frac{\sin\left(\frac{\delta(k^2)\epsilon t}{4\tilde\beta^3}\left(1+\frac{3m\epsilon}{\tilde\beta}\right)\delta\right)}{1+\frac{3m\epsilon}{\tilde\beta}}+\right.$$
$$\left.\mathrm{e}^{-\imath\frac{\delta(k^2)m\epsilon^2 t}{2\tilde\beta^3}}\frac{\sin\left(\frac{\delta(k^2)\epsilon t}{4\tilde\beta^3}\left(1-\frac{3m\epsilon}{\tilde\beta}\right)\delta\right)}{1-\frac{3m\epsilon}{\tilde\beta}}\right]. \quad \text{(D.4)}$$

This formula is not verry handy. Unfortunatlly there is not too much hope for simplifications. This comes from the denominator. If we could factor out the denominator we could treat the rest as an trigonometric expression and try to recombine the terms, but the denominator somehow leads to a missmatch of the amplitudes and therefore is verry hard to handel.

In order to get a more handy expression we define

$$I(k_1,k_2,m,\epsilon,\tilde\beta,t) \equiv \mathrm{e}^{\imath\frac{\delta(k^2)m\epsilon^2 t}{2\tilde\beta^3}}\frac{\sin\left(\frac{\delta(k^2)\epsilon t}{4\tilde\beta^3}\left(1+\frac{3m\epsilon}{\tilde\beta}\right)\delta\right)}{1+\frac{3m\epsilon}{\tilde\beta}}+$$
$$\mathrm{e}^{-\imath\frac{\delta(k^2)m\epsilon^2 t}{2\tilde\beta^3}}\frac{\sin\left(\frac{\delta(k^2)\epsilon t}{4\tilde\beta^3}\left(1-\frac{3m\epsilon}{\tilde\beta}\right)\delta\right)}{1-\frac{3m\epsilon}{\tilde\beta}} \quad \text{(D.5)}$$

so we can write

$$\int_{-\delta/2}^{\delta/2} \mathrm{e}^{\imath\frac{k_2^2-k_1^2}{4}\left(\frac{1}{\tilde\beta^2}-\frac{2}{\tilde\beta^3}\delta\bar\beta\right)\epsilon t}\cos\left(m\frac{k_1^2-k_2^2}{2}\left(\frac{1}{\tilde\beta^3}-\frac{3}{\tilde\beta^4}\delta\bar\beta\right)\epsilon^2 t\right)\mathrm{d}\delta\bar\beta$$
$$= \frac{2\tilde\beta^3}{\delta(k^2)\epsilon t}\mathrm{e}^{\imath\frac{\delta(k^2)\epsilon t}{4\tilde\beta^2}} I(k_1,k_2,m,\epsilon,\tilde\beta,t). \quad \text{(D.6)}$$

Bibliography

[Abb09] M. Abb, I. Guarneri, and S. Wimberger. Pseudoclassical theory for fidelity of nearly resonant quantum rotors. Phys. Rev. E **80** (2009), 035206. URL http://link.aps.org/doi/10.1103/PhysRevE.80.035206.

[Abr64] M. Abramowitz and I. A. Stegun. Handbook of Mathematical Functions with Formulas, Graphs, and Mathematical Tables. Dover, New York, ninth dover printing, tenth gpo printing edition (1964).

[Ald80] R. Aldrovandi and P. L. Ferreira. Quantum pendulum. American Journal of Physics **48** (1980), 660–664. URL http://link.aip.org/link/?AJP/48/660/1.

[And99] E. Anderson, editor. LAPACK users' guide. Software environments tools. Society for Industrial and Applied Mathematics, Philadelphia, Pa., 3. ed. edition (1999).

[Arf08] G. Arfken and H. J. Weber. Mathematical methods for physicists. Elsevier Academic Press, Amsterdam, Heidelberg, 6. ed., 5. [print., international ed.] edition (2008).

[Ash06] N. W. Ashcroft and N. D. Mermin. Solid state physics. Brooks/Coole Thomson Learning, Singapore, 33. [repr.], (college edition) edition (2006).

[Bal06] L. E. Ballentine. Quantum mechanics. World Scientific, Singapore, repr. edition (2006).

[Bha99] C. F. Bharucha, J. C. Robinson, F. L. Moore, B. Sundaram, Q. Niu, and M. G. Raizen. Dynamical localization of ultracold sodium atoms. Phys. Rev. E **60** (1999), 3881–3895. URL http://link.aps.org/doi/10.1103/PhysRevE.60.3881.

[Bre92] N. Brenner and S. Fishman. Pseudo-randomness and localization. Nonlinearity **5** (1992), 211. URL http://stacks.iop.org/0951-7715/5/i=1/a=009.

[Cas88] G. Casati, I. Guarneri, and D. Shepelyansky. Hydrogen atom in monochromatic field: chaos and dynamical photonic localization. Quantum Electronics, IEEE Journal of **24** (1988), 1420 –1444.

[Dub] R. Dubertrand, B. Probst, and S. Wimberger In preparation.

[Fis02] S. Fishman, I. Guarneri, and L. Rebuzzini. Stable Quantum Resonances in Atom Optics. Phys. Rev. Lett. **89** (2002), 084101. URL http://link.aps.org/doi/10.1103/PhysRevLett.89.084101.

[Fis03] S. Fishman, I. Guarneri, and L. Rebuzzini. A Theory for Quantum Accelerator Modes in Atom Optics. Journal of Statistical Physics **110** (2003), 911–943. URL http://dx.doi.org/10.1023/A:1022176306198.

[Fri06] H. Friedrich. Theoretical atomic physics. Springer, Berlin ; Heidelberg, [3. ed.] edition. Dt. Ausg. u.d.T.: Friedrich, Harald: Theoretische Atomphysik (2006).

[Gaz09] J.-P. Gazeau. Coherent states in quantum physics. Wiley-VCH, Weinheim (2009).

[Gia91] Chaos et physique quantique. Université Joseph Fourier Grenoble ; Ecole d'Eté de Physique Théorique 52, 1989, Les Houches, North-Holland, Amsterdam, XXXIII, 795 S. Nebent.: LesHouches 1989 (1991).

[Gol06] H. Goldstein, C. P. Poole, and J. Safko. Klassische Mechanik. Lehrbuch Physik. Wiley-VCH, Weinheim, 3. revised edition edition (2006).

[Gor06] T. Gorin, T. Prosen, T. H. Seligman, and M. Znidaric. Dynamics of Loschmidt echoes and fidelity decay. Physics Reports **435** (2006), 33 – 156. URL http://www.sciencedirect.com/science/article/B6TVP-4M7V9YY-1/2/16e2bcc2e1f0f3d2ab0cec38e670c087.

[Gre79] J. M. Greene. A method for determining a stochastic transition. Journal of Mathematical Physics **20** (1979), 1183–1201. URL http://link.aip.org/link/?JMP/20/1183/1.

[Gre84] D. R. Grempel, R. E. Prange, and S. Fishman. Quantum dynamics of a nonintegrable system. Phys. Rev. A **29** (1984), 1639–1647. URL http://link.aps.org/doi/10.1103/PhysRevA.29.1639.

[Gut90] M. C. Gutzwiller. Chaos in classical and quantum mechanics. Number 1 in Interdisciplinary applied mathematics. Springer, New York, NY (1990).

[Haa10] F. Haake. Quantum signatures of chaos. Springer series in synergetics. Springer, Berlin ; Heidelberg, 3., rev. and enlarged ed. edition (2010).

[Hau05] F. Haug, M. Bienert, W. P. Schleich, T. H. Seligman, and M. G. Raizen. Motional stability of the quantum kicked rotor: A fidelity approach. Phys. Rev. A **71** (2005), 043803. URL http://link.aps.org/doi/10.1103/PhysRevA.71.043803.

[Izr80] F. M. Izrailev and D. L. Shepelyanskii. Quantum resonance for a rotator in a nonlinear periodic field. Theoretical and Mathematical Physics **43** (1980), 553–561. URL http://dx.doi.org/10.1007/BF01029131, 10.1007/BF01029131.

[Izr86] F. M. Izrailev. Limiting quasienergy statistics for simple quantum systems. Phys. Rev. Lett. **56** (1986), 541–544. URL http://link.aps.org/doi/10.1103/PhysRevLett.56.541.

[Izr90] F. M. Izrailev. Simple models of quantum chaos: Spectrum and eigenfunctions. Physics Reports **196** (1990), 299 – 392. URL http://www.sciencedirect.com/science/article/B6TVP-46SNJ0T-2D/2/665eb1e4283e482da8a3aa0ff402bb2c.

[Jac01] P. Jacquod, P. Silvestrov, and C. Beenakker. Golden rule decay versus Lyapunov decay of the quantum Loschmidt echo. Phys. Rev. E **64** (2001), 055203. URL http://link.aps.org/doi/10.1103/PhysRevE.64.055203.

[Jal01] R. A. Jalabert and H. M. Pastawski. Environment-Independent Decoherence Rate in Classically Chaotic Systems. Phys. Rev. Lett. **86** (2001), 2490–2493. URL http://link.aps.org/doi/10.1103/PhysRevLett.86.2490.

[Jel89] R. J. Jelitto. Thermodynamik und Statistik. Akad. Verl.-Ges., Wiesbaden, 2. revised edition edition (1989).

[Ken04] A. Kenfack and K. Życzkowsk. Negativity of the Wigner function as an indicator of non-classicality. Journal of Optics B: Quantum and Semiclassical Optics **6** (2004), 396. URL http://stacks.iop.org/1464-4266/6/i=10/a=003.

[Lic85] A. J. Lichtenberg. Universality from resonance renormalization of Hamiltonian maps. Physica D: Nonlinear Phenomena **14** (1985), 387 – 394. URL http://www.sciencedirect.com/science/article/B6TVK-46G8PVX-42/2/5df337981c3e02103d729713f3c278dc.

[Lic92] A. J. Lichtenberg and M. A. Lieberman. Regular and chaotic dynamics. Number 38 in Applied mathematical sciences. Springer, New York ; Berlin ; Heidelberg, 2. ed. edition (1992).

[Nol05] W. Nolting. Viel-Teilchen-Theorie. Springer, Berlin ; Heidelberg [u.a.], 6., aktualisierte aufl. edition (2005).

[Obe99] M. K. Oberthaler, R. M. Godun, M. B. d'Arcy, G. S. Summy, and K. Burnett. Observation of Quantum Accelerator Modes. Phys. Rev. Lett. **83** (1999), 4447–4451. URL http://link.aps.org/doi/10.1103/PhysRevLett.83.4447.

[Per84] A. Peres. Stability of quantum motion in chaotic and regular systems. Phys. Rev. A **30** (1984), 1610–1615. URL http://link.aps.org/doi/10.1103/PhysRevA.30.1610.

[Rec80] A. B. Rechester and R. B. White. Calculation of Turbulent Diffusion for the Chirikov-Taylor Model. Phys. Rev. Lett. **44** (1980), 1586–1589. URL http://link.aps.org/doi/10.1103/PhysRevLett.44.1586.

[Sak09] J. J. Sakurai. Modern quantum mechanics. Addison-Wesley Longman, Reading, Mass. ; Bonn, rev. ed. edition (2009).

[San03] R. Sankaranarayanan and A. Lakshminarayan. Recurrence of fidelity in nearly integrable systems. Phys. Rev. E **68** (2003), 036216. URL http://link.aps.org/doi/10.1103/PhysRevE.68.036216.

[Sch96] L. S. Schulman. Techniques and applications of path integration. Wiley classics library ; A Wiley Interscience publication. Wiley, New York (1996).

[Sch01] W. P. Schleich. Quantum optics in phase space. Wiley-VCH, Berlin ; Weinheim (2001).

[Sch04] F. Schwabl. Statistische Mechanik. Springer-Lehrbuch ; Physics and astronomy online library. Springer, Berlin ; Heidelberg, 2., aktualisierte aufl. edition (2004).

[Sch05a] R. Schaback and H. Wendland. Numerische Mathematik. Springer-Lehrbuch. Springer, Berlin ; Heidelberg, 5. completely revised edition edition (2005).

[Sch05b] F. Schwabl. Quantenmechanik. Springer-Lehrbuch. Springer, Berlin ; Heidelberg, 6. revised edition edition (2005).

[She83] D. Shepelyansky. Some statistical properties of simple classically stochastic quantum systems. Physica D **8** (1983), 208.

[Tab89] M. Tabor. Chaos and integrability in nonlinear dynamics. A Wiley-Interscience publication. Wiley, New York (1989).

[Wei05] Y. S. Weinstein and C. S. Hellberg. Quantum fidelity decay in quasi-integrable systems. Phys. Rev. E **71** (2005), 016209. URL http://link.aps.org/doi/10.1103/PhysRevE.71.016209.

[Wim03] S. Wimberger, I. Guarneri, and S. Fishman. Quantum resonances and decoherence for δ-kicked atoms. Nonlinearity **16** (2003), 1381. URL http://stacks.iop.org/0951-7715/16/i=4/a=312.

[Wim04] S. M. Wimberger. Chaos and Localisation: Quantum Transport in Periodically Driven Atomic Systems. Ph.D. thesis, Ludwig-Maximilians-Universität München. URL http://edoc.ub.uni-muenchen.de/1687/1/wimberger_sandro.pdf (2004).

[Wim06] S. Wimberger and A. Buchleitner. Saturation of fidelity in the atom-optics kicked rotor. Journal of Physics B: Atomic, Molecular and Optical Physics **39** (2006), L145. URL http://stacks.iop.org/0953-4075/39/i=7/a=L01.

[Wu09] S. Wu, A. Tonyushkin, and M. G. Prentiss. Observation of Saturation of Fidelity Decay with an Atom Interferometer. Phys. Rev. Lett. **103** (2009), 034101. URL http://link.aps.org/doi/10.1103/PhysRevLett.103.034101.

Danksagung

Am Ende meiner Arbeit und meines Studiums möchte ich noch einige Personen erwähnen, denen ich viel zu verdanken habe.

Zuerst möchte ich Herrn Dr. Sandro Wimberger danken. Er hat dieses interessante Thema vorgeschlagen, mich in seiner Gruppe aufgenommen und mir damit ermöglicht, dies im Laufe des letzten Jahres zu bearbeiten. In den vielen und intensiven Diskussionen haben wir gemeinsam sehr viel über das System des gekickten Quantenrotors gelernt. Besonders dankbar bin ich ihm, dass er den Kontakt mit Herrn Prof. Guarneri hergestellt und mir einen Aufenthalt bei diesem in Como ermöglicht hat. Dieser hat meiner Arbeit eine andere Qualität gegeben.

Weiterer Dank gilt Herrn Prof. Dr. Thomas Gasenzer, der sich freundlicherweise bereit erklärt hat das Zweitgutachten zu schreiben.

I owe special gratitude to Prof. Italo Guarneri for allowing me to visit him in Como. Without this visit my thesis never would have reached the level it has reached now. His ideas and his confidence in approximations were impressive. Discussing with him was the best starting point I could have had and also influenced the work I did when I returned to Heidelberg.

For the time in Como I would also like to thank Laura, Gabriella, Gabriela and Matheo who shared their office with me. The coffee breaks made the day much more pleasant beside the extensive calculations I did. I owe gratitude to Antoine who was one of my room-mates in the students dormitory. His help and supply made it possible for me to have a nice time at Collegio Santa Teresa in Como.

Auch in meiner Zeit am Institut in Heidelberg haben mir meine Zimmergenossen die Zeit wesentlich versüßt. Für die lustige Zeit im Keller möchte ich David Jörg, David Breyel, Kambis Veschgini, Frank Hantschel, Benjamin Hess und Johanna Baschek recht herzlich danken. Besonders möchte ich Tobial Paul, Remy Dubertrand, Patrick Plötz, Ghazal Tayebirad, Carlos Parra-Murillo, Georgios Kordas, Nils Lörch und Conrad Albrecht, alle Mitglieder der Gruppe Wimberger, danken. Die gemeinsamen Mittagessen, Kaffepausen und Diskussionen haben meine Motivation, täglich den steilen Weg ins Institut zu gehen wesentlich gehoben. Auch Martina Abb, von der ich dieses Projekt übernommen habe, gebührt Dank. Ihre Erklärungen haben meinen Einstieg in die Arbeit wesentlich erleichtert.

Ein spezieller Dank geht an Patrick Plötz, Jörg Bochterle und David Jörg die sich bereit erklärt haben, diese Arbeit zumindest in Teilen Korrektur zu lesen und sich mit meinen teils wirren Gedankengängen zu beschäftigen. Wenn dabei ein lesebarer Text entstanden sein sollte, so haben diese Herren einen wesentlichen Anteil daran.

Ein Studium ist ohne Mitstreiter wesentlich schwerer zu bestehen. Daher gilt

mein Dank auch Jörg Bochterle, Felix Klein, Martin Ries, Christian Kieft, Enno Rohlack und Fridtjof Kowald. Ohne eure Unterstützung bei Praktika, Übungszetteln und diversen Prüfungen wäre das Studium wesentlich schwerer gewesen. Eure Freundschaft hat meine Zeit in Heidelberg bereichert.

Auch all den Leuten die in meiner Heidelberger Zeit meine Freunde geworden sind will ich hier danken. Nicht zuletzt meinen Mitbewohnern die vor allem in der Schlussphase meiner Diplomarbeit darunter zu leiden hatten, dass ich meinen Pflichten nur teilweise nachgekommen bin.

Ein besonderer Dank gilt meiner Familie. Sie haben mich in allen Entscheidungen seit der Schulzeit unterstützt und mir mein Studium ermöglicht. Sie haben mir erlaubt, zu dem zu werden was ich heute bin.

Erklärung:

Ich versichere, dass ich diese Arbeit selbstständig verfasst habe und keine anderen als die angegebenen Quellen und Hilfsmittel benutzt habe.

Heidelberg, den 30. September 2010 .....